New TDOA based localization method for HDR systems

Ahmadreza Jafari



Université Pierre et Marie Curie

Laboratoire d'Électronique et Électromagnétisme (L2E)

École doctorale : EDITE

Rapport de thèse

Spécialité : Électronique

Présentée par

Ahmadreza JAFARI

Nouvelle méthode d'estimation des différences de temps d'arrivée pour la localisation des objets connectés haut débit

Thèse en cotutelle dirigée par M. Aziz Benlarbi-Delaï et M. Philippe De Doncker

Soutenue devant le jury composé de :

Mme. M. Di Benedetto, *Professeur à l'Université de Sapienza Rome*	Rapporteur
M. C. Loyez, *Professeur à l'Université de Lille 1*	Rapporteur
M. F. Horlin, *Professeur à l'ULB*	Examinateur
M. B. Denby, *Professeur à l'UPMC*	Examinateur
M. P. De Doncker, *Professeur à l'ULB*	Directeur de thèse
M. A. Benlarbi-Delaï, *Professeur à l'UPMC*	Directeur de thèse
M. J. Dricot, *Professeur à l'ULB*	Examinateur
M. J. Sarrazin, *Maître de conférences à l'UPMC*	Encadrant de thèse
M. A. Ghiotto, *Maître de conférences à l'Université de Bordeaux*	Invité

Contents

Introduction

THE forthcoming vision of Internet of Things (IoT) and Internet of Everything (IoE) will immerse people in so-called Smart Environments involving a great number of sectors of applications such as smart habitat, smart-cities, environment monitoring, e-health... IoT and IoE tend to make everyday objects readable, recognizable, locatable, addressable and controllable via the widespread wireless deployment and the internet. Among these capabilities, localization and more extensively the ubiquitous positioning will play, in the next future, a key role to promote another emerging vision: a spatio-temporal Internet of Places (IoP), which would be able to structure and organize, by means of wireless energy aware approaches, the spatial content of Internet.

It is well known that in wireless local and personal area networks, the spectrum congestion, the low energy efficiency communications and the insufficient exploitation of the spatial resources are among the factors that may slow down its development in terms of throughput and autonomy. To overcome these unavoidable restrictions, wireless localization technology, as the mechanism for discovering spatio-temporal relationship between connected objects, appears here also as one of the key solutions. This is because dedicated localization techniques in wireless communication can help in developing more extensively the exploitation of spatial resources and allow driving optimized routing for low energy multi-hop communication and spectrum decongestion for Green ICT (Information and Communication Technology).

To propose optimized systems achieving both high data rate communication and precise localization, we define a well suited TDOA (Time Difference of Arrival) based method able to perform localization based on communication signals and data only. With this technique, unlike conventional TDOA estimations, it is possible to drastically decrease the complexity of required infrastructures by using either SIMO (Single Input Multiple Output), MISO (Multiple Input Single Output) or MIMO (Multiple Input Multiple Output) configurations in connected objects.

This whole study is made within the framework of the IEEE 802.11ad standard and WiGig alliance specifications, however the proposed solutions are compatible with other

standards and can be extended to other context aware applications requiring localization inputs such as robotics for example or smart shopping.

This thesis is organized as follows:

In the first chapter, the context and objective of this research are stated. First, new emerging applications demanding wireless high data rate communications are presented with a focus on the next generation of mobile networks (5G). Then, millimeter wave communication, and particularly 60 GHz technology, is explored as a solution to meet the requirements of mentioned high data rate applications. Energy aspects are also considered. All these elements of context lead to localization as one of the main tools required to achieve green radio systems. Furthermore, indoor localization, which is the final objective in the context of this research area, is explored regarding its growing recent applications.

In the second chapter, the state of art of 60 GHz communication systems and indoor positioning methods are presented. In the 60 GHz section, propagation characteristics, material impacts, technological aspects, modulation schemes and standards are briefly described. In the indoor positioning section, methods and metrics are presented, and TDOA is chosen as a promising solution for compact and asynchronous localization function in the context of ultra wide band high data rate millimeter wave communications.

In the third chapter, a new TDOA based method, well suited to 60 GHz communication systems, is presented. Based on Multiple Input Single Output (MISO) high data rate communication signal, this method is explored regarding two different approaches: TDOA estimation using Error Vector Magnitude (EVM) of received signal, and TDOA estimation using Channel Equivalent Response (ECR) performed in mono-band and multi-band configurations. The system description and formulations are presented in detail and the prediction of theory is confirmed through first stage of simulations. Finally, the IEEE channel is introduced and simulations are performed to illustrate the accuracy and efficiency of the proposed approach in a realistic environment.

In the fourth chapter, measurement campaigns and experimental results, acting as a second mean of theory and model validation, are presented. Coupling vectorial network analyzer based measurements and 60 GHz communication system based measurement, qualitative and quantitative results are obtained for different types of communication channel. As this research is led in the frame of European doctoral school EIT ICT labs, some measurements have been carried out in Berlin at Fraunhofer HHI.

Finally, section 5 concludes this work and presents the perspectives of this research.

Chapter 1

Context and objectives

1.1 Introduction

SOME wireless systems are expected to provide multi-gigabyte data rates, thus replacing cables for indoor communications. Wide-band communications using complex modulations such as OFDM (Orthogonal Frequency Division Multiplexing) are used more and more in short-range applications such as video streaming, wireless USB, wireless HDMI, etc. However, the current commercial wireless systems do not yet reach the necessary data rates for heavy applications involving for example HD video. In addition, the popularization of smart phones and tablets in recent years causes the ever growing traffic explosion in mobile communications. This fact has recently drawn increased attention to utilize higher frequency like millimeter-wave bands [1, 2, 3, 4].

In this chapter, first, emerging applications demanding wireless high data rate communications are explored, and solutions using millimeter-wave communication are seen as key elements of the context. Next, localization is proposed as a solution to deal with the energy consumption challenges in high data rate communications and also as a powerful tool that enables different new applications for indoor environments.

1.2 New applications demanding high data rate communications

Recent applications requiring high data rate wireless communication in indoor and outdoor environment are mainly categorized in four major divisions: wireless networking, wireless display, intelligent transportation and 5G.

1.2.1 Wireless networking and instant wireless synchronization

Wireless networking and instant wireless synchronization applications need massive data rates between mobile devices, telecommunication infrastructure equipment, and the cloud [5]. Furthermore, high-bandwidth data transfer applications involve the transparent bridging of various short-range wired connection technologies with wireless technology like USB, SATA, etc. The main applications of this category are [5, 6]:

- Gb/s wireless networking for office
- Rapid upload/download
- High bandwidth and rapid file transfer/synchronizing

1.2.2 Wireless display, distribution of HDTV, high quality audio and wireless docking

It has been a while since high data digital video (HDTV) penetrated in almost every home. HD video can be transmitted via cable connections that provide easily very high data rates. However, users would prefer to utilize a wireless solution to reduce the number of visible wires. Flat panel display which can be hanged on a wall, is an example of the need for a wireless video solution. The main applications of this category are [6, 7]:

- Desktop storage and display
- Projection to TV or projector in conference room or auditorium
- In-room gaming
- Streaming from camcorder to display
- Outside broadcast pickup
- Video streaming around the home
- Uncompressed baseband high-definition video
- Uncompressed high-quality audio

Wireless docking is another application of this category which is a combination of wireless display, wireless synchronization and wireless I/O. Let's consider a scenario where a tablet is wirelessly bridging to a dock that instantly connects the tablet to different monitors, keyboard, and mouse. And it is just by putting the tablet in range that connects it to all these peripherals needed to turn it into a full desktop system.

1.2.3 Intelligent transportation systems

Intelligent transportation systems (ITS) encompass a variety of safety, informational, and entertainment communications applications either between multiple moving vehicles

or between an in-vehicle system and infrastructure such as roadside equipment or between a train and a platform. In some regulatory domains, portions of the 60-GHz band is allocated for ITS. The main applications of this category are [8]:

- Car-to-car communication
- Monitoring and identifying of objects near vehicles
- Road guidance inside parking garages
- Rapid uploading of heavy files provided by embedded security IP camera

1.2.4 Access and future 5G

The popularization of smart phones and tablets in recent years causes the traffic explosion in mobile communications. As shown in Figure 1.1, the traffic of data on conventional networks increased during last years and is predicted to increase several times in the next 10 years.

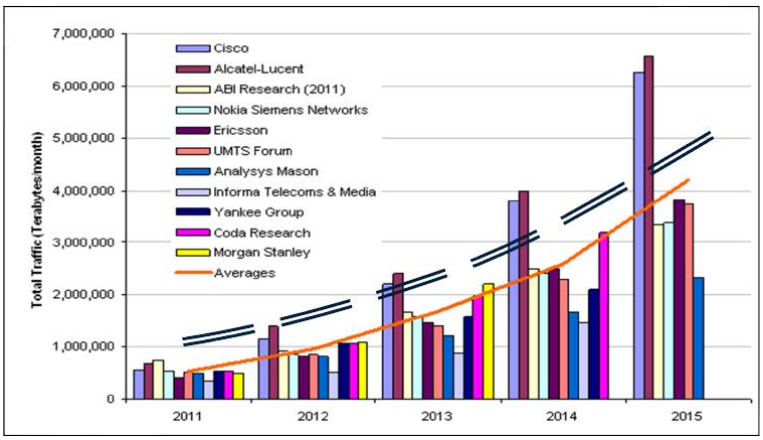

Figure 1.1: Traffic forecast.

To support the hundreds of times more traffic demands foreseen in 2020 and beyond, the so-called 5G era, new wireless high data rate communication standards and systems are required [3, 4]. Similarly, low-cost backhaul radio devices and massively broadband wireless relays may replace telephone poles and conventional repeaters in the telephone plant of the future.

Recently, European projects like MiWEBA (Millimetre-Wave Evolution for Backhaul and Access) and METIS (Mobile and wireless communications Enablers for the Twenty-twenty Information Society) are being funded [9, 10]. The goal of these projects is to base the foundation of 5G. One major goal of 5G technology developers is providing data rates of more than 10 Gbit/s in the mobile wireless access networks. The advancements in new radio concepts such as ultra dense networks, MIMO (Multiple Input Multiple

Output) systems, device-to-device, ultra reliable and massive machine communications are expected to support the increase in mobile data volume in future 5G [11].

Furthermore, it is predicted that IoT will be implemented in different applications of everyday life and by 2020, a total of about 50 billion connected devices is expected. Thus, researches related to the fields such as World Wide Wireless Web (WWWW), Dynamic Adhoc Wireless Networks (DAWN), and Real Wireless Communication will be taken into consideration in 5G.

Regarding the spectrum that will be used in 5G, considered frequencies are 28 GHz, 38 GHz, 60 GHz and the E-band. Among these frequencies, the availability of the 60 GHz band as unlicensed spectrum makes it a good candidate to provide Gb/s communications for short-range communication. Furthermore, several industrial standards such as 802.11ad have already been developed at 60 GHz [11, 12, 13].

Millimeter-wave based networks, will consider several type of wireless links such as back-haul, multi media mesh back-haul, point to point back-haul and front-haul [6, 7].

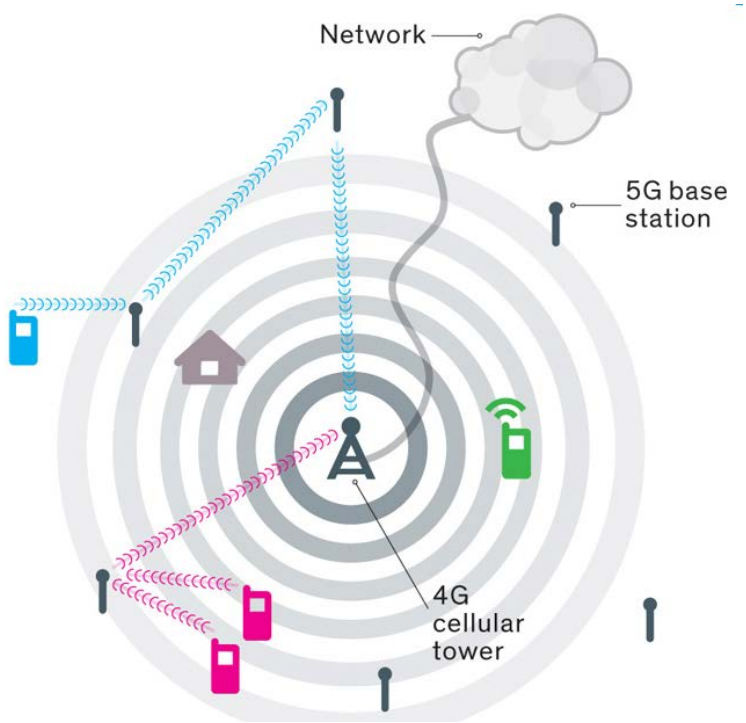

Figure 1.2: Applications regarding access and 5G: future mobile network schematic.

As shown in Figure 1.2, phones at the edge of a 4G cell could connect themselves to the millimeter-wave base stations (5G base station), thereby enabling a multi gigabit mobile connections. 5G is consequently expected to operate at 3 scales of network, hereby:

- Ad-hoc Wireless Personal Area Network (WPAN)
- 802.11 Wireless Local Area Networks (WLAN)

- 802.16 Wireless Metropolitan Area Networks (WMAN)

In next section, 60 GHz millimeter-wave communication systems are presented as a solution to achieve a reliable high data rate wireless communication in order to answer the requirements of emerging applications mentioned above [6, 7].

1.3 High Data rate communication: millimeter-wave solutions (60 GHz)

1.3.1 Benefits of millimeter-wave frequencies for Gb/s communication

As already mentioned, new applications for WPAN and WLAN require very high data rates and a very high level of QoS (Quality of Service) to meet user expectations. Millimeter-wave frequencies provide a unique opportunity to wirelessly enable these applications. Different approaches are being pursued to increase the overall wireless access network capacity and the maximum supportable data rate. One proposed solution is improving spectral efficiency, which requires individual radio link optimization simultaneously for many users [3, 4]. To implement this approach, one should deal with challenges like self-interference by adjacent cells and imperfections of the deployed hardware. This requires advanced and complex signal-processing techniques and high performance transceivers, which is neither easy nor always possible to achieve. The second solution is network densification (spectrum reuse) by reducing distance between base stations. This is an energy efficient solution but with more inter-cell interference, thus more complexity. The third solution is spectrum extension using millimeter-wave communications. Below 6 GHz, its difficult to allocate additional spectrum in low frequency because of satured existing frequency allocations. So, the solution could be utilizing higher frequencies like millimeter-wave bands. The large amount of radio spectrum available, combined with low cost CMOS (Complementary Metal Oxide Semiconductor) technology and new solutions of integrated antennas, make millimeter-wave spectrum a valuable candidate for new capabilities for future wireless communication networks. Advantages of using millimeter-waves regarding capacity increase techniques are shown in Figure 1.3.

Spectrum extension by means of millimeter-wave cellular overlay perfectly consistent into existing networks. Millimeter-waves normally offer a large bandwidth and a shorter range communication which leads respectively to densification of networks and more throughput. They also use beamsteering and multi-user MIMO techniques supporting point to point and point to multi-point communications which increase the spectrum ef-

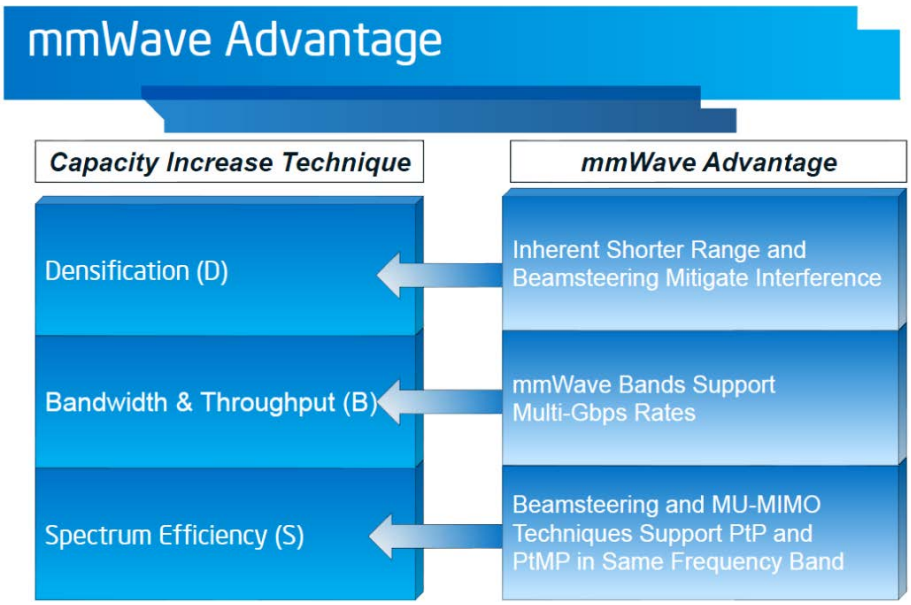

Figure 1.3: Millimeter-wave advantages.

ficiency (Figure 1.3). Using the large bandwidth available at frequencies in the 30–300 GHz range can lead to extend the spectrum. Recently, 28 and 38 GHz bands (where 1 GHz of bandwidth is available) have been explored in details to overcome the problem of future network capacity. 60 GHz band and the E band (71–76 and 81–86 GHz) are also among the bandwidths explored recently to provide multi-Gbps capacity for wireless communications.

1.3.2 Why 60 GHz?

1.3.2.1 Regulatory environment

Among the millimeter-wave bands, the vast amount of radio spectrum available at 60 GHz, is particularly a good candidate to be chosen as a relevant solution [7, 9, 14]. The 60 GHz band has not been heavily utilized because of the higher path loss of RF signals due to oxygen absorption. This has allowed regulators all over world to create 7 GHz frequency allocations, for unlicensed use. To have a better idea about this huge bandwidth, it should be mentioned that 7 GHz includes all AM radio stations, FM radio stations, all broadcast television allocations, all cellular telephony, and both 802.11 frequency bands, and still has room to spare. Representation of the allocated frequencies is illustrated in Figure 1.4.

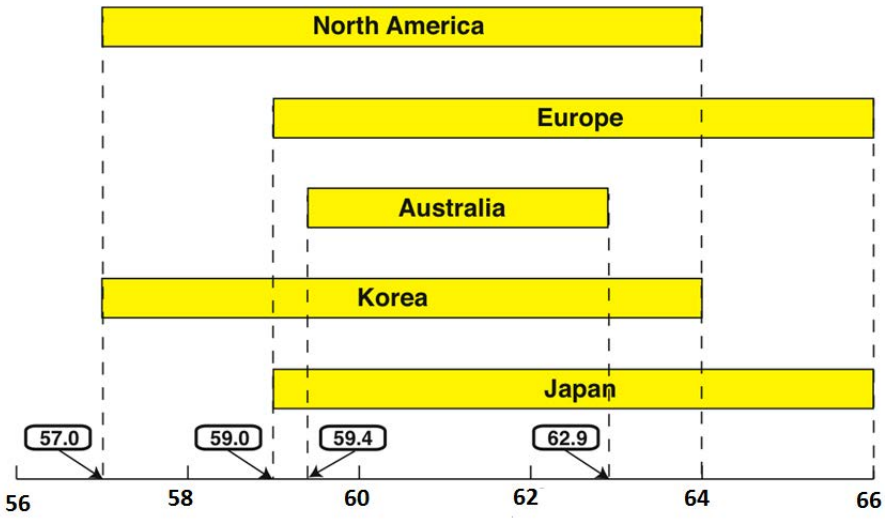

Figure 1.4: 60 GHz available bandwidth for millimeter-wave communication (GHz).

1.3.2.2 60 GHz implications

In addition to its huge bandwidth, 60 GHz, as any millimeter-wave frequency, exhibits other features that are of great interest for telecommunication. 60 GHz technology has many important characteristics which makes it a good choice to be used in high data rate local applications.

Using small wavelength allows small high-gain antennas. A 25 dB gain antenna has an effective aperture of approximately one square inch. High-gain antennas allow high equivalent isotropically radiated power (EIRP) with low-power RF amplifiers. High gain allows overlapping networks that do not interfere. Because antennas are highly directional at these frequencies, spatial reuse is enabled for collocated systems [7].

However, due to the wave attenuation in free space, the more the frequency increases the more the attenuation increases too, as indicated by Friis equation:

$$P_r = P_t + G_t + G_R + 20 * log_{10}(\frac{\lambda}{4\pi R}) \tag{1.1}$$

In this equation P_r and P_t are the received and transmitted powers expressed in dBm, G_t and G_R are respectively the gains, in dB, of transmitter (Tx) and receiver (Rx) antennas, λ is the wavelength and R is the distance between Tx and Rx. So the attenuation is much higher at 60 GHz than at 2.5 GHz, 5 GHz or any other usual radio frequencies (for example for R=10m, attenuations at 60 GHz and 2.5 GHz are respectively 88 and 60 dB), as shown in Figure 1.5 [15].

But, considering equation 1.2, for given aperture areas of Tx and Rx antennas (respectively A_t and A_r), shorter wavelengths propagate further compared to longer wave-

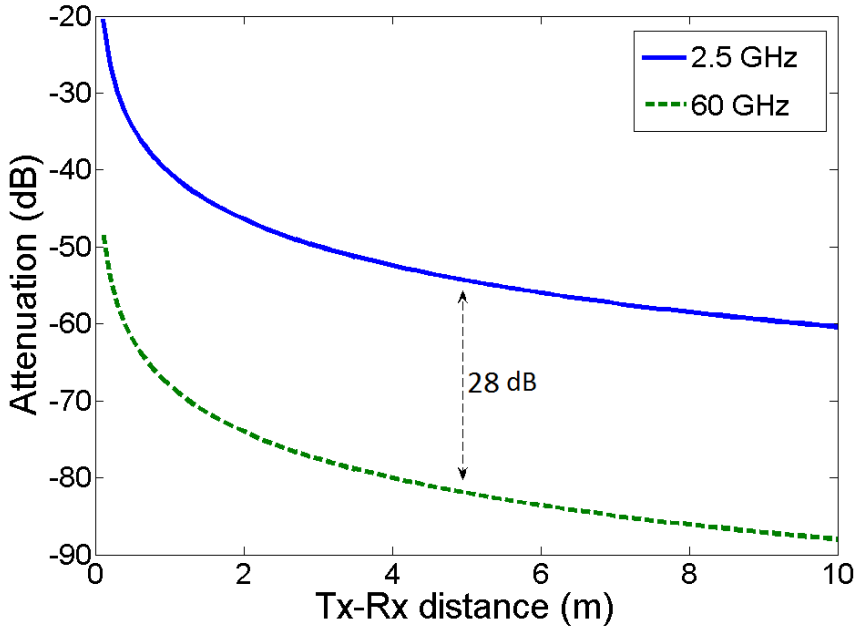

Figure 1.5: Path loss attenuation for 60 GHz and 2.5 GHz as function of the distance between Tx and Rx.

lengths [15].

$$\frac{P_r}{P_t} = A_r^{\text{eff}} A_t^{\text{eff}} \frac{1}{\lambda^2} \frac{1}{R^2} \tag{1.2}$$

This fact is due to the more directive transmission at higher frequencies (narrower beams). For example, a beam at 60 GHz will have about 27.6 dB extra gain compared to the beam at 2.5 GHz for the same antenna areas.

Thus, as long as directional transmissions are considered, millimeter-wave frequencies do not suffer from any inherent disadvantage relative to the lower frequencies. Moreover, directional transmissions may lead to reduce interference and at the same time, to increase spatial multiplexing capabilities for cellular applications.

Also, at 60 GHz, the peak of absorptions by oxygen molecules in the air is about $15dB/km$. In addition, 60 GHz also deals with the higher sensibility to obstacles and more attenuation in rainy weather. Due to all these reasons, inter-cells interferences largely decreased, which matches perfectly the concept of small cells.

In addition, there are not any widely deployed 60 GHz radiating sources in the home or office, so there is less chance for interference. Unlike the strict transmit power restrictions on ultra wide band unlicensed operation, the millimeter-wave band allows an EIRP that is significantly greater.

So, an effort exists to develop a wireless UWB (Ultra Wide Band) technology at 60 GHz. In this context ultra-high-speed systems employing mm-wave such as WiGig and

802.11ad have been standardized, however, they are not yet connected to the cellular networks. Since the release of 60 GHz spectrum by the FCC and other governmental bodies, tremendous progress has been made toward the realization of highly integrated 60 GHz radios for inexpensive and potentially ubiquitous consumer adoption. Progress in the areas of on-chip antennas, PAs (power amplifiers), LNAs (low noise amplifiers), VCOs (voltage control oscillators), mixers, ADCs (analog to digital converters), and mm-wave channel characterization will result in widespread commercial 60-GHz products [5, 7]. Progress is needed in antenna integration, lower power components, improved base-band and beam forming processing, and in creating more targeted and streamlined standards to bring 60 GHz and future mm-wave wireless devices to consumers [16, 17]. The recent achievement in 60 GHz technology and a global view of 60 GHz communication are presented in details in next chapter.

1.4 Energy aspects

Energy consumption in wireless networks is an essential factor with respect to its environmental impact as well as autonomy of the system. And this could be even more so in the case of 60 GHz communications compared to the conventional wireless networks due to strong millimeter-wave attenuation [18, 19, 20]. Hence, the energy efficient transmission technologies become one of the most important research topics and attract a lot of research projects, including MVCE (Mobile Virtual Center of Excellence), Green Radio project and cool silicon program targeting for low-power chip and network solutions [21].

1.4.1 Lower energy consumption thanks to high data rates

It may seem against the intuition to reach a low power device by using high-frequency, high-throughput wireless technologies. But, one should consider the fact that the suitability of a design for mobile applications is determined by the energy efficiency and not just the instantaneous power consumption. On the first look, it may seem that a typical high data rate 60 GHz wireless design consumes more power than other wireless technologies over higher distances. But this conclusion is misleading due to the fact that the total power consumption may be reduced by using a higher speed solution because of its ability to operate at a much lower duty cycle than slower radio technologies. Considering this fact, the power efficiency is determined by the energy required per bit transmitted. Then, in this case, the faster the radio technology, the lower the actual duty cycle and the lower the amount of energy necessary to transfer each bit of data. Furthermore, the overall power drain is reduced by using the host processor and storage for a shorter period of

time [7]. In addition, a high throughput system decreases the time required to complete a transaction and enables the user to quickly accomplish the data transfer. Therefore, using a high throughput communication at 60 GHz is helping to achieve an efficient energy consumer system. Even without considering duty cycle, higher bandwidths and higher data rates lead to better efficiencies. In fact it can be seen from Figure 1.6, that applying more bandwidth per communication link is a significant contributor for improved energy efficiency measured in Bits-per-Joule [21].

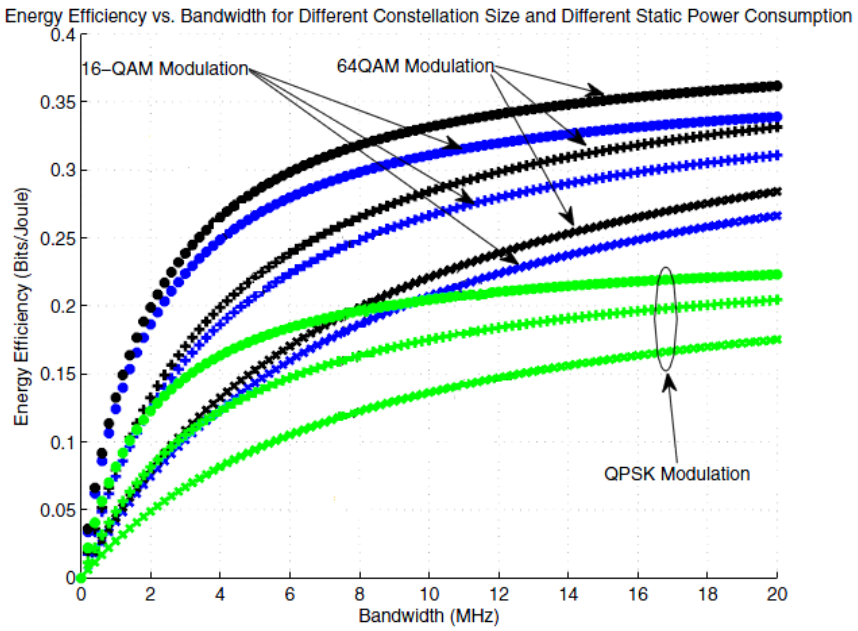

Figure 1.6: Energy efficiency versus bandwidth for different modulation schemes [21].

1.4.2 Lower energy consumption thanks to spatial capabilities

A simple way to estimate the energy budget of a given SISO communication is to consider the cost function C given by:

$$C = \beta d^{\gamma}. \tag{1.3}$$

where γ is a channel exponent (for free space: $\gamma = 2$), β is a coefficient related to antenna gains and operating wavelength, and d is the distance between Tx and Rx. This two degree of freedom equation (β, d) can lead to two approaches for optimizing the energy cost of a given communication system: beamforming, which optimizes systems regarding β and multi-hop, which optimizes systems regarding d.

1.4.2.1 Beamforming

Beamforming, which consists in reducing β, is used to achieve a directional signal propagation and a spatial selectivity. Beamforming is obtained by using a phased array and combining its elements in such a way that signals experience, at particular angles, constructive interference while others experience destructive interference [22].

Multiple antenna elements are utilized in beamforming to form a beam toward a defined direction. The signal strength is increased which is achieved by transmitting phase shifted signals from multiple antenna elements. The signals are phase shifted in a way that at the target direction, the signals are added up coherently. As the number of antenna (Na) increases the peak beamforming gain (Gb) increases (i.e. Gb [dB] = 10*log(Na)). For instance, approximately 12 dB of peak beamforming gain can be provided by a 16 isotropic elements antenna array.

Since many antenna elements can be packed in a very small area for millimeter-wave communications, beamforming is well suited at 60 GHz compared to 2.4 GHz and 5 GHz band. For example, a square antenna array with 16 antennas elements (4*4) can be packed in 1 cm^2 when adjacent antenna elements are separated by half wavelength (wavelength is 5 mm at 60 GHz). This fact is a very critical aspect to consider in required compact complex systems.

Furthermore, to achieve a green radio communication, focalization of energy, which generalizes the concept of beamforming, is a solution that can lead to a decrease in consumption and to increasing the range of the wireless communications. This is why underway development of 60 GHz standards consider strongly beamforming solution [23].

1.4.2.2 Multi-hops

In multi-hop networks, along the path between BS (base station) or Tx and the end user or Rx, there are one or more intermediate nodes.

The idea here is to refer to the fact that, assuming the distance d between Tx node and Rx node is a sum of elementary distances d_i, one can write that:

$$d^\gamma > \sum d_i^\gamma. \tag{1.4}$$

Regarding energy issues, compared with networks with single wireless link d, transmission over multiple short links d_i in multi-hop networks might require less transmission power and energy than that required over one hop link.

In such networks, additional nodes are required. They are radio-equipped and able to

communicate by propagating over wireless links. Communication paths between Tx and Rx nodes can be established by those intermediate nodes acting as relays to forward data toward the destination.

In multi-hop wireless networks, such as radio networks, sensor networks and ad hoc networks, the network topology can be changed by each node. A set of neighbors can be piloted by each node's adjustment of transmission power. Obtaining power-efficient routing algorithms is the primary goal of topology control. By using this technique, it is possible to maintain network connectivity and optimize performance metrics such as throughput and network lifetime [24].

So in conclusion, to be able to perform energy spatial focalization or to deal with routing algorithms in multi node networks, connected nodes should be able to determine their location.

1.5 The objective: a better utilization of spatial resources

1.5.1 Localization as a support for green radio

It has been mentioned that in the field of high data rate wireless communications, utilization of spatial resources can play a key role to perform either beamforming or multi-hops.

Beamforming allows focusing the transmitted signal toward the receiver only, thereby decreasing the wasted amount of energy, whereas multi-hop techniques enables smart routing in dynamic networks. The objective way to address the spatial resources is to be able to perform localization in a way to make it as familiar and seamless for the end user as communication.

Thus, as shown in Figure 1.7, proposing an efficient localization method which is adapted to high data rate millimeter-wave communication systems (particularly at 60 GHz), is the vision that this research deals with, in order to ensure green radio communication in the different contexts involving indoor mobility or, more recently in the lab, body area networks (BAN).

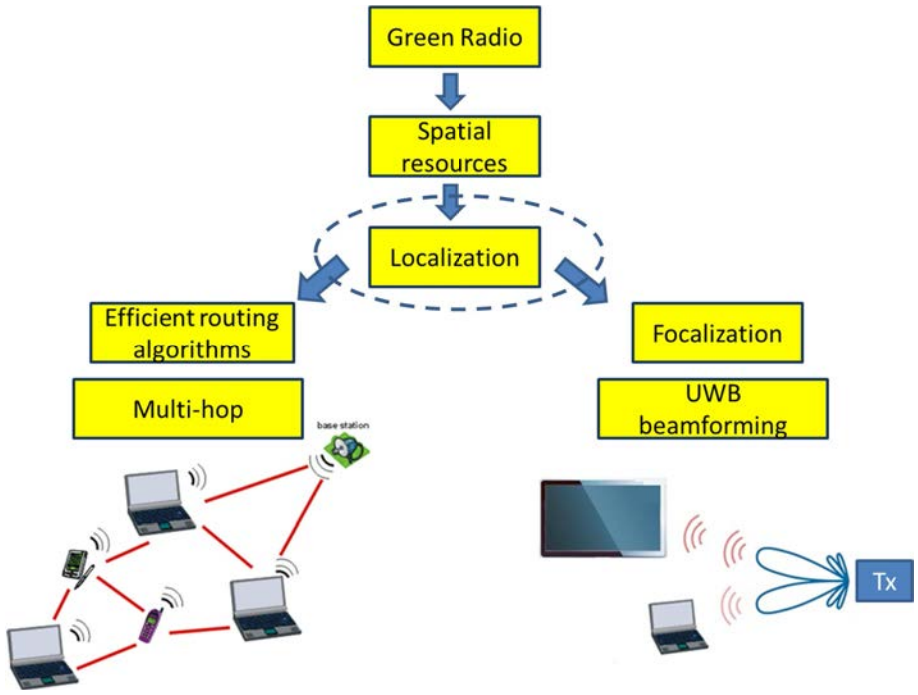

Figure 1.7: Green Radio: Localization.

1.5.2 Other applications of indoor localization

In previous sections, the impact of localization on the power consumption has been highlighted. In this section, the advantage of performing localization is explored regarding its applications in the world of high data rate indoor communications. The ability to localize and navigate persons and mobile devices in indoor environments has become more and more indispensable, while the performance of outdoor positioning has already become excellent, by using the global navigation satellite system (GNNS) [25].

Indoor positioning have become very popular in recent years and new applications have been developed and will be developed accordingly. Some examples are [8, 26]:

- Locating, monitoring and tracking people and things:
  This process would be similar to automobile GPS navigation applications however being done indoor where GPS does not work. Navigation in malls, public buildings and finding particular stores or offices in these areas are some examples of this category.
- Coordinating Joint Activities:
  Coordinating activity between people and things that are moving dynamically with respect to each other is another interesting issue in indoor localization. Identifying and locating a particular person who is nearby is one example of this application.
- Augmented reality (AR) and gaming:

AR is an increasingly powerful tool to superimpose graphics or sounds or information related to the environment on the users real view. For AR applications, localization awareness has an important impact. Gaming and entertainment are also relatively new areas for indoor localization. Location information can be applied in order to combine the virtual and real world and create a huge number of new applications.

- Situational awareness:
  Devices use positioning information to provide context on the surrounding environment and, in interactive applications, pinpoint the location of items or people of interest that may be nearby, for example, finding the right platform in train and bus stations.
- Applications related to safety:
  Detecting the location of medical personnel in a hospital or of firemen in a building on fire are some examples of this category.

1.6 Conclusion

In this section the recent ever-growing applications urging to use high data rate communication are presented. Demonstrations have been done that huge bandwidth is necessary to meet these emerging application's requirements and the 60 GHz band and more extensively millimeter-wave communication are seen as present and future potential promising solutions.

To overcome the energy consumption challenges for these high data rate communications, localization is introduced as a key function to perform either beamforming or multi-hops but also to develop spatial aware applications, for which different applications have been described in order to emphasize the importance of indoor localization itself.

Therefore, in the context of green radio, the subject of this research is to propose a simple and yet efficient localization method well-suited for 60 GHz wireless communications.

Chapter 2

State of the art of 60 GHz systems and indoor positioning methods

2.1 Introduction

It has been shown, in chapter 1, that 60 GHz appears to be a good candidate for present and future high data rate communications. Furthermore, localization techniques can play an important role application-wise as well as energy-wise. Consequently, in this second chapter, state of the art of 60 GHz technologies and systems is presented in order to highlight their suitability to perform both High Data Rate (HDR) communication and precise positioning. From the communication point of view, 60 GHz channel characteristics, technological aspects, modulation schemes and standards are explored. The second part of this chapter gives an overview of current positioning techniques. Angle of arrival measurements and distance related measurements leading to the determination of the main metrics (AOA, TOA, TDOA) are briefly described.

2.2 60 GHz communication systems

In spite of offering and providing many advantages, 60 GHz communication systems encounter different challenges and problems that may slow down their progress. These are defined hereafter.

2.2.1 Channel issues

Channel issues refer with all methods and approaches that allow a fair modeling of the behavior of radiated electromagnetic waves in a given environment. To target this modeling, propagation characteristic and material impact are to be addressed.

2.2.1.1 Propagation characteristics

The first property one should take into account for EM millimeter-waves propagation, is the atmospheric absorption. As shown in Figure 2.1, bands like 60 GHz that have high degree of atmospheric absorption and higher attenuation, are not suited for long range communication but are very convenient for short range applications. This is why, the majority of 60 GHz communication applications are in the category of WPAN, whereas, lower attenuation bands such as 77 and 240 GHz, are well suited for cellular, backhaul, fiber-replacement and sensing [5].

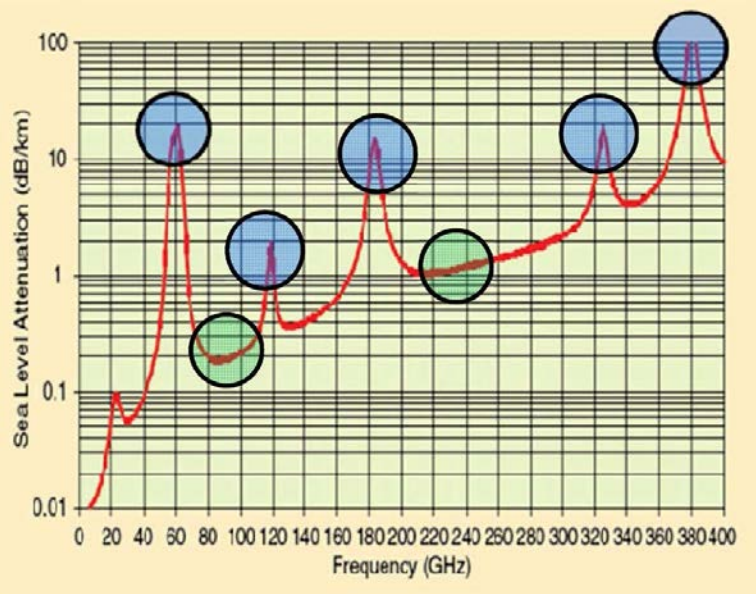

Figure 2.1: Atmospheric absorption of EM wave.

In addition to atmospheric absorption, all classical propagation phenomenons (reflection, diffraction,..) that happen in rural, urban and indoor environments must be taken into account. For that purpose, channel models are developed. In ray-tracing-based models, large scale and small scale fading, quasi-optical behavior of 60 GHz signals and polarization impact can be summarized in a general mathematical formulation dealing with the channel impulse response $h(.)$ and expressed as follow [27, 28]:

$$h(t, \phi_{Tx}, \theta_{Tx}, \phi_{Rx}, \theta_{Rx}) = \sum_i A^{(i)} C^{(i)}(t - T_{(i)}, \phi_{Tx} - \Phi_{Tx}^{(i)}, \theta_{Tx} - \Theta_{Tx}^{(i)}, \phi_{Rx} - \Phi_{Rx}^{(i)}, \theta_{Rx} - \Theta_{Rx}^{(i)}) \quad (2.1)$$

where t is time, ϕ_{Tx}, θ_{Tx}, ϕ_{Rx} and θ_{Rx} are respectively azimuth and elevation angle at Tx and Rx. $A^{(i)}$ is the gain for the i^{th} cluster and $C^{(i)}$ is the i^{th} cluster's channel impulse response and can be presented as:

$$C^{(i)}(t, \phi_{Tx}, \theta_{Tx}, \phi_{Rx}, \theta_{Rx}) = \sum_k \alpha^{(i,k)} \delta(t - \tau^{(i,k)}) \times \delta(\phi_{Tx} - \Phi_{Tx}^{(i,k)}) \delta(\theta_{Tx} - \Theta_{Tx}^{(i,k)}) \times \delta(\phi_{Rx} - \Phi_{Rx}^{(i,k)}) \delta(\theta_{Rx} - \Theta_{Rx}^{(i,k)}) \quad (2.2)$$

where δ is the Dirac function, $T_{(i)}$, $\Phi_{Tx}^{(i)}$, $\Theta_{Tx}^{(i)}$, $\Phi_{Rx}^{(i)}$ and $\Theta_{Rx}^{(i)}$ are the time and angles for the i^{th} cluster. $\alpha^{(i,k)}$ is the amplitude of the k^{th} ray of the i^{th} cluster. $\tau^{(i,k)}$, $\Phi_{Tx}^{(i,k)}$, $\Theta_{Tx}^{(i,k)}$, $\Phi_{Rx}^{(i,k)}$, $\Theta_{Rx}^{(i,k)}$ present the k^{th} ray of the i^{th} cluster's time and angles. Some contribution in this general formulation may be neglected if some assumptions are done [27, 28].

For example, using high gain antenna, which is a good solution for Line Of Sight (LOS) scenarios, can reduce the delay spread of the radio channel [29]. But in the case of Non Line Of Sight (NLOS) situations, antenna arrays and beamsteering techniques should be used in order to obtain a robust communication. Using circular polarization over linear polarization [30] is another way to decrease the multi-path effects. Recently, many channel measurements and modeling effort have been done at 60 GHz [27, 28].

2.2.1.2 Material impact

The path loss and transmission loss for many materials are significantly higher at 60 GHz compared to lower frequencies [31, 32, 33]. These higher path loss and transmission loss limit the use of 60 GHz for short range communication. Consequently, high gain antennas, relays and repeaters are required in order to have wider indoor coverage.

Hence, in order to dimension in a proper way a 60 GHz communication system, material penetration characteristics are an important factor to consider a realistic propagation channel. At millimeter-wave frequencies, wave penetration is defined mostly by the permittivity of the materials, because of the fact that most objects are large compared to the wavelength. In addition, the relative permittivity of a material determines the reflection and transmission coefficients of the wave impinging on that material. Thus permittivity for different materials at 60 GHz are presented in Table 2.1 [5, 34, 35]. To determine absorption related to these materials, let's consider a plane wave that can be written as:

Material	**Relative permittivity** (ϵ_r)
Acrylic Glass	2.5298-j2.5298
Chipboard	2.8556-j0.1586
Concrete	6.132-j0.3014
Glass	5.2839-j0.2538
Plasterboard	2.8096-j0.0461
Wood	1.5761-j0.0962
Human Body	7.98-j10.9

Table 2.1: Materials permittivity at 60 GHz.

$$E(\vec{r}) = E_0 e^{-j\vec{k}.\vec{r}} \tag{2.3}$$

with the propagation constant: $k = \omega\sqrt{\mu\epsilon}$ or $k = \omega\sqrt{\mu_0\epsilon_0\epsilon_r}$, in the case of non-magnetic materials. ϵ_r represents the complex relative permittivity of the medium where the wave is propagating. If α is the attenuation constant, we have then [34]:

$$\alpha = \Re(jk) = \omega\sqrt{\frac{\mu_0\epsilon_0'}{2}}\left(\sqrt{1+\left(\frac{\epsilon''}{\epsilon'}\right)^2}-1\right)^{1/2} \tag{2.4}$$

where $\epsilon' = \Re(\epsilon_0\epsilon_r)$ and $\epsilon'' = \Im(\epsilon_0\epsilon_r)$. α is in Np/m. To compare the attenuation involved by the different materials in Table 2.1, we express the attenuation in dB/cm with:

$$att_{[dB/cm]} = 20.\alpha.r.log(e) \tag{2.5}$$

where r is consequently equal to 1 cm.

Absorption results are given in Table 2.2 for classical materials found in a typical room. It can easily be observed that a 60 GHz wave will never propagate through a human body because of the severe attenuation. The absorption appears to be less strong in plasterboard. However, in addition to absorption involved in lossy materials, reflections have to be taken into account as well. In fact, a wall, for instance, obstructs a wave because it exhibits losses but also because part of the power is directly reflected at the wall-air interface. These reflections, as it will be shown, avoid communication between adjacent rooms at 60 GHz. However, it can allow a transmission in NLOS situations (in the case of an obstruction by a person for example) by taking benefits of strong multipaths. The reflection coefficient Γ on a plane interface can be expressed at normal incidence by [34]:

$$\Gamma = \frac{\eta_2 - \eta_1}{\eta_2 + \eta_1} \tag{2.6}$$

Material	**Absorbtion [dB/cm]**	**Reflection $\|\Gamma\|^2$ at normal incident [dB]**		**Transmission $\|T\|^2$ at normal incident [dB]**	
		Linear	**[dB]**	**Linear**	**[dB]**
Concrete	6.64	0.18	-7.43	0.81	-0.86
Glass	6.03	0.15	-8.08	0.84	-0.73
Plasterboard	1.50	0.06	-11.94	0.93	-0.28
Wood	4.18	0.01	-18.81	0.98	-0.05
Body	181	0.37	-4.23	0.62	-2.05

Table 2.2: Classical material's absorption, reflection and trasnmission.

where η_1 and η_2 are the intrinsic impedance of the fisrt and second medium respectively, as shown in Figure 2.2. In our case, we have: $\eta_1 = \eta_0 = \sqrt{\frac{\mu_0}{\epsilon_0}}$ for the air (with μ_0 the free space permeability and ϵ_0 the free space permittivity) and $\eta_2 = \sqrt{\frac{\mu_0}{\epsilon_0 \epsilon_r}}$ for non magnetic materials under consideration whose relative permittivity is ϵ_r (i.e. walls, body...). The power transmission coefficient is then given by:

$$|T|^2 = 1 + |\Gamma|^2 \tag{2.7}$$

Power reflection coefficient $|\Gamma|^2$ and power transmission coefficient $|T|^2$ have been calculated for different materials whose properties are reported in Table 2.1 and are given in Table 2.2. It can be observed that wood exhibits low reflection and high transmission. However, because of its quite severe absorption ($4.18 dB/cm$), 60 GHz signal will not likely be transmitted through it. The human body and concrete exhibit highest reflection.

Simply considering reflection at normal incidence shows that NLOS situations are going to be experienced quite often at 60 GHz. To give an even more realistic overview of the reflections that EM waves will undergo, reflection coefficients are now calculated for oblique incidences. In this case, one have to define polarizations for incident waves, namely Transverse Electric (TE) polarization (horizontal) and Transverse Magnetic (TM) polarization (vertical). Orientation of electric and magnetic fields for both polarizations can be seen in Figure 2.2 and Figure 2.3 respectively.

For TE and TM modes, reflection coefficient can be expressed using the lossy media Snell's law:

$$\Gamma_{TE} = \frac{\eta_2 cos(\theta_i) - \eta_1 cos(\theta_t)}{\eta_2 cos(\theta_i) + \eta_1 cos(\theta_t)} \tag{2.8}$$

$$\Gamma_{TM} = \frac{-\eta_1 cos(\theta_i) + \eta_2 cos(\theta_t)}{\eta_1 cos(\theta_i) + \eta_2 cos(\theta_t)} \tag{2.9}$$

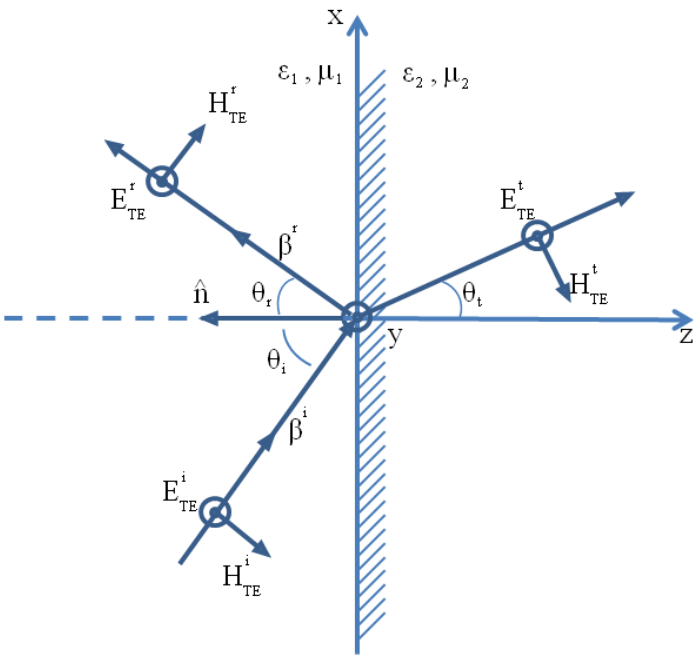

Figure 2.2: TE mode.

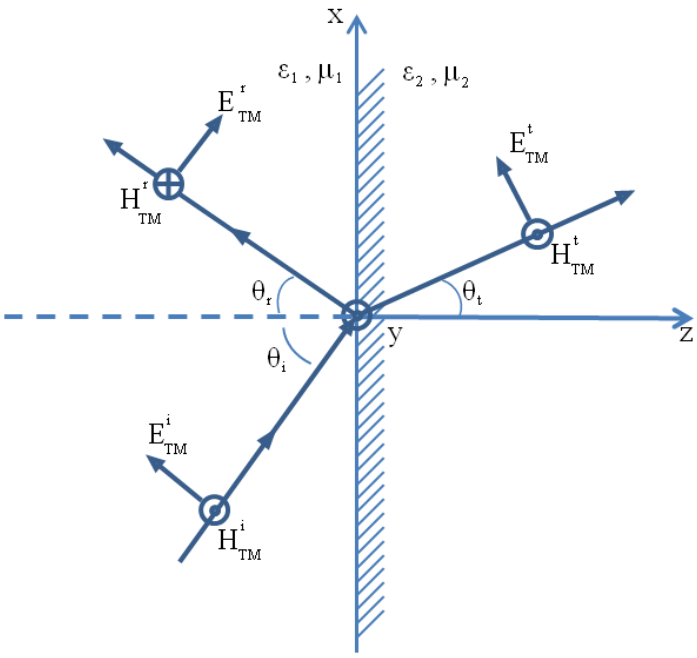

Figure 2.3: TM mode.

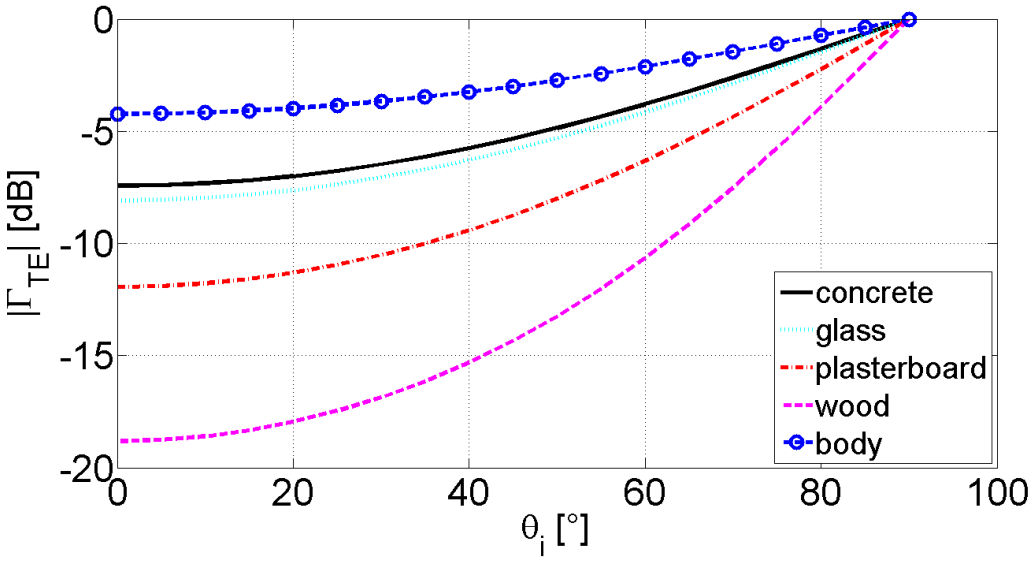

Figure 2.4: Reflection of TE.

where θ_i is the incident angle of the incoming wave and θ_t the reflection angle of the transmitted wave, as seen in Figure 2.2 and Figure 2.3. From the Snell's law of refraction, we know that:

$$sin(\theta_t) = \frac{k_1}{k_2} sin(\theta_i) \tag{2.10}$$

where $k_1 = k_0$ is the propagation constant in the air and k_2 in the material. This last equation can also be written as:

$$cos(\theta_t) = \sqrt{1 - \frac{k_1^2}{k_2^2} sin^2(\theta_i)} \tag{2.11}$$

and thus Γ_{TE} and Γ_{TM} can be calculated. Power reflection coefficient results are shown in Figure 2.4 and Figure 2.5, for TE and TM polarizations respectively.

It is worth noticing that the normal incidence case is not a singularity and that for higher conductivity materials, the reflection is pretty large. Except for wood, large amount of power is reflected and thereby not transmitted through considered materials. In TM polarization however, there existes an angle about which waves are penetrating materials. But even at this angle, there is few chance that a signal can be transmitted from one room to another. Indeed, transmitted waves will undergo propagation losses through the wall that are quite sever (see Table 2.2).

Furthermore, in our approach, we did consider only one air-wall interface whereas a second wall-air interface exists on the opposite side of the wall, thereby introducing even

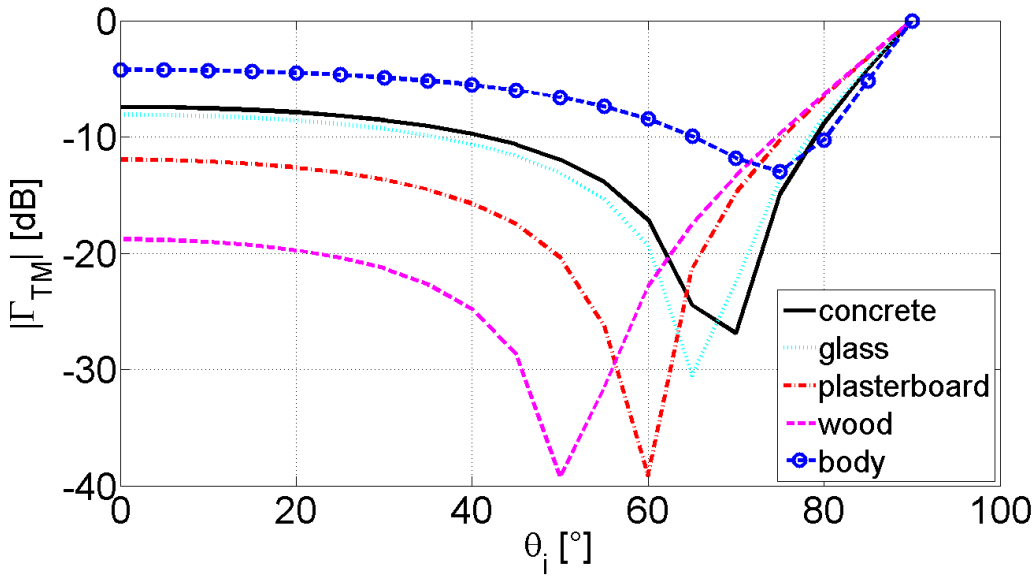

Figure 2.5: Reflection of TM mode.

more reflection and also possibility that some of the power remains contained within the wall itself (like in Fabry-Perot cavity for instance).

In conclusion, we have shown the great influence of obstacle's reflections at 60 GHz. Although this forbids between-rooms-communication, walls, ceiling and floor high reflectivity can be used by a wireless link in order to "bypass" an obstacle such as a person thanks to a strong NLOS multipath.

2.2.2 Technological aspects

Since the release of 60 GHz unlicensed bandwidth by the FCC and worldwide efforts to provide and develop standards and specifications in order to use this bandwidth for various applications, progress has been made concerning the design and realization of integrated 60 GHz circuits and radio systems. Progress in the areas of antennas design and integration, circuit components shuch as power amplifiers (PAs), low noise amplifiers (LNAs), voltage controlled oscillators (VCOs), mixers and analog to digital converters (ADCs), millimeter-wave channel characterization and beamforming techniques, makes the use of this bandwidth possible.

2.2.2.1 Integrated circuit technology and RF 60 GHz components

A demand for high-speed wireless connections and recent progress in silicon-based technologies have driven the development of wireless local area networks (WLANs) standards

operating at 60 GHz such as WiGig [14, 36]. Such applications require a low-cost and low-power implementation, which leads to implement system-on-chip for the transceivers and use of advanced CMOS nodes.

The choice of integrated circuit (IC) technology depends on:

- Implementation aspects:
  Issues such as power consumption, efficiency, dynamic range, linearity requirements are among implementation aspects.
- System requirements:
  Issues such as transmission data rate, modulation scheme, cost and size, transmit power, bandwidth are related to system requirements.

At mm-wave, there are three competing IC technologies:

- Gallium Arsenide (GaAs) and Indium Phosphide (InP) technology:
  GaAs technology offers low noise, fast and high gain implementation but suffers from poor integration and expensive implementation.
- Silicon Germanium (SiGe) technology such as Heterojunction Bipolar Transistor (HBT) and Bipolar junction transistor and CMOS (BiCMOS):
  SiGe technology allows low noise, fast and high gain implementation and is a cheaper alternative to the GaAs.
- Silicon technology such as CMOS and BiCMOS:
  CMOS technology performance is not remarkable considering gain and noise and linearity but it provides cheaper product with a high degree of integration [2].

None of these technologies can meet all the implementation challenges and system requirements mentioned above at the same time. However, it should be considered that the size and cost are the key factors regarding mass deployment and market exploitation. Considering this point of view, CMOS technology is the leading candidate among the others. Recent progress make it possible to obtain thinner CMOS technology such as 28 nm compare to 130 nm in past years [36, 37].

The 5 mm wavelength of 60 GHz allows integration of analog and microwave components and obtaining monolithic microwave integrated circuits (MMICs) onto a single chip or package. CMOS processes have also reached transition frequencies of hundreds of gigahertz [38]. Hence, the performance of 60 GHz system is improved by using multi-chip solutions and mixed signal equalization [39, 40].

In next sections, considering wireless radio systems, the most important RF components such as LNA, PA, mixer and oscillator are explored in more details.

Low Noise Amplifier (LNA)

Performance of 60 GHz radio systems depends significantly on low-noise figure and

Frequency (GHz)	**3 dB BW (GHz)**	**Gain (dB)**	**NF (dB)**	**CMOS technology (nm)**
60	12.5	11.4	3.88 (at 55.5 GHz)	90
60	12	8	4.5 (at 60 GHz)	65
60	14.1	20.6	4.9 (at 58 GHz)	65
64	8	15.5	6.5 (at 64 GHz)	90

Table 2.3: Examples of features of 60 GHz band LNA using CMOS technology.

high gain and linearity at the receiver which is related to RF LNAs. Considering semiconductor process, voltage, and temperature variations, LNA should be designed to provide stable performance. This is more difficult in mm-wave systems due to the need for more stages to achieve needed gain, and greater variations in device parameters [39, 40]. As shown in Table 2.3, some examples in design of LNAs are illustrated regarding frequency, 3 dB bandwidth, gain, noise figure and CMOS technology [41].

Power Amplifier (PA)

The transmitter's PA is a key function to establish the link budget and the power requirements (and hence battery life) at 60 GHz communication systems. Reasonable linearity for the specific used modulation scheme, and adequate efficiency and output power for long battery life must be taken in consideration in a 60 GHz PA design. Achieving these characteristics is a challenging task due the large dynamic ranges required for certain modulation schemes such as orthogonal frequency division multiplexing (OFDM) to the low-voltage supplies of modern CMOS.

According to the standards, 60 GHz devices are considering both OFDM and single-carrier frequency domain equalization (SC-FDE) modulation. The linearity requirements for PA are due to the peak-to-average power (PAPR) ratio of the particular chosen modulation. Smaller PAPR in single carrier modulation implies a less linear PA. Using Doherty architecture, envelope tracking, self biasing (which also can improve device lifetime), and power combining are among the solutions proposed in literature to improve the linearity requirements of a PA [42, 43, 44, 45]. As shown in Table 2.4, some examples of PA designs are illustrated regarding technology, gain, saturation power, 1dB compression point and power-added efficiency [36].

Mixer

Mixers are used to up-convert or down-convert the base-band signals in radio transceivers, respectively in Tx and Rx. They may be active or passive. Active mixers modulate transconductance which provides a conversion gain through transistors that serve as amplifying elements while passive mixers modulate a switch resistance and re-

Gain (dB)	P_{sat} **(dBm)**	OCP_{1dB} **(dBm)**	**Peak PAE %**	**CMOS technology (nm)**
15.3	12.5	14.8	12	28
24.5	16.5	8	11.7	28
10	12.5	20.6	-	32
21.2	17.4	15.5	14	40
22	10.5	15.5	10.2	40

Table 2.4: Examples of 60 GHz PA features using CMOS technology.

RF freq (GHz)	**IF freq (GHz)**	**CG (dB)**	**RF BW (GHz)**	**CMOS technology (nm)**
57-66	10-14	14	> 9	65
58-66	4	5	8	120
58.3-62.5	0-3	-4.1	6	65
57.1-63.3	0.1	4.5	6.2	90
59-65	0.1	4	6	130

Table 2.5: Examples of 60 GHz mixer using CMOS technology.

sult in conversion losses by using diodes or non amplifying transistors as simple switches. At 60 GHz, passive mixers are easier to implement compared to active mixers. Passive mixers have lower power consumption and higher linear performance [46, 47, 48]. In Table 2.5, some examples of designs of mixers are illustrated regarding different important parameters [49].

Oscillator

One of the fundamental building block of most wireless systems is the VCO which provides stable frequency sources for Tx and Rx. In order to cover the entire bandwidth available about 60 GHz, very large absolute and relative tuning ranges should be considered in the design phase [50]. At 60 GHz transistors operate closer to the maximum frequency of oscillation in CMOS which results in lower LO power [46]. As shown in Table 2.6, some examples in VCO designs are illustrated regarding different main parameters [51].

Regarding all the progress in technological aspects mentioned above, in Table 2.7, some recent fabricated 60 GHz transceivers, are presented [52].

f_{min} (GHz)	f_{max} (GHz)	TR $[GHz]/[\%]$	Num of VCOs	PN@1MHz $[dBc]/[Hz]$	Supply [V]	Power [mW]	FoM [dBc]	FoM_T [dBc]	Area $[mm^2]$	CMOS tech (nm)
48.8	62.3	13.5/24.3	1	-96	1.2	30.0	176	184	0.11	65
54.0	61.0	7.0/12.2	1	-85	1.2	14.9	170	172	0.25	65
57.1	66.1	9.0/14.6	2	-75	1.1	26.5	157	160	0.018	45
63.0	81.0	16.0/22.2	2	-89	1.1	21.0	178	184	0.013	40
56.0	60.4	4.4/7.4	1	-97	1.0	22.0	179	176	0.075	65
43.7	51.7	8.0/16.8	1	-85	1.0	32.0	166	170	-	90
3.2	7.3	4.1/69	1	-114	1.2	20.0	177	193	0.27	65

Table 2.6: Examples of 60 GHz VCO using CMOS technology.

2.2.2.2 Antenna

Many criteria should be considered for antenna designing at 60 GHz. Requirements of being low cost, small in size, light in weight, and high gain should be considered. Furthermore, 60 GHz antennas require an almost constant gain and high efficiency over a 5 GHz bandwidth. Integrating and combining antennas directly on chip is another issue to be taken into consideration. Using on-chip antennas offers the possibility of removal all connections between RF circuits and the antenna, which leads to obtain cost reduction and flexibility in circuit design [53, 54, 55].

To reach a similar gain with in-package antenna gains, on-chip antennas should benefit from techniques like electromagnetic band-gap structures, frequency selective surfaces, and meta-materials [56, 57]. To overcome the lossy ground of on-chip antenna, rhombic antenna can be utilized. For arrays, smaller antennas, such as the dipole and Yagi are suggested [58]. For long-range WPAN applications (more than 10 m) and also for outdoor mm-wave backhaul and future cellular systems, high directive antenna arrays should be used [59].

In addition, phased antenna arrays or high gain steerable antenna array that can be integrated into the RF front-end electronics are required to deal with the multi-path effects specially in NLOS scenarios. In switched beam arrays, the main beam selects one of a set of predefined orientation and are well-suited to mitigate some 60 Ghz challenges like: interconnect effects, low-output-power amplifiers, and high-noise-figure components [60, 61].

TX Data Rate	TX EVM	TX Power	RX gain	RX BB bandwidth	RX NF	RX input power	RX Error Rate
3.8 Gb/s (OFDM-16QAM)	-20.7 dB	> 16 dBm	N/A	0.85 GHz	4.5-5.5 dB (stand-alone LNA)	N/A	N/A
2 Gb/s (OFDM-QPSK)	N/A	6 dBm	35 dB	N/A	14 dB	N/A	N/A
7 Gb/s (16QAM)	< -17 dB (TX-RX)	10.2 dBm (P_{1dB})	30 dB	0.95 GHz	5.5 dB	-45 dBm	N/A
2.5 Gb/s (π/2-QPSK)	-22 dB	8.5 dBm	N/A	N/A	7.1 dB	-78 dBm	N/A
2 Gb/s (QPSK)	N/A	10-12 dBm (P_{1dB})	38-40 dB	N/A	5-6.7 dB	N/A	N/A
4 Gb/s (16QAM)	-20.2 dB (TX-RX)	5.3 dBm (P_{1dB})	42 dB	1.9 GHz	5.5-7 dB	N/A	N/A
5 Gb/s (QPSK)	-21.9 dB	6.4 dBm	54 dB	2.5 GHz	6.1 dB (59.5 GHz)	-52 dBm	$< 8^{-7}$ (5 Gb/s)

Table 2.7: Comparison of recent fabricated 60 GHz transceivers.

Phase arrays that sweep continuously the main beam are more expensive but, compare to switched beam arrays, have the advantage of being more powerful and flexible.

2.2.3 Modulation schemes and MAC protocols

For 60 GHz radio, the choice of modulation scheme relies on:

- the propagation channel
- the use of high gain antenna/antenna array
- the limitations imposed by the RF technology [39-46]

It should be noticed that, although simple modulation schemes such as single carrier (SC) can be used to meet some hardware constraints, they exhibit significantly less spectral efficiency. Hence, to find a robust and permanent solution, these simpler modulation techniques are not the best choice. For frequency selective channels with high multi-path effects, an OFDM is a better choice since it can mitigate the multi-path effects by providing flat fading smaller bandwidths. It is done by dividing the high-rate stream into a set of parallel lower rate sub-streams. Furthermore, using OFDM decreases the complexity of the system for multi-giga-bits systems by simplifying the equalization process. OFDM is also well suited at 60 GHz regarding its ability to decrease ISI (Inter Symbol Interference) effects. But it is sensible to phase noise from inter subcarrier interference (ICI) and requires large PAPRs.

SC provides lower PAPR, less sensitivity to phase noise and is not transmitted in the frequency domain. Furthermore, SC is cheaper because of requiring lower resolution in analog-to-digital converters.

OFDM may still provide better overall performance in highly frequency selective channels and, continuous phase modulation strategies have also been considered to mitigate the nonlinearity of power amplifiers (using cyclic prefix, pilot training structure) [62, 63].

In Table.2.8 the modulation schemes for IEEE 802.11.ad standard are illustrated.

Control (CPHY)		
Coding	Modulation	Raw Bit Rate
Shortened 3/4 LDPC, 32x Spreading	π/2-DBPSK	27.5 Mbps
Single Carrier (SCPHY)		
Coding	Modulation	Raw Bit Rate
1/2 LDPC, 2x repetition 1/2 LDPC, 5/8 LDPC 3/4 LDPC 13/16 LDPC	π/2-BPSK, π/2-QPSK, π/2-16QAM	385 Mbps to 4620 Mbps
Orthogonal Frequency Division Multiplex (OFDMPHY)		
Coding	Modulation	Raw Bit Rate
1/2 LDPC, 5/8 LDPC 3/4 LDPC 13/16 LDPC	OFDM-SQPSK OFDM-QPSK (DCM) OFDM-16QAM OFDM-64QAM	693 Mbps to 6756.75 Mbps
Low-Power Single Carrier (LPSCPHY)		
Coding	Modulation	Raw Bit Rate
RS(224,208) + Block Code(16/12/9/8,8)	π/2-BPSK, π/2-QPSK	625.6 Mbps to 2503 Mbps

Table 2.8: Modulation schemes for IEEE 802.11.ad.

2.2.4 Standards

After the establishment of an unlicensed band at 60 GHz by US Federal Communications Commission (FCC), different frequency allocations and standards have been considered for this bandwidth by other regulatory organizations around the word. Currently, there are many standardization and commercialization efforts underway for 60 GHz networks by different engineering organizations. IEEE 802.15.3c, WirelessHD, IEEE 802.11ad, the WiGig standard, and ECMA 387 are among current standards which target 60 Ghz systems [5, 6, 64, 65]. In next sections, the progress of these standardization efforts are explored in details.

2.2.4.1 WirelessHD standards

In April 2006, the WirelessHD Consortium was founded to develop the WirelessHD standard in order to create wireless video area networks (WVANs). The consortium was founded by SiBEAM Inc, a spin of company from University of California, in collaboration with many other companies such as Mediateck, Intel, Samsung Electronics, Co., Ltd, Sony Corporation. WVANs were supposed to stream either compressed or uncompressed high quality audio and video for products shuch as computer and portable devices. Thus, the WirelessHD specification defines a system for short-range high data rate 60 GHz ad-hoc wireless communication networks dedicated to high-definition multimedia data [5].

The WirelessHD specification defines a physical layer capable of short range (10 m) communications with high speed data rates up to 7.139 Gbps. The frequency band used in this standard is between 57 GHz and 64 GHz (2.5 GHz bandwidth for each channel). It should be mentioned that, by using a 4*4 MIMO system benefiting from spatial multiplexing, four times of the later data rate (28.552 Gbps) can be obtained. Three different physical layer are considered for the ad-hoc network: Low Rate PHY (LRP), Medium Rate PHY (MRP) or High Rate PHY (HRP). LRP uses OFDM with BPSK modulation and offers a maximum datarate of 40 Mbps while HRP uses QPSK, 16 QAM and 64 QAM modulations and offers a a maximum datarate of 7 Gbps. Time Division Multiple access (TDMA) modulation piloted by protocol layer is defined for all these three physical layers which share a common frequency channel. The data is transmitted using OFDM modulation with a preamble dedicated for synchronization. For NLOS operation, beam-steering is used in all physical layers. Beam-steering in radio systems is accomplished by altering the RF signals' relative phases or by switching the antenna elements [5, 6].

The WirelessHD Consortium is actively promoting WirelessHD technology, but recently there is a general shift of focus in the industry towards IEEE 802.11ad.

2.2.4.2 IEEE 802.15.3c-2009 standard

Standards for Wireless Personal Area Networks (WPAN) is developed by IEEE 802.15 working group. Among the IEEE 802.15 standards family, IEEE 802.15.3c-2009 standard is developed in 2009 for millimeter-wave-based high data rate (more than 20 Mbps) WPANS. IEEE 802.15.3c-2009 shares many similarities with the WirelessHD standard and defines an alternative physical layer (PHY) and medium access layer (MAC) specification. It supports data rates about 5 Gb/s and includes three distinct PHYs [5, 6, 65]:

- Single carrier (SC) mode:
  Using PSK/QAM modulation, SC mode is tasked to trade reduced peak data rates for improved peak/average power ratios. The SC mode is thus considered to be a

better fit for low power and complexity systems which typically participates in a PAN (phones, MP3 players etc.).

- High speed interface (HSI) mode:
  Using OFDM for low latency bidirectional data transfer, HSI mode can be used for applications requiring high speed communication.
- Audio/visual (AV) mode:
  For multi-path environment, the OFDM-based AV mode performs better and so can offer greater range than SC-based modes, albeit at the expense of power consumption. It is used for uncompressed HD audio and video streaming. In this specification, the AV mode is exactly the same as the HRP PHY in WirelessHD although the MAC layer is different between the two specifications.

It should be mentioned that by using beamforming techniques it is possible to increase the range of communication. No commercially available equipment employs this standard yet.

2.2.4.3 ECMA 387

ECMA International is an association for the purpose of preparing and developing standards related the fields of ICT and electronics. The ECMA 387 standard defines specifications to facilitate bulk and streaming data transfer for three device types:

- High-end video/audio streaming devices:
  For communication up to 10 meters considering both LOS or NLOS links.
- Economical data/video devices:
  For communication up to 3 meters, considering only the LOS operation.
- Very inexpensive data-only devices:
  For a 1-m range LOS communication operation.

Four frequency channels are defiend in this standard, each with a bandwidth of 2.16 GHz and a symbol rate of 1.78 Gs/s [66]. The goal is to support bit rates up to 10 Gb/s. In the case which higher data rates are required, the possibility of channel aggregation is also predicted in ECMA 387 specifications. Also, the possibility of using the 60 GHz wireless device as an intermediate network node between source and sink is taken into consideration in the standard to provide a structure adapted to high definition media interface protocol adaptation layer (HDMI PA). No commercially available equipment employs this standard yet.

2.2.4.4 WiGig and IEEE 802.11ad

In April 2009, the Wireless Gigabit Alliance (WGA) was founded to define specifications for transmission of data, audio and video in the millimeter-wave frequency band considering both LOS and NLOS environments. The WiGig alliance has cooperated closely with the IEEE 802.11ad technical group which develops standards for Wireless Local Area Networks (WLAN). The two groups merged into a single standard. In December 2012, the Wi-Fi Alliance and WGA planed to consolidate activity in Wi-Fi Alliance. The final standard is part of the emerging array of 4G cellular technologies, and support short-range (1m - 10m) 60 GHz wireless communication of data over an ad-hoc network at data rates up to 6.75 Gbps. It also supports switching between the 2.4 GHz, 5 GHz and 60 GHz bands. Provisions for beam steering are also included, in order to deal with 60 GHz propagations path loss [5, 6, 67]. Other protocol adaptations will be conducted by Wi-Fi Alliance in collaboration with other organizations such as VESA, PCI-SIG and USB-IF.

The IEEE 802.11ad-2012 DMG PHY supports three distinct modulation methods:

- Spread-spectrum modulation
- Single carrier (SC) modulation for low power
- Orthogonal Frequency Division Multiplex (OFDM) modulation (the OFDM PHY)

Although, OFDM modulation has a large peak to average power ratio (PAPR) compared to single-carrier modulation, it has a great advantage regarding energy per bit and is robust to multi-path environment. These two factors are really important considering the throughput. As mentioned in last chapter, in this research work, highdata rate communication are investigated, thus, the OFDM PHY of IEEE 802.11ad-2012 is more relevant to our work. The OFDM considered in this standard is based on a 512-point FFT (Fast Fourier Transform) with 336 data carriers, and 16 fixed pilot tones. The individual OFDM carrier modulation may be SQPSK, QPSK, 16 QAM or 64 QAM. The cyclic prefix is fixed at 25 percent of the symbol period. With the support of WiFi alliance, IEEE 802.11ad is currently the most noticed standard regarding companies which product devices in 60 GHz unlicensed band. Thus, in this research work the theory, simulation and measurements are done considering the main characteristics of this standard (regarding the bandwidth and modulation) [5, 6, 67].

Currently, it seems that IEEE 802.11ad will become the most widely deployed 60 GHz technology. In spite of being pioneer of the commercialization of 60 GHz band, WirelessHD technology, may let its place to IEEE 802.11ad. Nevertheless, WirelessHD technology may endure in some high-performance niche applications.

In Table.2.9 these mentioned standards for 60 GHz communications are compared to each other regarding bandwidth, data rate, and range.

Standard	**Bandwidth (GHz)**	**Data rate (Gbps)**	**Range (m)**	**Features**
WirelessHD	57-64 (2.5)	7.138-28.552	10	Beamforming, MIMO
IEEE 802.15.3	57-64 (2.5)	7.138-28.552	10	Beamforming, MIMO
ECMA 387	57-66 (4*2.16)	6.35	10	-
IEEE 802.11.ad	2.4, 5, 60 (2.16)	6.75	10	Beamforming, MIMO, Tri band

Table 2.9: Comparison of standards of wireless communication.

2.2.5 Conclusion

In order to provide the requirements of recent and also future high data rate applications, 60 GHz wireless networks must deliver, with high energy efficiency and reliability at a low cost, Gb/s data rates. Several ongoing challenges, including channel consideration, design of low cost on-chip antennas and arrays, high-performance RF components in CMOS technology, choosing the efficient modulation techniques and well suited MAC protocols that are suitable for frequency selective channel at 60 Ghz were surveyed. Thanks to the recent progresses in each criteria mentioned above and development of different standards and efforts to commercialize 60 GHz products, nowadays it is possible to expect using 60 GHz technology in tremendous variety of indoor and outdoor applications. In next section, techniques and metrics of localization for wide-band wireless indoor networks are presented.

2.3 Indoor positioning methods

Wireless indoor positioning systems have become very popular in recent years and have been used in applications such as asset tracking, self-organizing sensor network and location sensitive billing. There exist mainly three typical location estimations: triangulation, scene analysis and proximity. In this section, different existing methods of localization considering important performance characteristics like accuracy, complexity and cost are compared. The process of determining a location may be called location sensing, geolocation, position location, or radio-location, if it uses wireless technologies. Different applications require different types of location positioning algorithm, i.e. the method of determining location, making use of various types of metrics such as Time Of Arrival (TOA), Angle Of Arrival (AOA) and Received Signal Strength (RSS). In addition

there are different types of location positioning systems regarding their physical layer and infrastructure. There are four different topologies systems:

- Remote positioning system (mobile signal transmitter, several fixed measuring units, master station).
- Self-positioning (mobile measuring units, several transmitters in known locations).
- Indirect remote positionig.
  In this case a wireless data link is provided and sends measurement results from a self-positioning measuring reference to the remote side.
- Indirect self-positioning.
  In this case, a remote positioning side sends measurement results to a mobile reference via a wireless data link.

Depending on the type of measurements available, computing inverse problem, i.e. finding the location from the measured data, is usually done by triangulation using two different techniques:

- Angulation.
  Angulation locates an object by computing angles relative to multiple reference points. Angle of arrival (AOA) method is in this category.
- Lateration.
  Lateration estimates the position of an object by measuring its distances from multiple reference points. So, it is also called range measurement technique. RSS, TOA and Time Difference Of Arrival (TDOA) are in this category [68, 69, 70].

In next parts, both measurements based on angle and distance are explored in details.

2.3.1 Angle related measurements

Angle Of Arrival measurements can be divided in two main categories:

2.3.1.1 Method utilizing receiver antenna's amplitude response

This category is based on the reception pattern of an antenna. Practically, the beam of the receiver antenna is rotated and the direction of the transmitter corresponds to the maximum obtained signal strength. A typical beam of antenna is presented in Figure 2.6. If the transmitted signal is not stable in terms of power, then a non rotating antenna or at least two stationary antennas with known anisotropic antenna patterns should be added to the system in order to calibrate out the variations regarding the transmitter signal power variation. In this way, the receiver is able to differentiate the signal strength variation caused by the anisotropy in the reception pattern from transmitter signal vari-

ations [71, 72]. Such techniques are used in marine radio navigation, avalanche rescue, wildlife tracking.

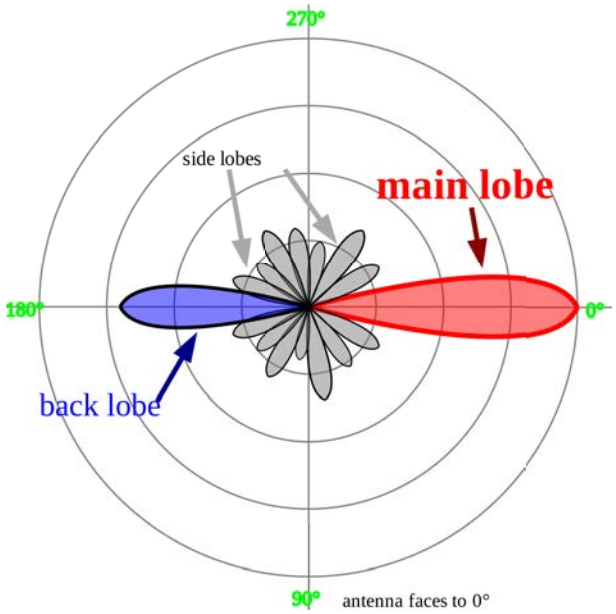

Figure 2.6: Antenna beam.

2.3.1.2 Method utilizing receiver antenna's phase response

This category of measurement techniques, which is also known as phase interferometry [73], benefits from phase differences in the arrival of a wave front. This method requires an antenna array or a large receiver antenna in each reference device (RD) and determines the direction of arrival of the signal by calculating the difference in received phases between each antenna of the array. As shown in Figure 2.7, an N elements antenna array with a uniform distance d separation can be used to calculate the bearing of the transmitter. Considering the hypothesis in which the distance between a transmitter and an antenna array is much larger than d, then the distance between two array elements can be calculated approximately by:

$$R_i = R_0 - idcos\theta \tag{2.12}$$

Where R_0 and R_i are respectively the distances between the 0^{th} and i^{th} antenna elements and the transmitter, d is distance between two adjacent antenna elements, and θ is the bearing of the transmitter with respect to the antenna array. Then the phase difference ϕ of adjacent antenna elements leads to obtain θ according to $\phi = 2\pi\frac{dcos\theta}{\lambda}$. For high SNR (signal-to-noise-ratio), this method offers an accurate positioning systems but is very sensitive to multi-path affected environments and does not have good performance since

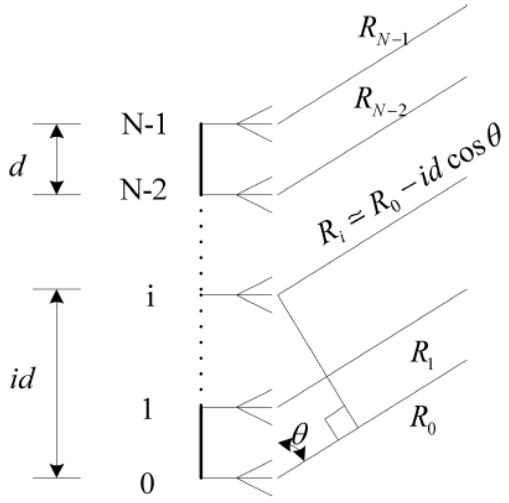

Figure 2.7: Antenna array.

accuracy of AOA measurements relies on shadowing and antennas directivity [73]. In the case that multi-paths affect the accuracy, using maximum likelihood (ML) algorithms is a solution to reduce errors but requires rigorous stochastic calculations and hence increases the complexity of the system [74, 75, 76, 77]. Another solution for AOA measurement methods is based on subspace-based algorithms. High resolution methods like MUSIC (multiple signal classification) and ESPRIT (estimation of signal parameters by rotational invariance techniques) are among these algorithms [71].

2.3.2 Distance related measurements

2.3.2.1 Received Signal Strength (RSS) measurements

This method uses the signal strength at a receiver to estimates the distances between RD and MD [78, 79]. If the transmitted power, P_t, is a priori known, then knowing the RSS leads to the distance d between RD and MD, using the Friis equation:

$$RSS(d) = \frac{P_t G_t G_R \lambda^2}{(4\pi)^2 d^2} \tag{2.13}$$

where, G_t and G_R are respectively the gains of transmitter and receiver antennas and λ is the wavelength. The advantage of this technique is the fact that they do not require synchronization and any additional hardware, and do not increase the power consumption and cost. There is a relation between distance and received power, as developed in Friis equation. However, environmental factors, already briefly presented in section 2.1.1, such as reflection, diffraction and scattering should be also considered in a realistic approach.

Based on empirical evidence, random and log-normally distributed random variable with a distance-dependent mean value can model these effects as defined in [80, 81]. Then distance estimation can be done by using ML approaches. Consequently, this technique remains highly environment-dependent and its accuracy is directly related to a priori knowledge of the propagation channel.

2.3.2.2 Time Of Arrival (TOA) measurements

The distance from the MD to the RD is directly proportional to the propagation time. Distances between neighboring sensors can be estimated from these propagation time measurements. TOA-based systems uses this fact to localize the MD. As shown in Figure 2.8, in order to perform 2-D positioning, TOA measurements have to be made with respect to signals from at least three RD.

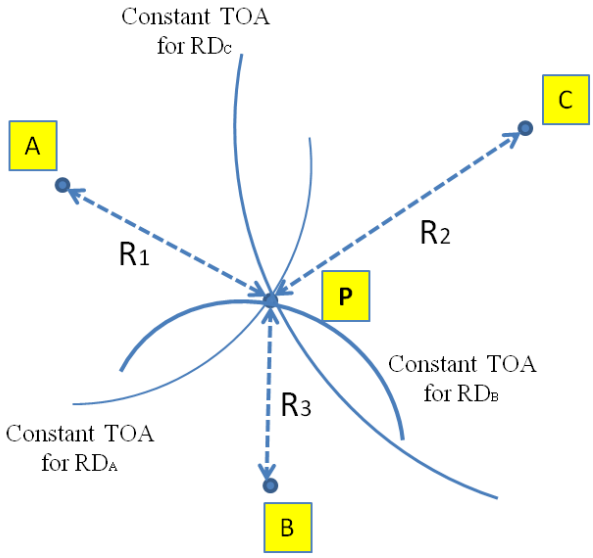

Figure 2.8: TOA positioning method.

One-way propagation time and round-trip propagation time measurements are among TOA measurements. The difference between the sending and receiving time in Tx and Rx are measured in one way propagation time method. This method requires a precise synchronization between Rx and Tx which is a costly task. Generalized cross-correlation method is mostly used to obtain the time delay [71, 82, 83, 84].

In order to avoid this latter fact, round-trip propagation time measurement is proposed which uses two way ranging (TWR) [85, 86]. In round-trip propagation time measurements, the difference between the time when a signal is sent by an RD and the time when the signal returned by the MD is received at the original RD, is measured. The same clock is used to compute the roundtrip propagation time, thus there is no synchronization

problem. In this case, the major error source is the delay required for handling the signal in the MD. This internal delay could be either known via a calibration, or measured and sent to the RD to be subtracted.

Another way to avoid synchronization problem is to use both RF and ultrasound hardwares [87], benefiting from much smaller speed of sound compare to the speed of light (RF). Use of ultra wide band (UWB) signals is also suggested for time measurements methods to obtain accurate distance estimation [88, 89]. Because of the large bandwidth offered by UWB, its pulse has short duration which leads to achieve a good time resolution.

2.3.2.3 Time Difference of Arrival (TDOA) measurements

The idea of TDOA is to determine the relative position of the mobile receiver by examining the difference in time at which the signal arrives at it from multiple measuring units. As presented in Figure 2.9, multiple reference devices transmit signals to the receiver (mobile device) and the relative position of MD is determined by estimating the TDOA, from which the loci of a constant range difference between two RD (i.e. a hyperbola curve), is obtained.

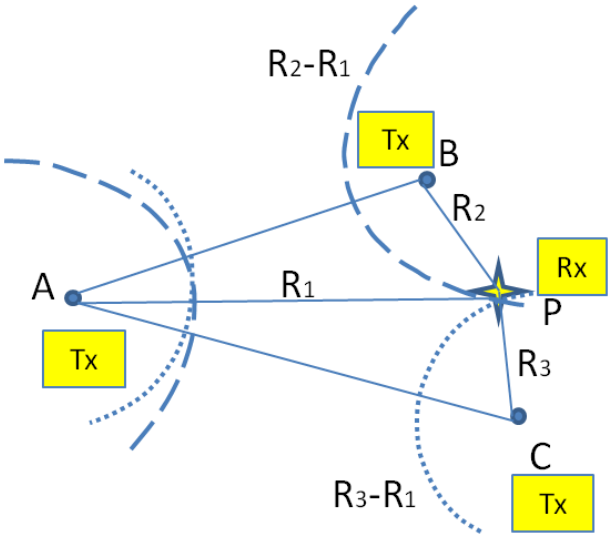

Figure 2.9: TDOA positioning method using hyperbolic system.

For each TDOA measurement, the transmitter lies on a hyperboloid with a constant range difference between the two measuring units. The equation of the hyperboloid is given by:

$$R_{i,j} = \sqrt{(x_i - x)^2 + (y_i - y)^2 + (z_i - z)^2} - \sqrt{(x_j - x)^2 + (y_j - y)^2 + (z_j - z)^2} \quad (2.14)$$

where (x_i, y_i, z_i) and (x_j, y_j, z_j) represent the fixed transmitter i and j, and (x, y, z) represent the coordinates of the target. A 2-D target location can be estimated from the

Solution	**Year**	**Principle**	**Application**	**Accuracy**
Sappire Dart	2010	TDOA	Indoor applications	< 30 cm
Segura	2010	TDOA	Mobile robot	20 cm
Ubisense	2011	TDOA, AOA	Automation	< 15 cm
Zebra	2011	TDOA	Logistics	< 30 cm

Table 2.10: Examples of commercially available TDOA solutions.

intersections of two (or more) TDOA measurements, as shown in Figure 2.9. Two hyperbolas are formed from TDOA measurements at three fixed measuring units (A, B, and C) to provide an intersection point, which locates the target P.

TDOA can also be estimated from the cross correlation between the signals received at a pair of measuring units. Frequency domain processing techniques are usually used to calculate τ (TDOA) [71, 73, 90, 91, 92, 93, 94].

TDOA method requires that the measuring units share a precise time reference and reference signals, but does not impose any requirement on the mobile target. Thus the complexity is within the infrastructure and not within the mobile device.

Table 2.10 exhibit TDOA-based commercial solutions' performance, pointing out that TDOA metric could be well suited for precise indoor applications.

2.3.3 Conclusion

To choose a proper positioning method for a specific application, one should notice that the prerequisite information has to be known. For example, in indoor UWB systems, reference devices have a defined position but prior information about mobile device is not available and in many cases, there is no synchronization between RDs and MD. These facts impose the choice of positioning method which are relative time methods, such as TDOA and AOA. It should be noticed that using TDOA and AOA methods simultaneously can improve the accuracy of positioning.

In addition, in this section, different methods of localization are explored: it is mentioned that AOA method offers high accuracy for high SNR at the expense of high complexity, cost and power consumption. Furthermore, it is sensible to multi-path environments. RSS is too sensitive to the environment and thereby does not offer a good accuracy. TOA exhibits a good performance but suffers from synchronization problem between RDs and MD which makes it a costly choice. TDOA has a good accuracy but suffers from synchronization problem between RDs.

In this research work, a localization method is introduced for 60 GHz systems that is

based on TDOA determination because of its well suited advantages in wireless indoor applications [85, 86, 95, 96]. Due to the huge available bandwidth at 60 GHz, the proposed method uses just one RD, so does not require the synchronization of RDs. Therefore, not only this approach benefits from the advantages of TDOA, but also deals with the synchronization problem. All these features are explored in details in next chapter.

2.4 Conclusion

In this chapter, first the 60 GHz state of art is surveyed. It considers the requirements of recent and future high data rate applications, with a focus on technical aspects and standards. It is mentioned that for the HDR indoor application, the most recent and important standard to be considered is IEEE.802.11ad.

Then, in the second part localization methods well suited for indoor applications are explored with a focus on angle and distance related measurements. It is mentioned that among different metrics, TDOA methods offer a good accuracy and can be a good choice regarding high data rate indoor applications.

Thus in this research work, a TDOA-based localization method well suited for 60 GHz HDR systems will be introduced in next chapters. It will be shown that the new proposed method benefits from communication signals to locate the MD.

Chapter 3

New TDOA approach using communication signals

3.1 Introduction

To achieve a green radio communication, focalization of energy is one solution that can lead to decrease the consumption. In addition, different applications for indoor localization have been presented with a focus on TDOA localization techniques, described as an accurate and reasonable option for UWB systems. Therefore in this chapter, we study and propose a novel TDOA-based localization method well-suited to 60 GHz high data rate communication. This approach benefits from wide band interferometry techniques and can be applied on HDR communication based on the IEEE.802.11.ad. After a brief description of conventional TDOA estimations, we define our approach and establish the direct problem. To treat the inverse problem we explore two important features associated to HDR communication. The first is EVM (Error Magnitude Vector) based and the second is ECR (Equivalent Channel Response) based. We conclude this chapter by considering the channel impact, the influence of the TDOA estimation on the quality of communication, and by testing this method for one dimension localization.

3.2 TDOA metric

As presented in chapter 2, section 2.3, radio localization systems are mainly based on metrics (AOA, TOA, TDOA...) that are extracted from dedicated signals including narrow band, large band and impulse radio shapes. Such added dedicated signals in

an already complex high data communication system will undoubtedly increase energy consumption and cost. As we target green communication based on the capability to take benefit from spatial resources, we propose a novel TDOA based localization approach that reduces the complexity of the final connected system.

3.2.1 Conventional TDOA method

The two dimensions localization technique investigated in this research area, is based on the TDOA (Time difference of Arrival). As mentioned in section 2.3.2.3, in a conventional way, i.e a MISO-like (Multiple Input Single Output) configuration, the MD can retrieve its position by receiving a specific set of signals from at least 3 cooperative RD, and the couple of TDOA leading to MD self-localization is estimated by calculating successively the difference between τ_1 and τ_2, τ_2 and τ_3, and τ_1 and τ_3, as shown in Figure 3.1.

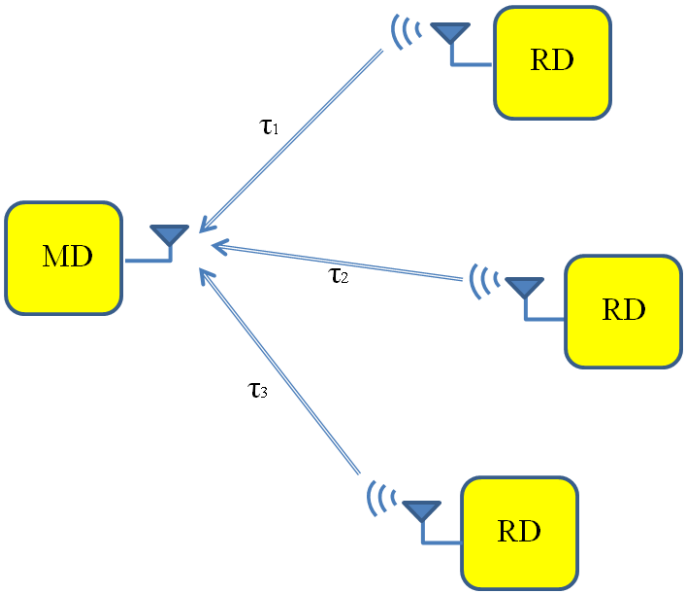

Figure 3.1: Conventional TDOA positioning method using a MISO-like configuration (RDs are reference devices and MD is a mobile device).

Typically the specific signal is an impulse radio one and although the synchronization of RD and mobile device MD is not always necessary in this technique, RDs are to be synchronized. For short range applications, this first constraint imposes a very fine synchronization and hence a high degree of complexity, which contributes to justify the novel solution we propose. The second constraint is linked to the shape of signals of interest. They are instantaneous bandwidths that are not always well suited for OFDM format usually used in modern HDR communication.

3.2.2 New TDOA method

To overcome this synchronization requirement, the RDs are supposed, in the proposed solution, very close to each-other (small baseline) and are driven by the same oscillator. Moreover, the proposed alternative solution is compliant with 60 GHz communication signals in order to avoid added complexity and hence consumption. Furthermore, it uses non instantaneous bandwidth and a single front-end. For sake of clarity, we only treat TDOA metric without performing in depth localization. However, some 1D localization results are presented in the last section of this chapter.

The principle is the same as presented in 3.2.1 but for determining one TDOA, one can use easily and depending on the targeted applications, either SIMO (Single Input Multiple Output) or MISO (Muliple Input Single Output) configuration. The two close antennas, separated by a baseline B, form a dual antennas system which can also be considered either in RD or MD. Hence, this versatility allows us to consider four different possibilities of which two are SIMO based and two are MISO based. In Figure 3.2, a SIMO configuration is presented.

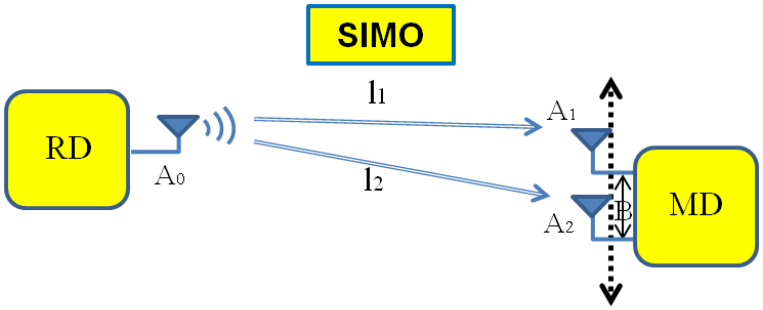

(a) MD calculates its position.

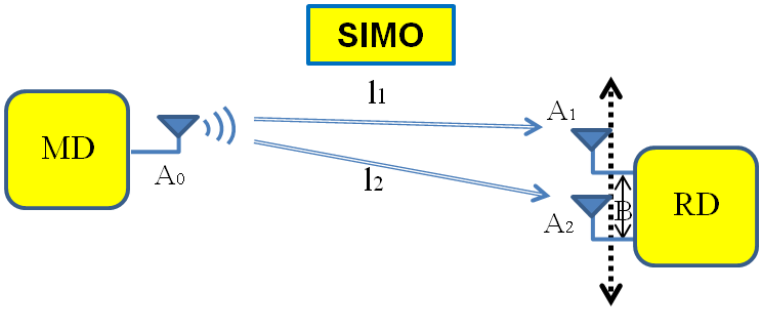

(b) RD calculates MD's position.

Figure 3.2: New TDOA positioning method, SIMO configuration.

In Figure 3.2a, RD acting as a transmitter sends, via antenna A_0, the signal to MD acting as a receiver in order to calculate, using a dual antenna system, its own position. In

Figure 3.2b, MD acting as a transmitter sends, via antenna A_0, the signal to RD acting as a receiver in order to calculate, using a dual antenna system, the MD position and sends back the position information to MD.

In Figure 3.3, a MISO configuration is presented.

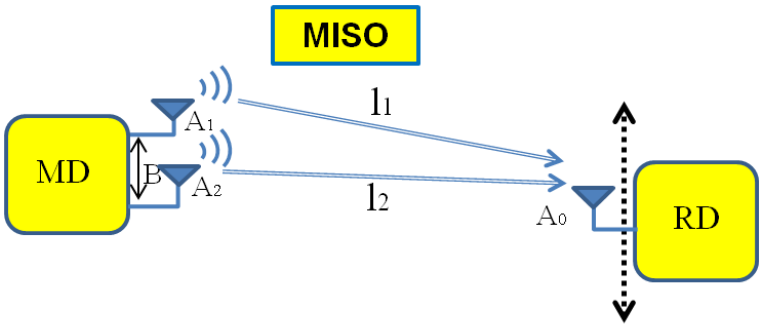

(a) RD calculates MD's position.

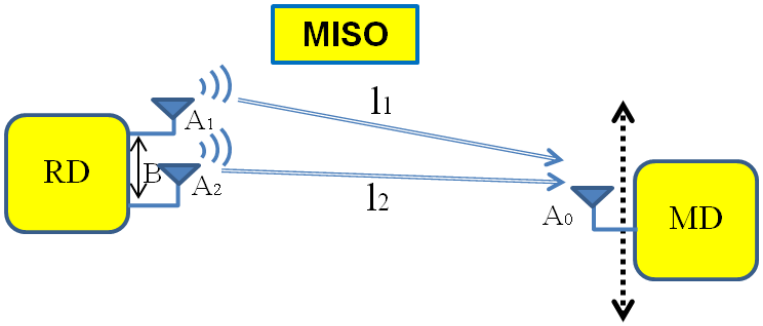

(b) MD calculates its position.

Figure 3.3: New TDOA positioning method, MISO configuration.

In Figure 3.3a, MD acting as a transmitter sends the signal, via a dual antenna system, to RD acting as a receiver in order to calculate, using antenna A_0, the MD position and send back the position information to MD. In Figure 3.3b, RD acting as a transmitter sends the signal, via a dual antenna system, to MD acting as a receiver in order to calculate, using antenna A_0, its own position.

In this research work, from these four available possibilities, a MISO system considering a dual antenna on RD (Figure 3.3b), is chosen in order to have the added complexity only at the fixed RD and hence to let the MD as simple as possible.

In this configuration, the process of calculating the TDOA is done by MD benefiting from communication signals. But it should be emphasized that a SIMO system can also be used to perform this technique (with a dual antenna system at MD), which is completely reciprocal.

Considering Figure 3.3b, A_0 is expected to be, for example, an antenna array for radio coverage needs, whereas A_1 and A_2 may be single elements or sub-arrays of a single antenna array. In this case, the transmitter playing the role of RD uses a dual-antenna system (A_1 and A_2) in order to create, in the received power spectrum, an interferometry pattern stating the direct problem (Figure 3.4). From this received magnitude modulated spectrum and its impact on EVM and ECR, it is possible to extract, by means of solving the inverse problem, the TDOA of interest (Figure 3.4).

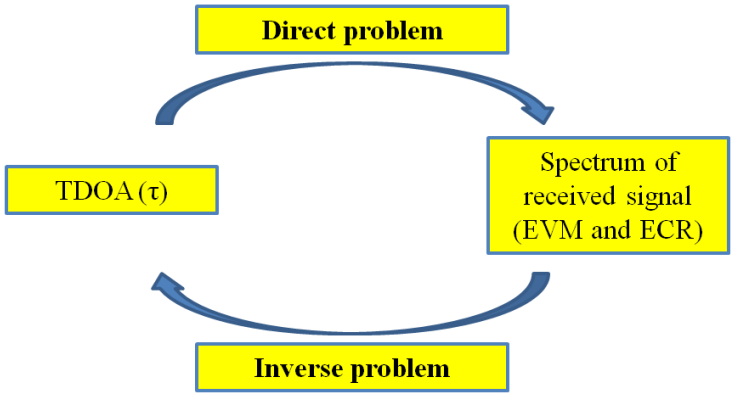

Figure 3.4: Introducing direct and inverse problems

.

Hence, a single mobile receiver can locate itself according to a single co-located antennas transmitter. The expected decrease of accuracy due to the small baseline B, few wavelengths, between the two transmitting antennas is compensated by the use of the huge available bandwidth at 60 GHz (at least 2 GHz for one channel and up to 7 GHz if aggregation is considered). This approach seems to be potentially well suited to perform localization and data transmission simultaneously without adding much complexity compared to existing systems [69, 97, 98, 99]. Further details are given in next paragraphs.

3.2.3 Mathematical analysis and the direct problem

In order to explore the principle of this novel approach in more details, a simple model is derived in this part. As presented in Figure 3.3b, the RD has two antennas A_1 and A_2 seperated by a distance B (baseline). The distance between MD and the antenna A_1 is l_1 and the distance between MD and A_2 is l_2. In the case of LOS (Line Of Sight) ideal channel between RD and MD, the delays of propagation are respectively $\tau_1 = l_1/c$ and $\tau_2 = l_2/c$, with c the speed of light. In the case where only a Continuous Wave (CW) is considered, A_1 and A_2 transmit the same signal:

$$x_1(t) = x_2(t) = Ae^{i2\pi ft} \tag{3.1}$$

At the receiver, both signals are captured, but one is delayed by $\tau = (l_2 - l_1)/c$ from the other. The received signal is called $x_R(t)$. Assuming an ideal channel and the acquisition time is negligible compared to the time behavior of MD, the detected signal, S, is presented, at each time, as a function of f parametrized by τ, and can be written as:

$$S_\tau(f) = \frac{x_R x_R{}^*}{2} = A^2(1 + cos(2\pi f\tau)) \tag{3.2}$$

The shape of $S_\tau(f)$ is a DC offset cosine-wave with a frequency period of $F_p = \frac{1}{\tau}$ from which the TDOA (i.e., τ) can be easily extracted.

We show in Figure 3.5, different magnitude modulated spectrums for different values of τ. As presented in this figure, in the case of $\tau = 0.25$ ns and considering a bandwidth $\Delta F = 7$ GHz centered at $F_0 = 63.5$ GHz, it is possible to visualize at least one periodicity on the modulated spectrum. But in the case of $\tau = 0.12$ ns, the periodicity on the modulated spectrum is not detectable. In such cases introducing a predetermined delay τ_p can help to make the periodicity detectable and, hence, to extract the TDOA. This solution will be explored further in next section.

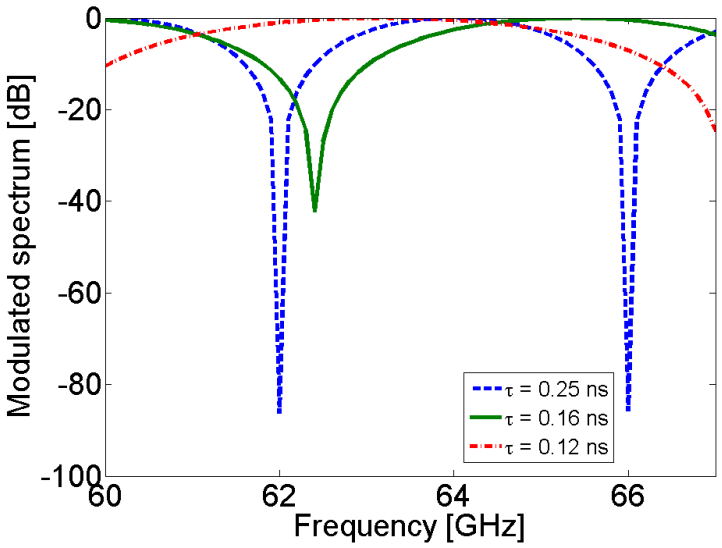

Figure 3.5: Analytical received interfered spectrum in a simple MISO case, $\Delta F = 7$ GHz, $F_0 = 63.5$ GHz.

It is mentioned in last sections that considering the MISO system, the localization information can be directly inferred from the frequency domain interferometry pattern in the received communication signal. As shown in Figure 3.5, this approach can be done using a mono-band signal with a bandwidth large enough to detect the whole interferometry pattern or at least a part of it, which is enough to extract the periodicity of interferometry pattern. In the case that the bandwidth is too small to detect the interferometry

pattern, a multi-band solution, can be proposed to deal with this problem. If the multiple bands are concatenated to each other, as shown in Figure 3.6, the whole interferometry pattern can be covered. If the multiple bands are not adjacent, one can retrieve the whole interferometry pattern by means of adequate interpolation (Figure 3.7).

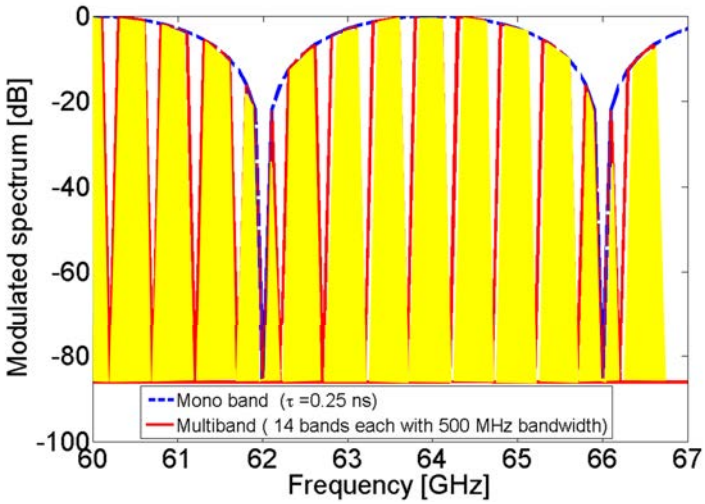

Figure 3.6: Analytical received interfered spectrum in a simple case using multi-band with concatenation.

These two cases are explored in details in next sections considering the IEEE.802.11ad standard.

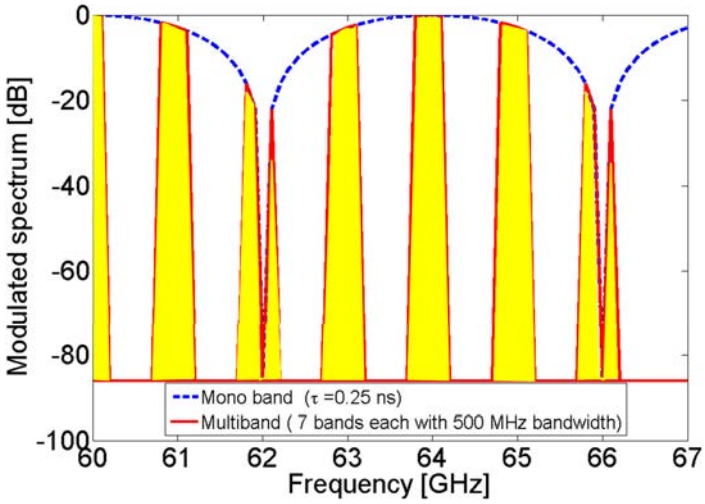

Figure 3.7: Analytical received interfered spectrum in a simple case using multi-band with interpolation.

3.2.4 Inverse problem

In all considered scenarios, the baseline B is relatively small (few wavelengths), and hence, so is the TDOA. So, to observe and extract small TDOA, compatible with indoor applications, a wide-band signal is required. To be able to visualize one period in frequency domain, the communication system should then have a bandwidth ΔF equal to the frequency period F_p.

Expecting TDOA less than $\frac{B}{c}$ (Figure 3.3b), the required bandwidth ΔF should be greater than $\frac{c}{B}$. However advanced signal processing, which is not considered in this report, can help to reduce this bandwidth, and contributing hence to powerful inverse problem resolution. As it will be shown in next sections, we used another approach by introducing a delay line to artificially increase the τ value.

It should be mentioned that, the channel has been considered identical for both paths. However, a more realistic channel is explored later on which complicates the inverse problem resolution.

More details for practical realistic cases with UWB OFDM signals, are presented in next sections. First, a TDOA-based estimation method using received signal EVM is presented and a multi-band approach is proposed in order to increase the precision. Then a similar but more accurate approach which uses the ECR properties and NLS (Non Linear Least Squares) estimation method is proposed. In all sections, theory, system descriptions and simulations of each proposed method are presented.

3.3 TDOA extraction using IEEE 802.11ad standard

To model the IEEE 802.11.ad standard direct and inverse problems, a more detailed calculation is needed.

We consider here the MISO scenario already described and presented in Figure 3.3b. In the frame of IEEE 802.11ad standard, A_1 and A_2 transmit the same OFDM 60 GHz signal with a sample rate frequency F_s, N sub-carriers and M data sub-carriers ($M < N$). If $x(t)$ is the base-band complex envelope (CE) signal and, $x_{RF}(t)$, the RF representation of the transmitted signal, following equations are obtained [100, 101, 102, 103]:

$$x(t) = \sum_{k=-N/2}^{N/2-1} c_k e^{i2\pi k F_s t/N} = \sum_{k=-M/2}^{M/2-1} c_k e^{i2\pi k F_s t/N} \tag{3.3}$$

and

$$x_{RF}(t) = \Re\left(x(t)e^{i2\pi F_{RF}t}\right) \tag{3.4}$$

where $\Re$ is real part operator, c_k are complex coefficients, with k the carrier index and F_{RF} the RF frequency. Calling channel gains between A_1 and MD, and A_2 and MD, h_1 and h_2, respectively, the time invariant channel impulse responses in the CE domain for the two different delays of propagation, τ_1 and τ_2, are:

$$h_1(t) = h_1 e^{-i2\pi F_{RF}\tau_1}\delta(t-\tau_1) \tag{3.5}$$

and

$$h_2(t) = h_2 e^{-i2\pi F_{RF}\tau_2}\delta(t-\tau_2) \tag{3.6}$$

where δ is the Dirac function.

However, in many cases and specially when B is small, $(\tau_2 - \tau_1)$ is not large enough to exhibit at least one period with the operational bandwidth. Thus, a fixed delay, τ_p, is applied between A_1 and A_2, as suggested in [104], to be able to extract the TDOA even in cases for which the defined bandwidth is not enough for visualizing periodicity in the received interfered spectrum. Considering the delay τ_p, the equation 3.6 can be written as:

$$h_2(t) = h_2 e^{-i2\pi F_{RF}(\tau_2+\tau_p)}\delta(t-\tau_2-\tau_p) \tag{3.7}$$

The received signal at MD, $y(t) = x(t) \otimes h(t)$ (operator $\otimes$ refers with the convolution product), in CE domain is equal to:

$$y(t) = h_1 x(t-\tau_1)e^{-i2\pi F_{RF}\tau_1} + h_2 x(t-\tau_2-\tau_p)e^{-i2\pi F_{RF}(\tau_2+\tau_p)} \tag{3.8}$$

The two antennas at RD being relatively close to each other, $h_2 = h_1$ is considered as a first approximation. Assuming that $\tau_t = \tau_p + \tau_2 - \tau_1 = \tau_p + \tau$ and considering a perfect LOS scenario, the received signal in the frequency domain can be presented as follows:

$$Y(f) = h_1 \sum_{k=-M/2}^{M/2} c_k \delta(f - kF_s/N) e^{-i2\pi(kF_s/N+F_{RF})(\tau_2+\tau_p-\tau_t)} \left[1 + e^{-i2\pi(kF_s/N+F_{RF})\tau_t}\right] \tag{3.9}$$

$$Y(f) = h_1 \sum_{k=-M/2}^{M/2} c_k \delta(f - kF_s/N) e^{-i2\pi(kF_s/N+F_{RF})(\tau_2+\tau_p-\tau_t)} \times 2e^{-i\pi(kF_s/N+F_{RF})\tau} cos(\pi(kF_s/N + F_{RF})\tau_t) \tag{3.10}$$

On one hand, from equation (3.9), it can be shown that, in the received spectrum, carriers k are canceled for certain values of τ_t which can lead to estimate the actual TDOA (i.e., τ). On the other hand, from equation (3.10), it can be inferred that the envelope of received signal spectrum (and ECR) is periodic and the periodicity is directly related to τ_t. Knowing the value of τ_p, TDOA can be easily derived by this approach.

3.3.1 Simulation setup

3.3.1.1 Geometry of acquisition

The considered scenario is presented in Figure 3.8.

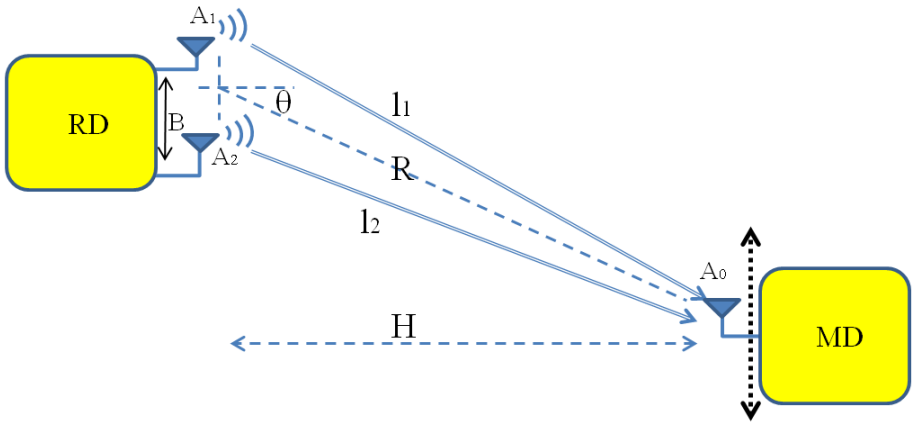

Figure 3.8: Geometry of acquisition for TDOA measurements

.

MD is distant from RD by a distance R and seen with an angle θ. The baseline B is normally set to few wavelengths which corresponds loosely to a maximum TDOA of 0.5 ns up to 1 ns.

3.3.1.2 SystemVue simulation

To perform simulations of the scenario depicted in Figure 3.8, we use a commercially available simulator called SystemVue which is an EDA (electronic design automation) environment. It enables users to access to different libraries and physical layer (PHY) of wireless communication systems. Using this simulator, it is possible to generate and study many forms of modulations and signals compatible with popular systems such as OFDM, Zigbee, GPS, and LTE.

The Figure 3.9 is the image, in SystemVue, of the geometry of acquisition presented in Figure 3.8. As there is no spatial parameter, the baseline B and the angle θ are taken into

account by adding a delay τ, provided by delay block, such as $\tau = \frac{B}{c} sin(\theta)$. As shown in this figure, a data pattern block delivers the message and a custom OFDM source block is used to generate WiGig signals. Channels are modeled here by a simple path loss model and a noise block is added to analyze results in terms of signal to noise ratio.

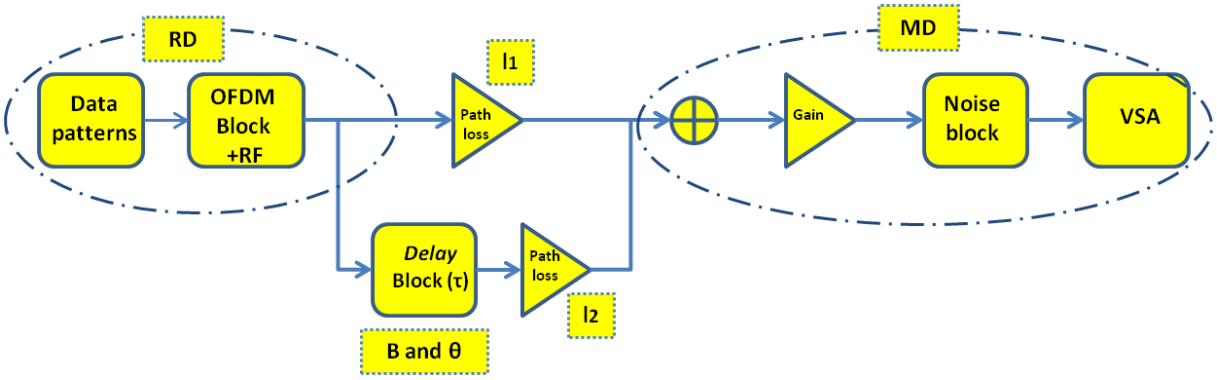

Figure 3.9: Block diagram in SystemVue modeling the geometry of acquisition depicted in Figure 3.8.

To demonstrate the functionality of this block diagram, a simple example, considering an OFDM signal corresponding to IEEE.802.11ad standard, is generated with a 4 QAM modulation. The OFDM parameters are set to F_s = 2,64 GHz, N = 512 and M = 354 for all the simulations. At the receiver, a vectorial signal analyzer (VSA) is added to demodulate the received signal.

Simulation results are presented in Figure 3.10. Due to the interference of the two signals, the spectrum of the received signal is modulated in amplitude as expected. In addition, other useful information such as constellation, EVM curve, signal in time domain and channel equivalent response are also presented in this Figure.

Meanwhile, the constellation of received signal shows that the communication is done with a reasonable average of EVM, 2.1%. The TDOA can be derived from the position of the zeros in spectrum or from maxima in error vector magnitude or from the periodicity of equivalent channel frequency response. These two last different approaches are explained further in next sections.

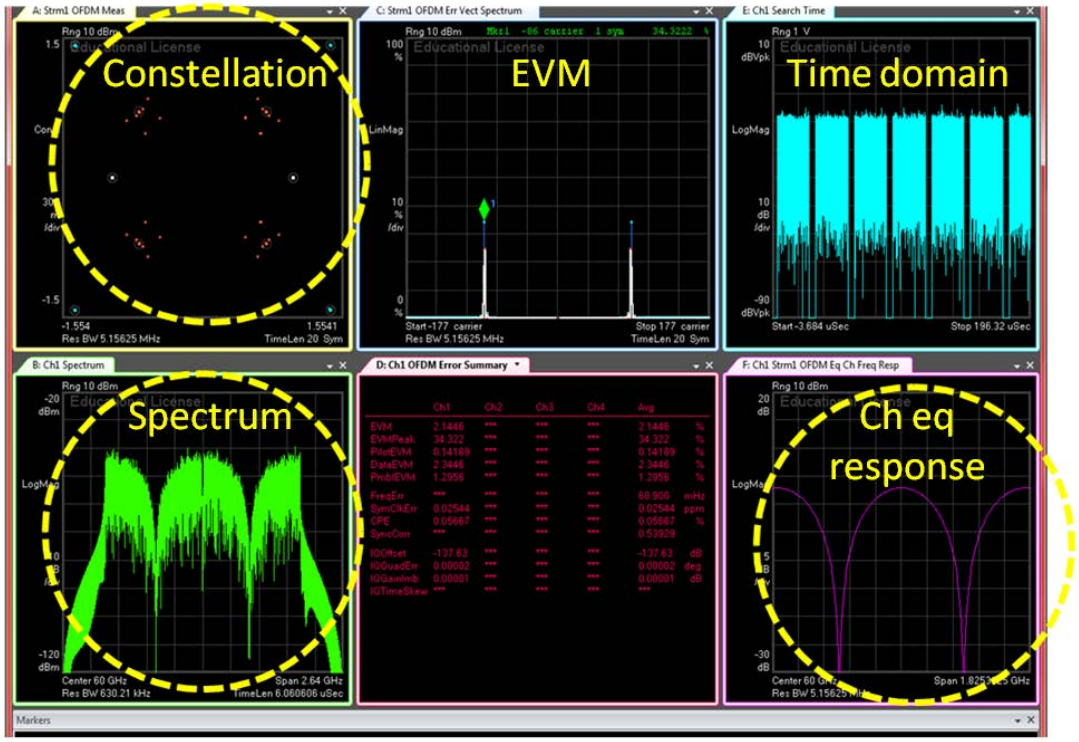

Figure 3.10: Analysis of the received OFDM signal using SystemVue simulator

.

3.3.2 TDOA estimation using EVM of received signal

From equation (3.9), it can be shown that in the received spectrum, carriers k are canceled for values of τ given by:

$$\tau_t = \frac{(2n+1)}{2(\frac{kF_s}{N} + F_{RF})} \qquad n = 0, 1, 2, ... \tag{3.11}$$

Equation (3.11) can also be presented as follows:

$$\frac{kF_s}{N} = \frac{(2n+1)}{2\tau_t} - F_{RF} \qquad n = 0, 1, 2, ... \tag{3.12}$$

where $\frac{kF_s}{N}$ is the k^{th} sub-carrier base-band frequency. The frequency difference between two consecutive null sub-carriers (or minimum power sub-carriers in practice), $F_n = \frac{k_n F_s}{N} + F_{RF}$ and $F_{n+1} = \frac{k_{n+1} F_s}{N} + F_{RF}$, is written as:

$$F_{n+1} - F_n = \frac{\Delta k F_s}{N} = \frac{1}{\tau_t} \qquad n = 0, 1, 2, ... \tag{3.13}$$

where $\Delta k = k_{n+1} - k_n$ and we supposed $\tau \geq 0$. Equation (3.13) shows that τ_t can be obtained by measuring the difference between indexes of two consecutive minimum sub-carriers which are defined by highest EVM values of received signal. Therefore, the value of $\tau = \tau_2 - \tau_1 = \tau_t - \tau_p$ is also obtained.

As already explained, τ_p is applied in order to ensure visualizing periodicity in the received interfered spectrum. Equation (3.10) shows that τ_t, which is also equal to $\tau_t = \tau_p + \tau$, can be obtained from the period of the received spectrum. It can be easily shown that the limit value of τ_t that guarantees to perform, in the considered bandwidth, a good estimation of the period is:

$$\tau_{min} = \frac{3N}{2MF_s} \tag{3.14}$$

The value τ_{min} is considered to ensure at least one and a half period in the bandwidth. The value τ_p, should be then large enough that for the highest negative value of $TDOA$, τ_{min} will be obtained, thus:

$$\tau_p = \tau_{min} + max(TDOA) \tag{3.15}$$

where $max(TDOA)$ is equal to baseline length divided by speed of light in vacuum (B/c). Then, τ_{max} is obtained as follows:

$$\tau_{max} = \tau_p + max(TDOA) \tag{3.16}$$

As an example, for a 15 cm baseline and 2 GHz bandwidth, the optimum value of τ_p is equal to 1250 ps. It should be noticed that to avoid a larger loss of the information carried

by the OFDM symbols and also to avoid increasing the delay too much, a proper baseline should be chosen.

Thus, τ_p, which plays in a certain manner the role of a bias point that should be chosen in a relevant way, helps to build an entire period inside the given bandwidth. It is obvious that this trick does not contribute in any way to enhance the accuracy of the measurement which is mainly limited by the bandwidth.

Making use of equation (3.11), we plot the values of τ_t that ensure the cancellation of at least one couple of carriers. Results for $n = 0, 1, 2$ are plotted in Figure 3.11. In order to ensure the cancellation of one and only one couple of carriers, we have to choose the values of τ_p that give us just one solution for equation (3.11).

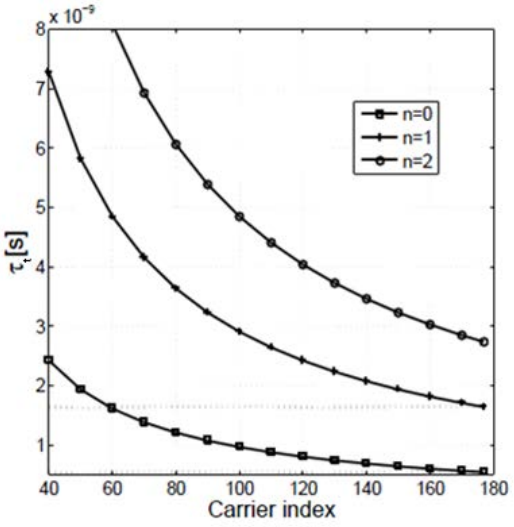

Figure 3.11: Solutions of equation 3.11 for $n = 0, 1, 2$ with defined OFDM parameters.

3.3.2.1 Simulation results

To demonstrate the feasibility of our approach, a 60 GHz communication system is simulated using SystemVue software. Knowing the range of τ values that can be measured with the OFDM signal used, in a realistic geometry of acquisition, τ and τ_p are respectively set to 0.23 ns and 1.37 ns. The value of TDOA corresponds to a geometrical acqusition where B=8 cm and $\theta = 60°$, with a distance between RD and MD of about two meters.

Therefore, according to equation (3.13), $\Delta k = 170$ is expected. It should be emphasized that if the delay τ_p was not considered ($\tau_p = 0$), then the baseline should have been chosen equal to B=40 cm in order to obtain an exploitable EVM diagram.

Figure 3.12a and Figure 3.12b present respectively the constellation and the EVM of the received signal when the SNR, given by the noise block, is set to 30 dB. As shown in

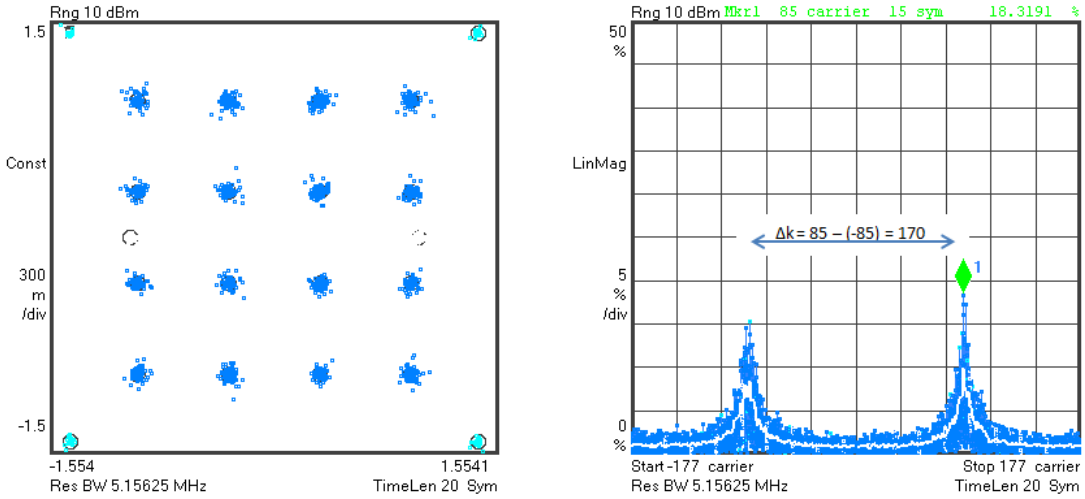

(a) Constellation.

(b) EVM.

Figure 3.12: Simulation by SystemVue: constellation and EVM of received signal in LOS scenario.

Fig. 3.12a, the constellation at the Rx presents a high quality communication in the LOS case. A precise estimation of TDOA can be performed by looking at the EVM of received signal. As shown in Figure 3.12b, the average EVM of received signal is about 2.5 % but at the minimum power sub-carriers the EVM is about 15 %. Therefore, the position of minimum power sub-carriers can be easily distinguished among the other sub-carriers. Figure 3.12b confirms the value of 170 for Δk, as predicted by the theory. This technique is a promising one as the localization data are carried by the minimum power sub-carriers, and therefore readily available from base-band processing.

In order to confirm the effectiveness of this solution, we show in Figure 3.13a the theoretical results obtained for $\tau_t = 1.47$ ns and $\tau_t = 3$ ns, while keeping other parameters unchanged. Results in EVM diagram are given in Figure 3.13b. The good agreement validates this approach but should still be confirmed in realistic environment. One should notice that for $\tau_t = 3$, ns a greater number of carriers have high EVM values which may contribute in a degradation of the quality of communication. Evaluation of a such impact is given in 3.4.2.

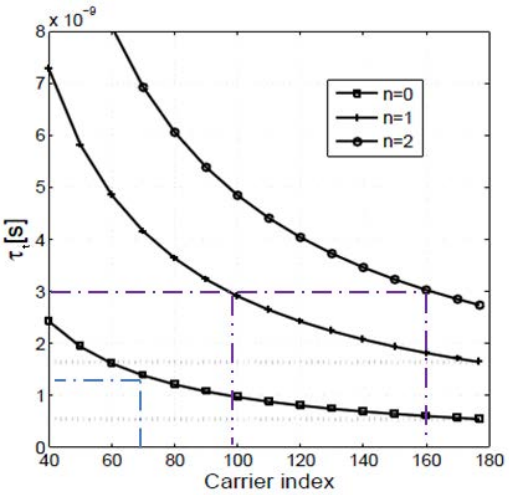

(a) Theoretical curve.

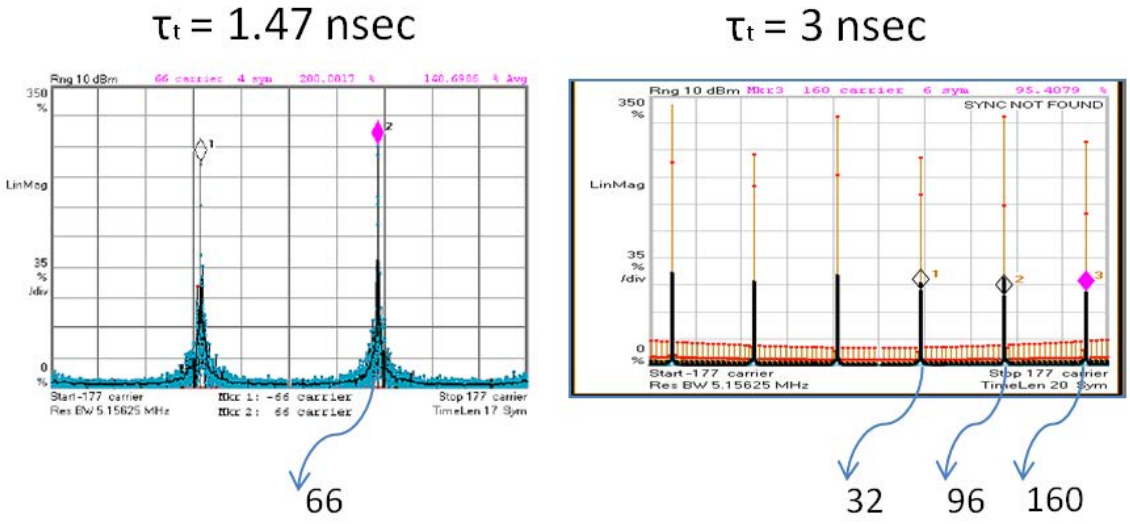

(b) Simulation results (EVM).

Figure 3.13: Comparison of the theory and simulation results for TDOA extraction from EVM diagram.

3.3.2.2 Conclusion

In this section, a new technique to measure asynchronously TDOA in UWB OFDM wireless systems is described. This technique is particularly suited for localization in 60 GHz networks using 802.11ad specifications. It has been shown that, under the hypothesis of LOS and using two very close reference devices, it is possible to estimate the useful metric for 1D position of a Mobile Device in a room, by exploiting the cancellation of one and only one pair of carriers.

This solution has the advantage of permitting to conceive a relatively compact reference device equipped with two antennas. Moreover it has the advantage of allowing localization and communication at the same time, unlike classical TDOA measurements.

3.3.3 TDOA estimation using equivalent channel response (ECR)

In the context of high data rate indoor communication and in order to mitigate the effect of multi-paths, most commonly used OFDM systems estimate the equivalent channel response using a cyclic-prefix, zero padding or Golay codes to perform an equalization [105]. Thus, the equivalent channel response (ECR) is readily available in OFDM systems and our method can directly benefit from this data in order to estimate the TDOA.

Here, in the inverse problem, the obtained TDOA is estimated using a non linear least square method (NLS) applied on the ECR. It has the ability to estimate with a better accuracy the TDOA even if the bandwith is not well suited. In Figure 3.14 the TDOA estimation algorithm is presented.

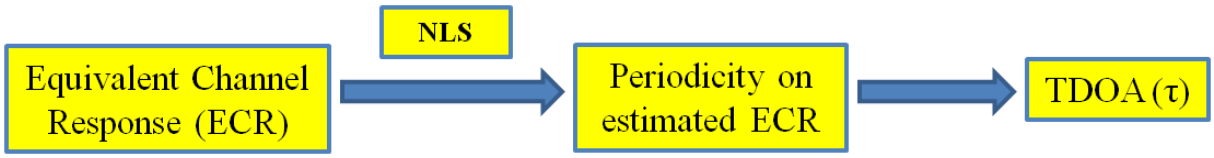

Figure 3.14: TDOA estimation algorithm using NLS applied on ECR

.

3.3.3.1 Simulations results

Simulations are done using Agilent SystemVue and VSA software to confirm the theory presented in last section. In the first case a $\tau = 0$ is considered, thus $\tau_t = \tau_p$. The spectrum

and the channel equivalent response of received signal are presented in Figure 3.15a and Figure 3.15b and are, as expected, in agreement with calculations.

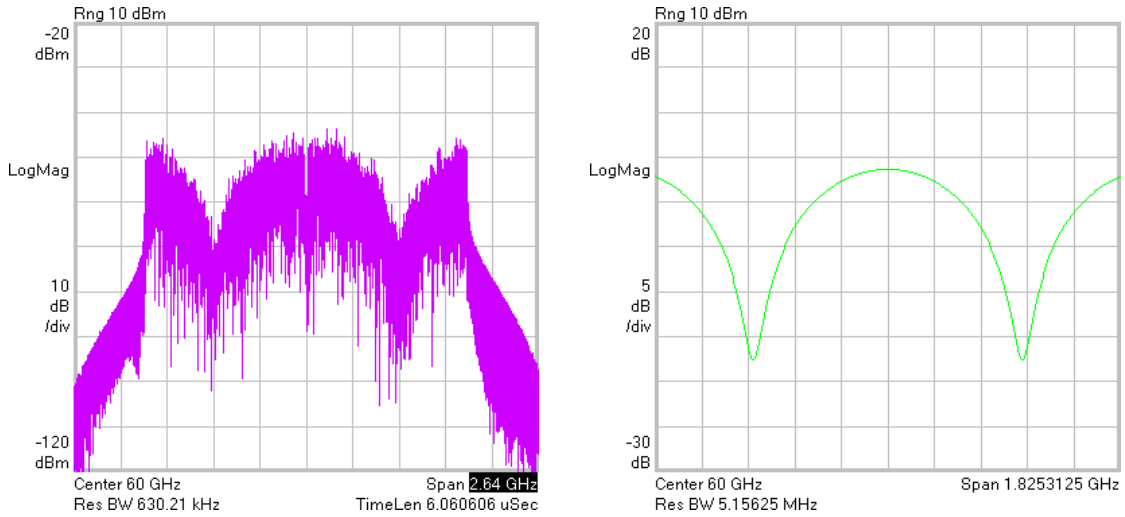

(a) Spectrum. (b) Channel equivalent response.

Figure 3.15: Spectrum of received signal and channel equivalent response (ECR) in LOS scenario and with $\tau = 0$, $\tau_p = 1250$ ps, $\Delta F = 2$ GHz, and SNR=20 dB.

In the second case, a $\tau > 0$ is considered, thus $\tau_t = \tau_p + \tau$ and a larger value of τ is obtained, so the periodicity in the spectrum is smaller (Figure 3.16a). In the third case, a $\tau < 0$ is considered, thus $\tau_t = \tau_p - \tau$ and a smaller value of τ is obtained, so periodicity in the spectrum is greater (Figure 3.16b).

These simulations considering simple case of LOS are presented here in order to describe the direct problem. In a realistic environment, the ECR is influenced by noise and multi-paths and in order to extract the periodicity, NLS estimation should be applied. The TDOA estimation (inverse problem) is explored in following paragraphs and realistic simulations using Matlab are presented after the definition of channel, in section 3.4.1.2.

3.3.3.2 TDOA estimation

In the case of inverse problem, a non linear regression based on the least square method is used to have an estimation of the received spectrum or equivalent channel response and calculate the periodicity. In least square method the minimum of sum of residuals squares should be calculated to estimate one signal, for example, equivalent channel response y_i:

$$r_i = y_i - \hat{y}_i \tag{3.17}$$

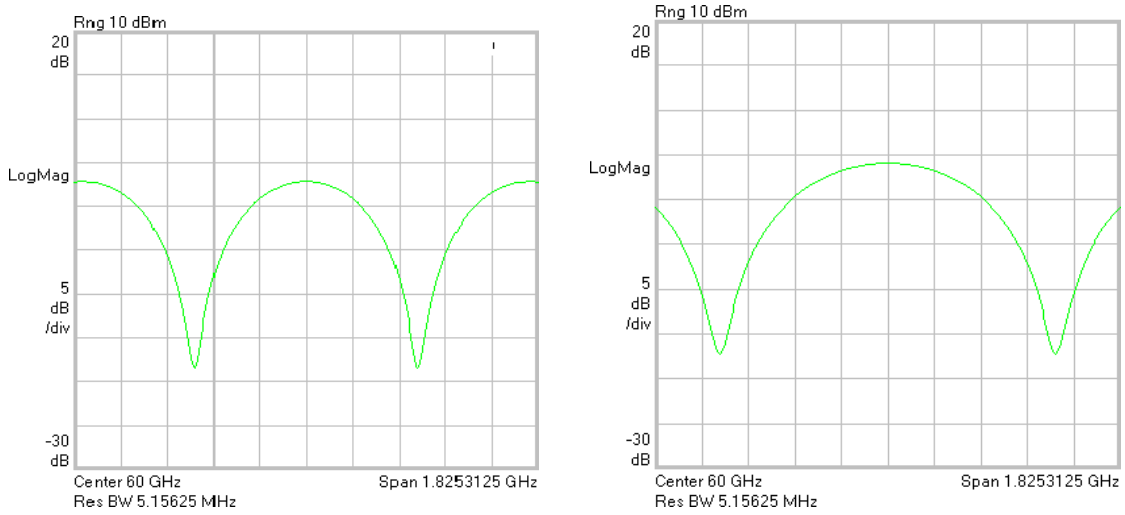

(a) $\tau > 0$. (b) $\tau < 0$.

Figure 3.16: Channel equivalent response (ECR) considering different τ

where r_i is the i^{th} residual and $\hat{y}_i$ is the estimation model. Fourier model considered for this regression allows to obtain an estimation of the equivalent channel response which will give naturally the period. The Fourier model is:

$$\hat{y}_i = \beta_0 + \sum_{i=1}^{n} \beta_1 cos(\beta_2 f) + \beta_3 sin(\beta_2 f) \tag{3.18}$$

where β_0, β_1, β_1 and β_3 are the coefficients of the defined model. Then, the sum of residuals square is presented as S:

$$S = \sum_{i=1}^{n} r_i^2 = \sum_{i=1}^{n} (y_i - (\beta_0 + \sum_{i=1}^{n} \beta_1 cos(\beta_2 f) + \beta_3 sin(\beta_2 f)))^2 \tag{3.19}$$

The minimum of function S should be calculated in order of to obtain the coefficients of the defined model

$$\partial S/\partial \beta = 2 \sum_{i=1}^{n} r_i \partial r_i / \partial \beta_j = 0 \qquad j = 1, .., m \tag{3.20}$$

To solve the problem, the Levenberg-Marquardt algorithm is then used [106, 107]. An example of performing the NLS method is shown in Figure 3.17. The perodicity of ECR is easily retreived leading to the estimation of TDOA.

3.3.3.3 Conclusion

In this section, a new TDOA estimation method in UWB OFDM wireless systems, based on the periodicity of the received envelope, is described. Compared to EVM approach, this solution has the advantage of using the envelope of received signal or channel

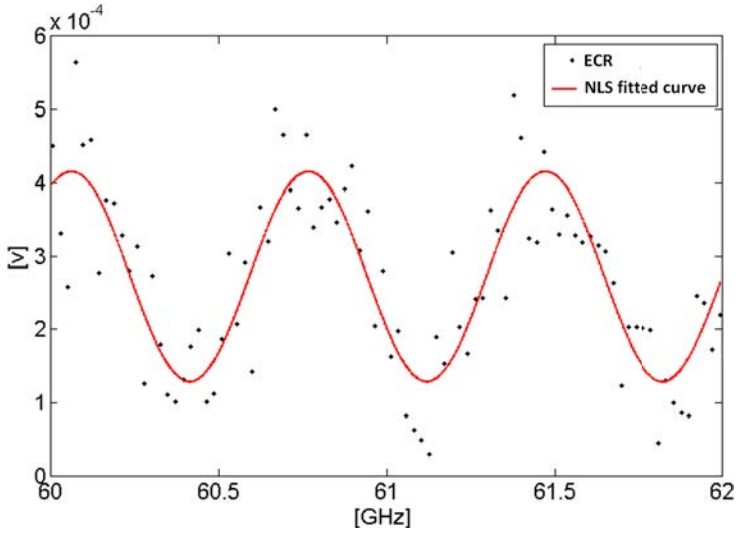

Figure 3.17: An example of NLS applied on ECR.

equivalent response (ECR), which is an available data in recent high data rate communication systems. Using NLS method to estimate the periodicity of received envelope, makes this approach more accurate compared to EVM approach. Meanwhile, this solution has all the advantages of EVM approach: permitting to conceive a relatively compact reference device equipped with two close antennas and allowing localization at the same time as communication, unlike classical TDOA measurements.

3.3.4 Multi-band approach

In this section, we investigate an extension of our method which is well suited for very small TDOAs. To cover the required large bandwidth, one can use a multi-band approach.

As previously mentioned, the new proposed TDOA principle is based on interferences in the received signal spectrum. So when a larger bandwidth is provided, a more precise TDOA can be achieved and hence a more accurate localization. So if, the OFDM signal is transmitted several times with different RF sub-carriers between 60 to 67 GHz and signal post processing is used, the TDOA can be extracted by considering the whole bandwidth in this range.

As shown in Figure 3.8, the configuration of RD and MD for this approach is exactly the same as in the last section. A_1 and A_2 transmit the same OFDM signal having baseband sample frequency F_s and N carriers at the same time with $F_{RF} = 60GHz$. Then, the same signal is transmitted about a different F_{RF}, for instance, 62 GHz, 64 GHz, etc. With a post processing, the whole spectrum can be obtained. Simulation results are presented

in Figure 3.18. More results will be explored in chapter 4 with experiments.

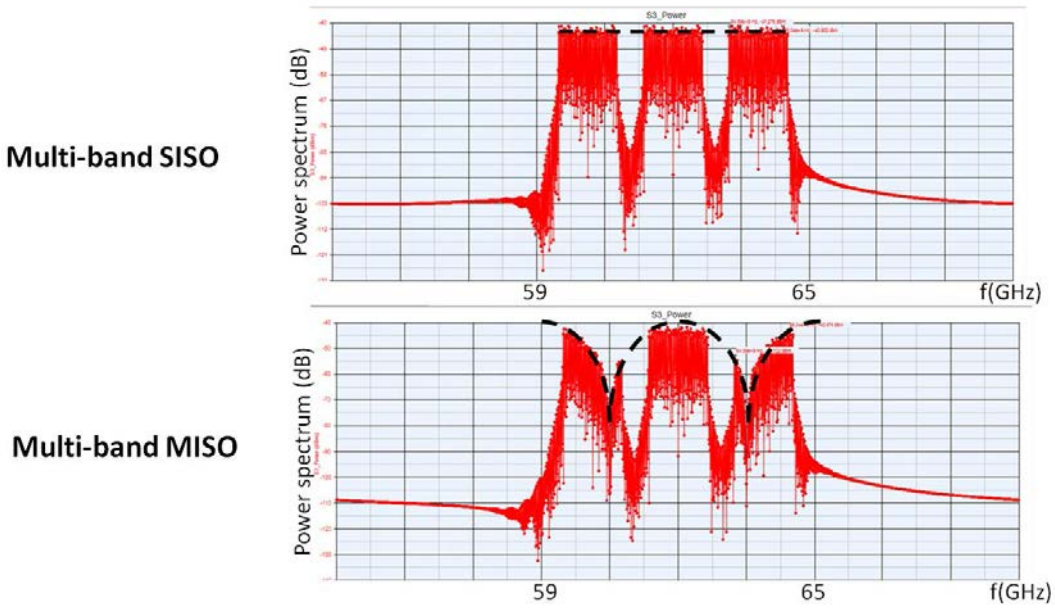

Figure 3.18: Simulation results of multi-band approach (3 bands with $\Delta F = 2GHz$centered at 60 GHz, 62 GHz and 64 GHz).

3.4 Limitations and validity domain

3.4.1 Channel consideration

3.4.1.1 Simple multi-path influence on 60 GHz TDOA estimation using EVM

In the whole former study only LOS channel is considered. In this section, the simple multi-paths contribution and their influence on the TDOA and on the localization precision are investigated for different cases. As before, this whole study is made within the framework of the WiGig alliance and IEEE.802.11 ad specifications. At the first part of this chapter another simulation of pure LOS case serving as a reference data, is demonstrated, then the different multi-paths are also studied to compare the pure LOS and multi-path cases [100].

Pure LOS case

Knowing the values of τ that can be measured with our OFDM signal, the configuration given in Figure 3.8 is used with B=40 cm. For this configuration, the reference device is chosen with A_1 and A_2 supposing that A_1 transmits the same signal as A_2 with a delay

τ_p. The value of τ_p is chosen to measure $\tau = \tau_2$-τ_1 with the maximum of dynamic range. The distance between RD antennas is chosen to observe the cancellation of a single pair of carriers. A simulation example of a MD localization with this method is implemented by

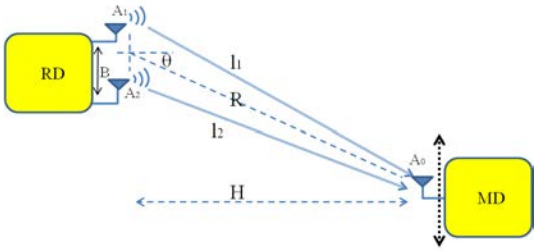

(a) RD and MD configuration.

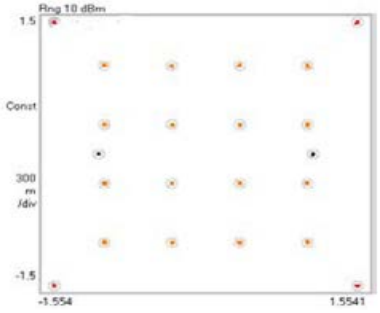

(b) Constellation of received signal in LOS scenario

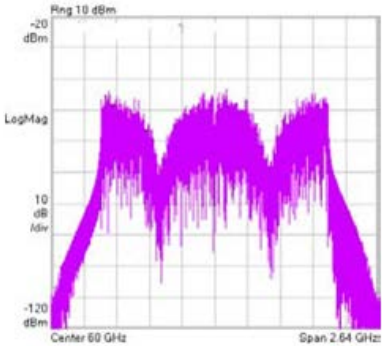

(c) Spectrum of received signal in LOS scenario

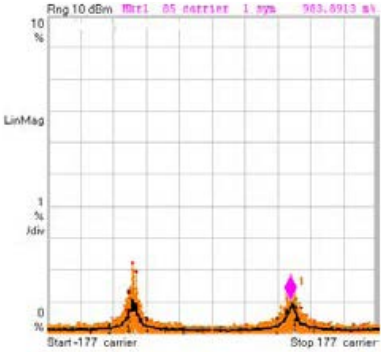

(d) EVM of received signal in LOS scenario.

Figure 3.19: Geometry of acquisition and communication features in LOS scenario.

using the SystemVue and VSA 89600 software. For a fixed point in the room, for example for a 40 cm baseline and a MD which is located 2 m apart from RD (H=1 m, $\theta = 60°$ in Figure 3.19a), the theoretical value of $\tau_t = \tau_p + \tau_2 - \tau_1$ for a LOS propagation between the RD antennas and the fixed point is calculated. $\tau = 1.1$ ns is obtained and thus according to equation (3.11),$|k| = 85$ is expected due to the theory. The result obtained by the simulation confirms the value calculated by the theory.

Figure 3.19b, Figure 3.19c and Figure 3.19d present respectively the constellation, the spectrum and the EVM of the received signal which leads to detect the nulls. As shown in Figure 3.19b, the constellation at the Rx presents a high quality communication in the LOS case. However, it is shown in Figure 3.19c, that the spectrum of the signal is totally deformed and the position of nulls leads us to obtain the TDOA [100]. A precise calculation of TDOA can be done by looking at the EVM of received signal, as shown in Figure 3.19d (the cancellation is presented in $|k| = 85$ as expected).

Multi-path case

The same simulation example is implemented for different multi-path cases. As shown in Figure 3.20a, for each case, one multi-path is added to the configuration of the LOS case. The calculated TDOA value is not anymore the same as the theoretical expected value due to the multi-path influence on the received signal spectrum.

For the same configuration of RD and MD, different NLOS paths are studied. The maximum coherence bandwidth at 60 GHz for the indoor environment is about 50 MHz [98]. So the maximum delay spread is about 20 nsec. Here, the case corresponding to a NLOS which is 300 cm (10 nsec) is presented to study an even worse case with a bigger error.

Figure 3.20b, Figure 3.20c and Figure 3.20d present respectively the constellation, the spectrum and the EVM of the received signal of this multi-path case. As shown in Figure 3.20b, the constellation at the Rx presents worse communication performance in the multi-path case than the pure LOS case. It is shown in Figure 3.20c, that the spectrum of the signal is totally deformed and the position of nulls changed, which affects the determination of the TDOA. As shown in Figure 3.20d, the maximum EVM of received signal is not the same as the case of pure LOS [100].

According to equation (3.11), $|k| = 85$ is expected due to the theory but the result obtained by the simulation does not confirm this value since the NLOS contribution affects the position of the nulls in the spectrum and changes the position of the maximum EVM. In this case the peak of EVM is at $|k| = 71$, so the TDOA error is 16.5 % [100].

Influence of multi-path on TDOA error

To demonstrate the influence of NLOS on TDOA error, different cases are studied. The theoretical TDOA considered for this configuration is 1.1 nsec. A range of multi-paths which are 40 cm to 3 m longer than the LOS path are chosen. The delay corresponding to these values vary from 1.3 nsec to 10 nsec.

In Figure 3.21, these different cases are presented. For each multi-path, 0 dB normalized power corresponds to the case for which the multi-path power loss is only due to the free space attenuation corresponding to the multi-path length (40 cm to 3 m). Smaller normalized powers represent different power losses due to absorption or reflection. It is shown in Figure 3.21 that for each path, if the power loss due to the reflection and absorption is 12 dB more than the path loss itself, then the TDOA error is less than 5 %. So the calculated TDOA, even in case of multi-path contributions, is close to the theoretical value [100].

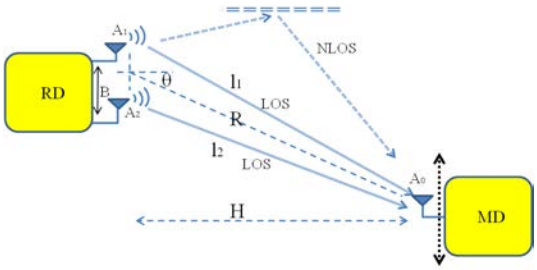

(a) RD and MD configuration in multi-path scenario.

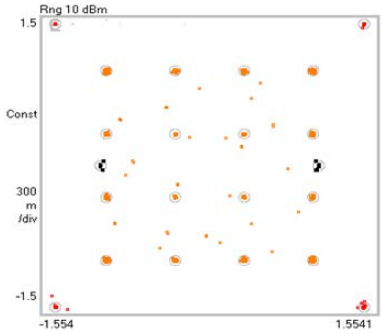

(b) Constellation of received signal in multi-path scenario.

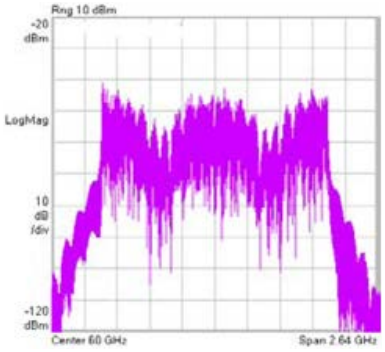

(c) Spectrum of received signal in multi-path scenario.

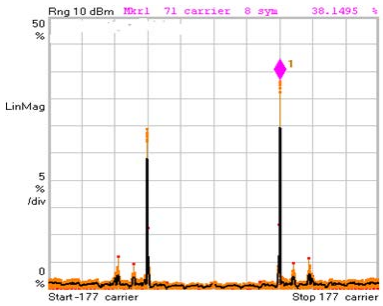

(d) EVM of received signal in multi-path scenario.

Figure 3.20: Geometry of acquisition and communication features in multi-path scenario.

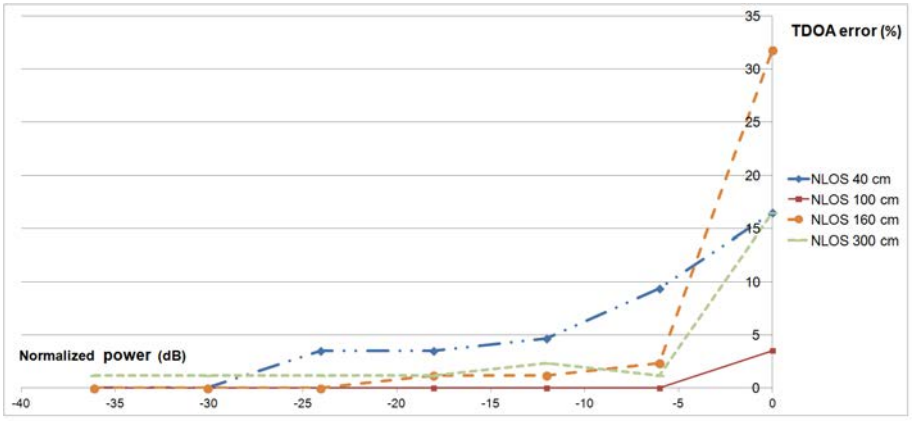

Figure 3.21: TDOA error for different NLOS Scenarios.

In Figure 3.22, the same scenarios but this time normalized to the LOS power loss are presented. It is shown in Figure 3.22, that for each multi-path, if the power loss due to the reflection and absorption is 8 dB more than the LOS path loss, then the TDOA error is less than 5 %. While considering reflection and absorption values presented in

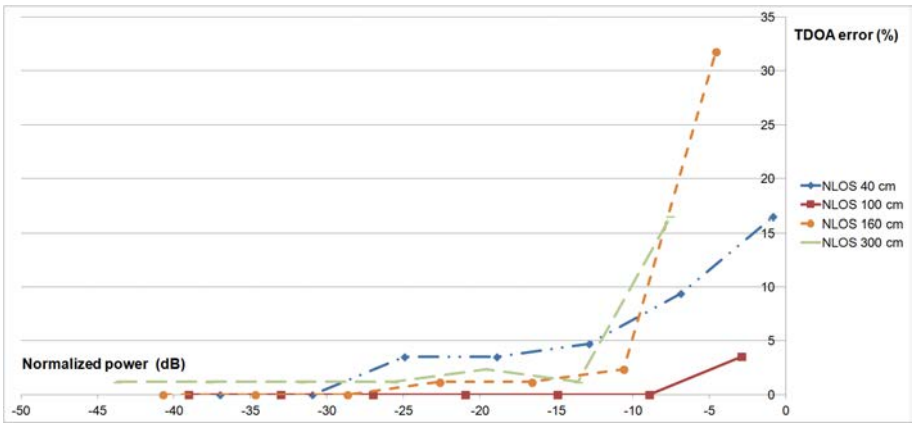

Figure 3.22: TDOA error for different NLOS Scenarios.

Table 2.2. in chapter 2, these first approach results let us think that our technique may be promising for 60 GHz indoor communications (at least when a LOS path is available).

3.4.1.2 IEEE channel influence on 60 GHz TDOA estimation using ECR

As already mentioned in section 2.2.1, the wireless channel environment may affect drastically the performance of wireless communication systems. Developing high performance and bandwidth-efficient wireless systems is laid on understanding the channel characteristics. It is even more important in the case of high data rate broad band 60 GHz communication.

Mainly, indoor channels are modeled under the hypothesis that they have static or quasi-static conditions. By looking at the measurements implemented in indoor channels, it has been verified that multiple clusters with multiple rays should be defined to model the channel. There are different statistical models for defining the indoor channel propagation. Two-ray models or exponential models are the two most popular models. In this research the channel is considered based on IEEE.802.11ad channel model. The channel impulse response is calculated by statistical approaches which consider uniform and Rayleigh distributions respectively for amplitude and phase of each ray in a cluster [108, 109]. The channel impulse response expression has already been presented in chapter 2.

The new proposed method is evaluated by performing simulations considering the IEEE 802.11.ad channel. It should be mentioned that communication aspects are not studied in this section and only the channel is explored to validate the proposed approach. In other words, the channel estimator of the OFDM scheme is supposed to be perfect. Simulation by ray tracing combined with the statistical definition of intra-cluster paths is used to generate channel model [110]. The simulations are done with Matlab.

Several functions are created to consider principal rays such as direct path, simple reflexions and double reflexions. Then for each ray, intra clusters are generated using Rayleigh distributions and the whole channel response is calculated. In all these functions, calculations are done by considering geometrical parameters (related to position of Rx and Tx) and physical parameters such as frequency, wavelength, permitivitty of walls, polarization, etc. A 2 GHz bandwidth, which corresponds to IEEE 802.11.ad standard and a conference room with a dimension of 10*10*3 m^3, are considered for the simulations. The reference device is placed at the center of the room at the height of 1.5 m. Different positions for MD have been considered: 1 to 5 m range differences from the RD and with an angle θ varying from 0° to 90° ($TDOA > 0$) and from 0° to -90° ($TDOA < 0$), as shown in Figure 3.23.

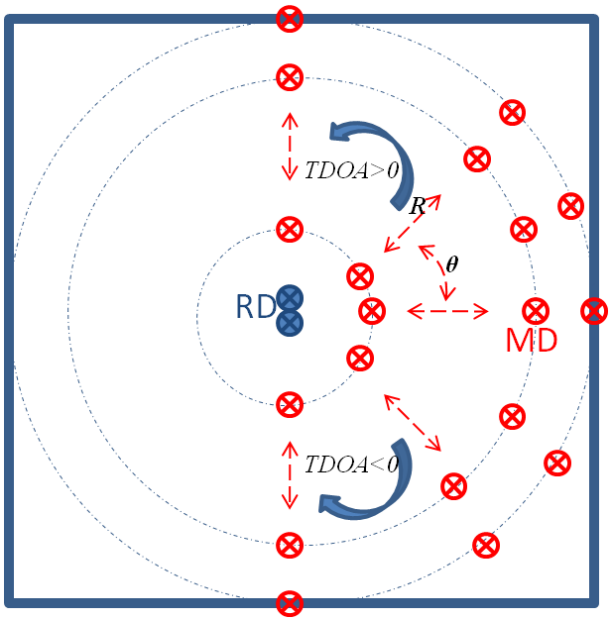

Figure 3.23: RD at the center of room and schematic of different positions of MD.

For each configuration, the channel impulse response between A_1 and MD is calculated. Then the same calculation has been done between MD and A_2 considering a delay shift in order to apply τ_p. Then the two channel impulse responses are added together and the frequency response of the whole MISO channel is calculated by applying the Fourier transformation.

The envelope of the resulted channel is then fitted by applying the non linear least square (NLS) method and Fourier model as described in section 3.3.3.2, in order to obtain τ, and therefore, the TDOA. The whole algorithm is shown in Figure 3.24.

An example of the MISO channel impulse response is presented in Figure 3.25. The first two points represent the two direct paths. Multi-paths whose power are 30 dB less

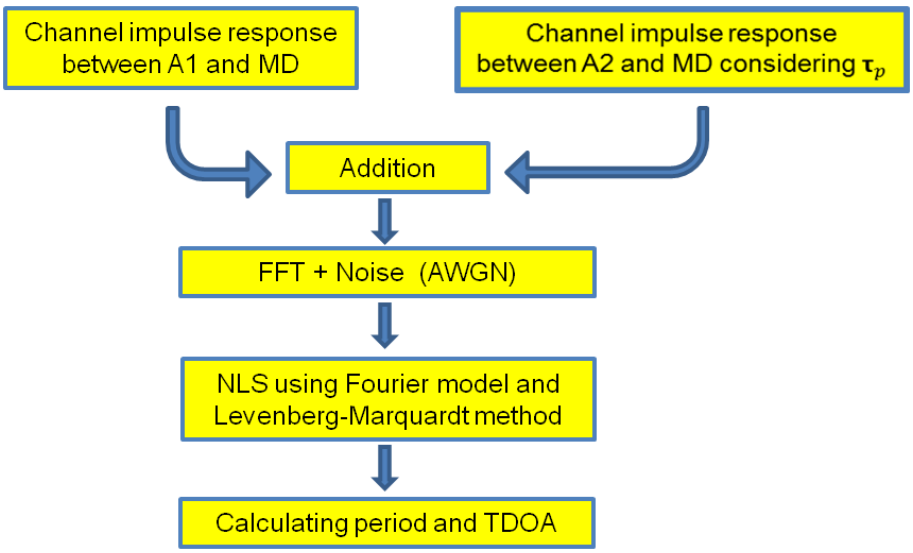

Figure 3.24: Simulation algorithm for TDOA estimation.

than the direct paths are not represented in Figure 3.25 for sake of clarity, but are taken into account during TDOA estimation.

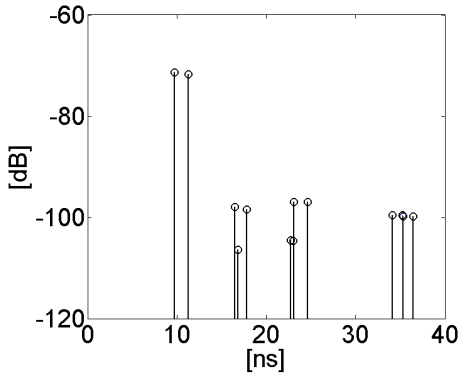

Figure 3.25: Addition of the two channel impulse response ($RD_{A_1} - MD$ and $RD_{A_2} - MD$) .

In Figure 3.26, the frequency channel response of the whole system (considering an additive white Gaussian noise (AWGN)) and its fitted curve by using NLS method and Fourier model is shown. As it is presented, these curves are periodic and the period is equal to τ_t.

Simulations for different locations of MD are conducted. Throughout the simulation study, the baseline is set at 16 cm, a $\tau_p = 1283$ ns is considered and a 10 dB SNR is defined at the receiver by adding an AWGN to the frequency response to the two added channel. Estimated TDOA are compared to actual ones that are geometrically determined. In Figure 3.27 estimated TDOA values are compared to actual TDOA values and errors are shown in meters in Figure 3.28. Results are ordered according to the radial distance R

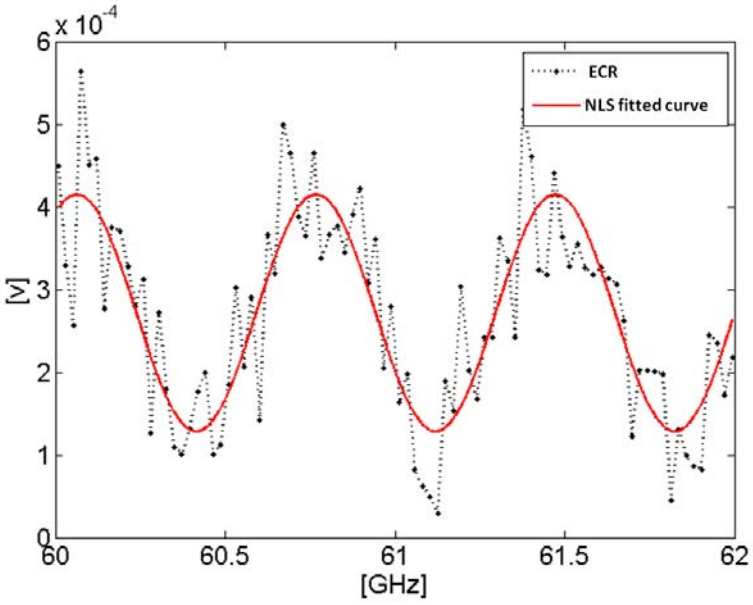

Figure 3.26: The frequency channel response and its fitted curve.

between RD and MD. Figure 3.27a, 3.27b, and 3.27c show results for R=1 m , R=3 m, and R=5 m, respectively. The different TDOA values are obtained by varying the angle θ according to Figure 3.23. For each location (so for each TDOA under consideration), 500 simulations are performed since noise and channel's clusters parameters follow statistical distributions.

It can be seen from Figure 3.27a that estimated TDOA values are reasonably close to actual TDOA values. In the case of R=1 m, the mean error is 4.3 ps with a mean variance of 0.176 ps and a maximal variance of 0.244 ps. In spatial domain the root mean squared error (RMSE) is 3.8 cm with a mean variance of 0.04 cm and a maximal variance of 0.24 cm.

Figure. 3.27b and Figure 3.27c show approximatively the same results for the Tx-Rx distance of R=3 and R=5 m, but with higher value of mean error and variance for the case of R=5 m. In this case, the mean error is 10 ps, with a mean variance of 0.19 ps and a maximal variance of 0.388 ps. In spatial domain the RMSE is 23 cm with a mean variance of 1.7 cm and a maximal variance of 11 cm. These values are illustrated in Table. 3.1.

This is due to higher influence of multi-paths for these positions that are closer to the walls. This assumption has been validated by calculating the Ricean factor K [110], and it has been found that the average K for R=5 m is 6.4 dB, whereas for R=1 m, it is 16.6 dB and for R=3 m it is 9.8 dB. The Rician factor allows to compare the power of

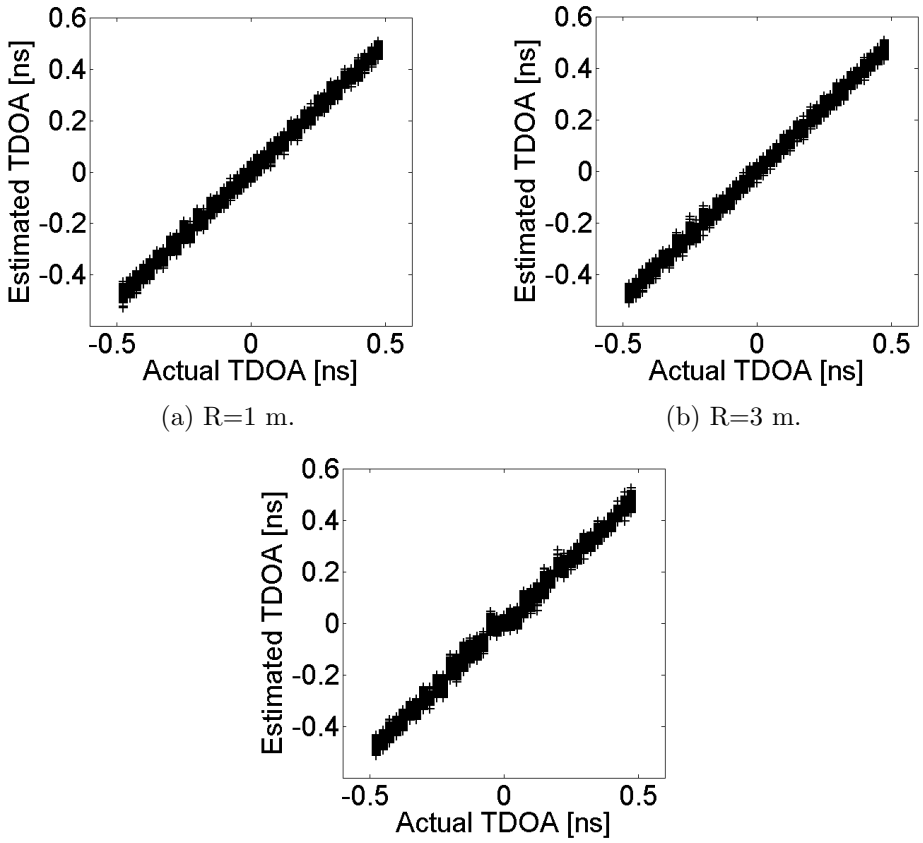

(a) R=1 m.

(b) R=3 m.

(c) R=5 m.

Figure 3.27: Estimation errors for different R, Baseline=16 cm.

line-of-sight and multi-paths and is calculated as [110]:

$$K = \frac{max_{(i,k)}[\alpha^2_{(i,k)}]}{\sum_{(i,k)} \alpha^2_{(i,k)} - max_{(i,k)}[\alpha^2_{(i,k)}]} \tag{3.21}$$

where, $\alpha_{(i,k)}$ is the k^{th} ray magnitude of the i^{th} cluster.

Same results are presented in spatial domain in Figure 3.28a, 3.28b, 3.28c, for R=1 m, R=3 m and R=5 m, respectively. As shown in Figure 3.28a, for the case R=1 m, the spatial error is generally below 8 cm. Figure 3.28b and Figure 3.28c show higher values of errors. In these cases, errors are generally less than 40 cm and always less than 75 cm for R=3 m, and always less than 95 cm for R=5 m. Consequently, it can be seen that the proposed method allows performing localization with a decent accuracy.

The cumulative distribution functions (CDF) of estimation errors in spatial domain are presented in Fig. 3.29 for R=1 m, R=3 m, R=5 m separately, and for all R values respectively. The CDF represents the probability that the spatial error is less than the given threshold presented in x-axis. To obtain these results, the spatial locations consid-

	R=1 m	**R=5 m**
Average error in time domain	4.3 ps	10 ps
Spatial domain RMSE	3.8 cm	23 cm

Table 3.1: Average error in time domain and spatial domain RMSE for R=1 m and R=5 m

.

ered in Figure 3.27 are taken into account. As shown in Figure 3.29, for the case R=1 m, the spatial error is below 10 cm for 97 % of cases whereas cases with R=3 m and R=5 m show higher values of errors. For R=3 m and R=5 m, errors are less than 15 cm and 30 cm for 80 % of cases respectively. Consequently, it can be seen that the proposed method allows performing localization with a decent accuracy. The CDF of all spatial errors for all different R values is also presented in Figure 3.29. It is shown that for 80 % of the cases (considering different R from 1 m to 5 m), the spatial error is less than 17.5 cm.

The cumulative distribution function of spatial error for different values of τ_p, for a 2 GHz bandwidth and a 15 cm baseline, is presented in Figure 3.30. The CDF represents the probability that the spatial error is less than the given threshold presented in x-axis. To obtain these results, all the spatial locations considered in Figure 3.28 (for all R values) are taken into account. The best result is obtained for τ_p = 1250 ps, as determined in section 3.3.2. It is shown that for 80 % of the cases (considering different R from 1 m to 5 m) the spatial error is less than 15 cm.

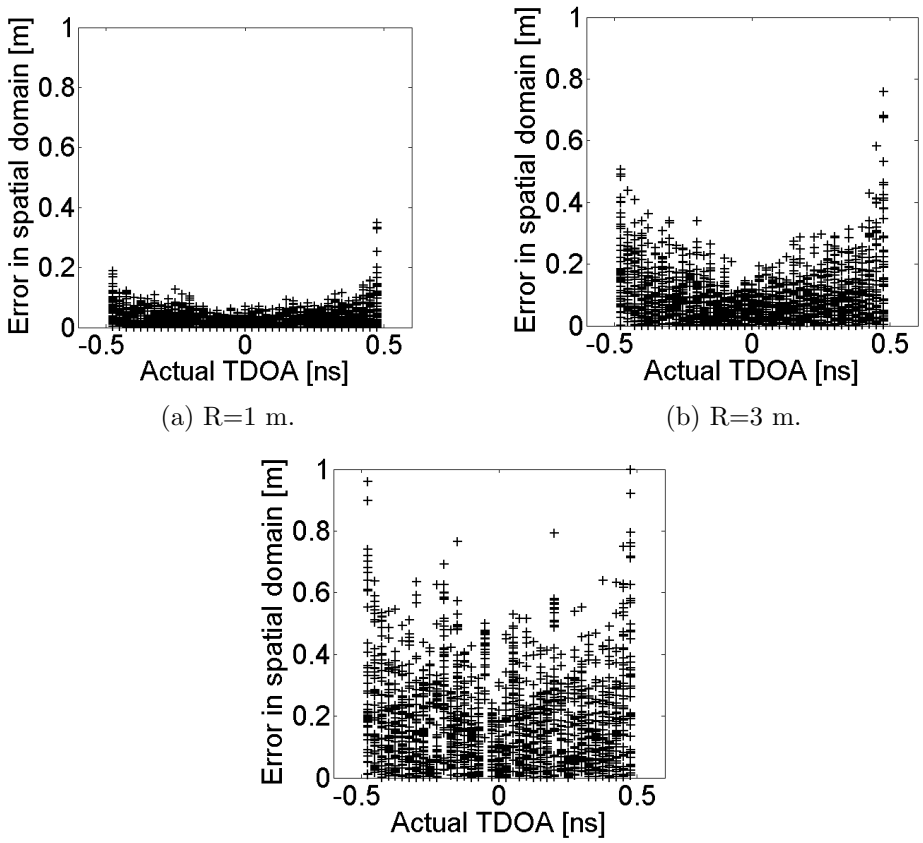

(a) R=1 m.

(b) R=3 m.

(c) R=5 m.

Figure 3.28: Estimation errors in spatial domain for different R, Baseline=15 cm.

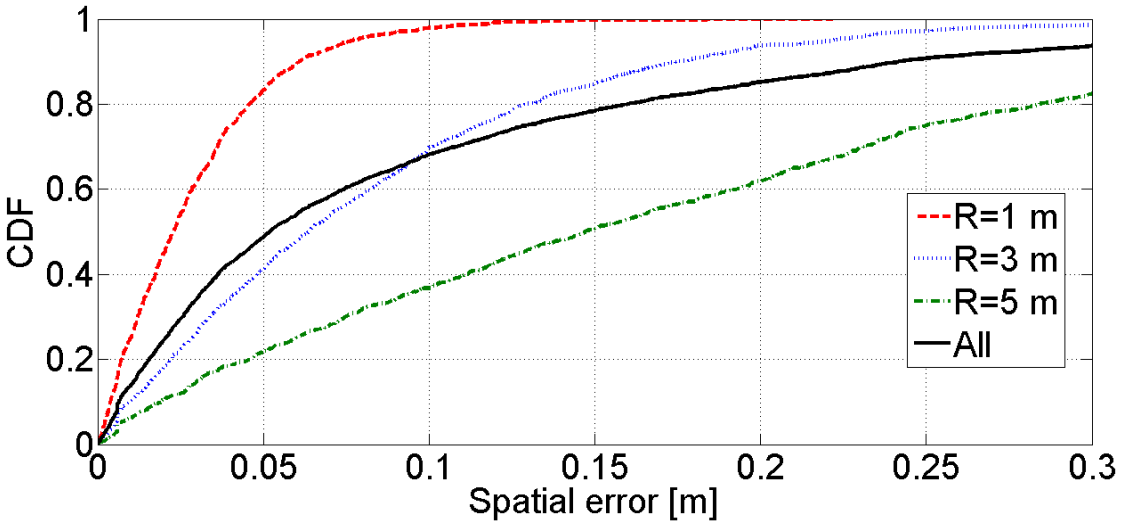

Figure 3.29: CDF of estimation errors in spatial domain for different R, Baseline=16 cm, $\tau_p = 1283$ ns.

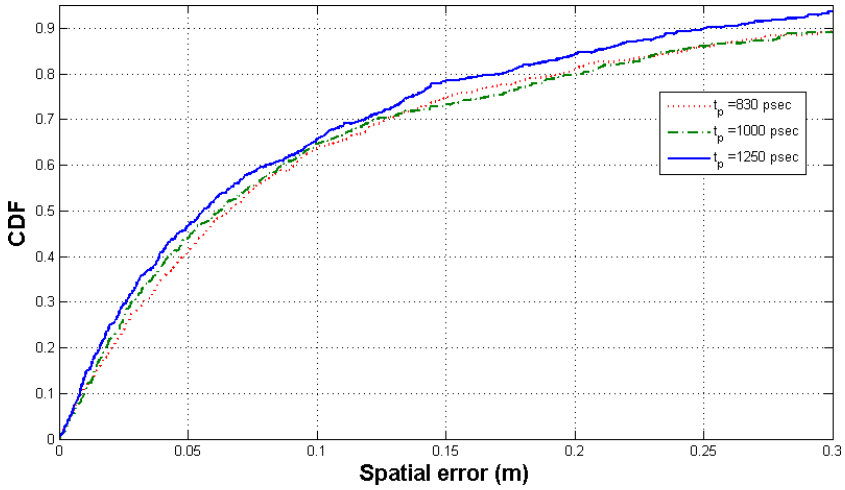

Figure 3.30: CDF of all simulation results considering 3 different τ_p.

3.4.2 Quality of communication

The proposed method of TDOA estimation is based on nulls in the ECR where high EVM occuring, or on ECR's periodicity. The question we pose here is considering much larger τ_t (more than $\frac{B}{c}$), how communication quality drops. For that purpose, Figure 3.31 shows the average EVM of 2 GHz bandwidth communication with respect to the number of null subcarriers involved by different τ_t values. As shown, increasing the number of null sub-carriers lesser than a threshold level (about 6 null-subcarriers) does not change drastically the value of EVM. The threshold level is much larger than the maximum number of nulls corresponding to the maximum TDOA that can be reached in many applications. For example, for a 30 cm baseline, the maximum TDOA is equal to 1 nsec (which introduce 2 null sub-carriers in the case we consider 2 GHz bandwidth). Thus, the value of EVM is reasonably low in most cases, which leads to achieve simultaneous communication and localization. Even by comparing the SISO case with different MISO cases, it can be inferred that the value of EVM is really close to the the case of SISO. It means that having some null subcarriers does not change much the overall EVM.

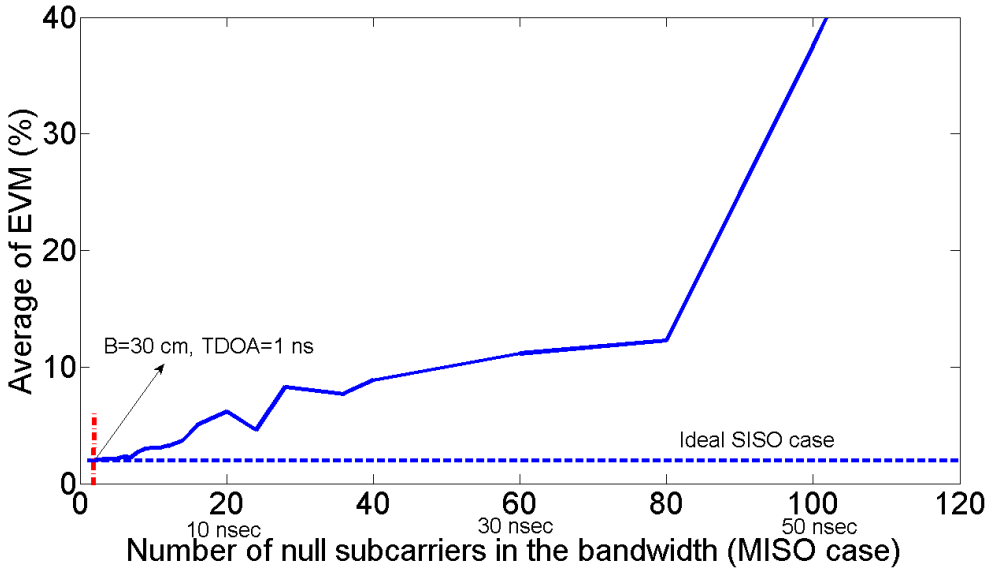

Figure 3.31: EVM versus number of null sub-carriers (Bandwidth=2 GHz)

.

3.5 Conclusion

In this chapter, a new TDOA based localization is introduced. Theory of this technique is studied, then confirmed by simulations. It has been shown that this approach is well adapted for 60 GHz systems and has the advantage of performing localization and communication simultaneously. Furthermore, contrary to classical TDOA methods, this approach deals with the problem of RDs synchronization by using only one RD composing of a dual antenna system. This fact is key factor which leads to achieving a localization system that do not add much complexity on the main existing communication system. A MISO configuration is considered in order to create, in the received power spectrum, an interferometry pattern. The interferometry pattern on the EVM or ECR of the received signal is then used to extract the TDOA value. Channel effect is also considered in the simulations, and the obtained results show a good accuracy for the proposed approach. To obtain an estimation with a good precision NLS method is used. It is shown that even by considering the IEEE.802.11ad channel in the hypothesis of LOS scenario, it is possible to estimate a 1D position of a mobile device.

Chapter 4

Measurements and experimental results

4.1 Introduction

In this chapter, three campaigns of measurements are performed and presented. The objective is to validate the theory and simulations results obtained for the scenario depicted in chapter 3. In the first campaign, measurements using vectorial network analyzer (VNA) are presented. Due to the high quality of their components and to the well defined calibration procedure, they serve as a reference to measurements carried out by 60 GHz communication systems. In the second section, implemented measurements using millimeter wave Tx/Rx module (Vubiq) and a digital storage oscilloscope (DSO) using a vectorial signal analyzer interface (VSA) are studied for free space and guided scenarios focusing on multi-band solutions. Measurements using a second communication system called "Highrate Transceiver"are then presented in the third section and finally, a multi-band approach, at lower frequencies, is studied in the forth section.

4.2 Measurements using VNA

4.2.1 Experimental setup and test conditions

To validate the theory and simulation results, a first measurement campaign using a VNA is conducted. Serving as a reference for the other types of experimental validation we led, this 2 GHz bandwidth and 256 frequency points set-up operating about 60 GHz

is presented in Figure 4.1. To be able to use longer cables to cover distances R up to 2.5 m, Reference Device (RD) and Mobile Device (MD) are connected to a lower frequency Rohde Schwartz ZVA24 via a frequency extension to measure the forward transmission scattering parameters (S_{21}).

Actually ZVA24 is a VNA operating in the frequency range of 10 MHz to 24 GHz and is used instead of a 60 GHz VNA to easier implement the measurements in which long cables are needed. To be able to conduct the measurements with 2 GHz band about 60 GHz, a special configuration is considered, as mentioned in [111]. A 14.75-15.25 GHz bandwidth is generated by ZVA24 source, then quadruplers are used to up-convert this bandwidth to a 59-61 GHz bandwidth. Omni-directional antennas are used at the RD antennas and open waveguide at MD. The baseline B is set to 16 cm.

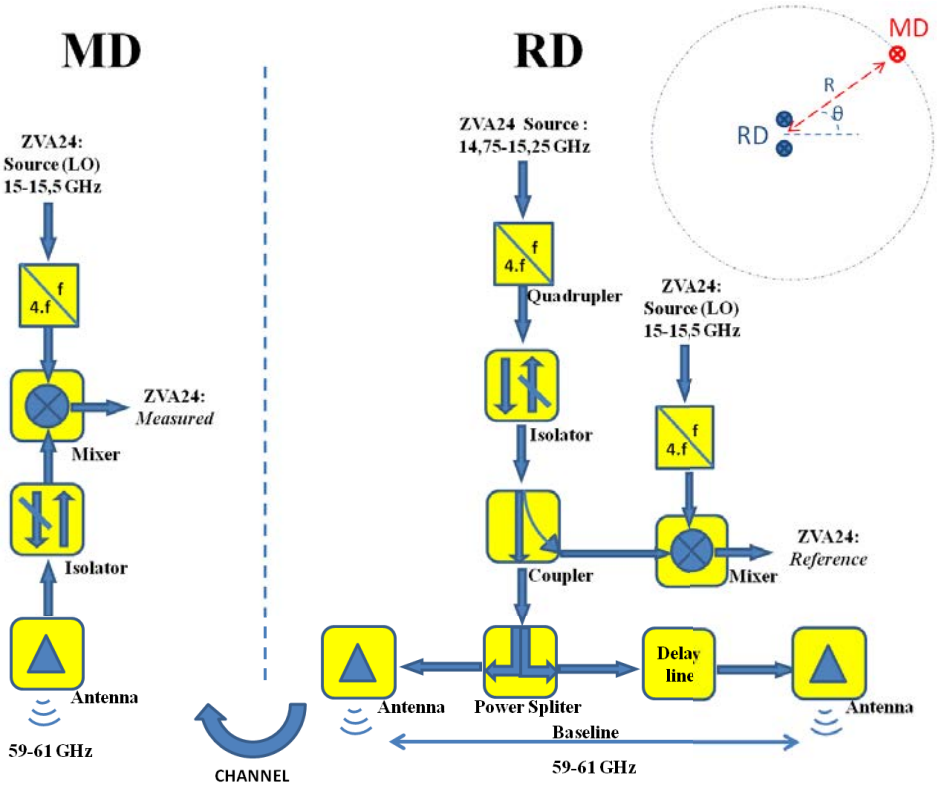

Figure 4.1: VNA (ZVA24) Measurement configuration schematic.

For this campaign, two different rooms and different positions for mobile device have been considered. R values range from 1 to 2.5 m, with θ varying from $-90°$ to $90°$ have been studied (Figure. 4.1). The first room is a laboratory in which there are lots of instruments and hence subject to dense multi-path propagation, and the second room is a lobby. The photography of the experimental set up is presented in Fig. 4.2.

(a) Measurements in room 1.

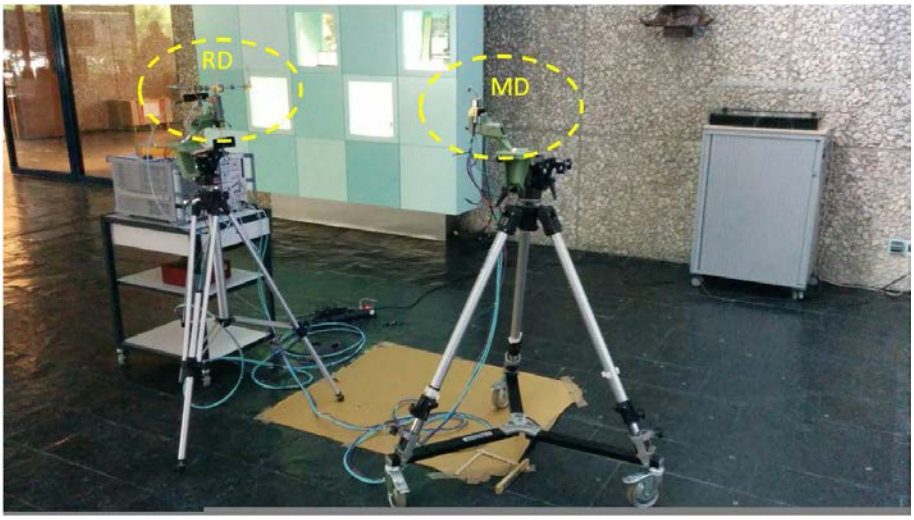

(b) Measurements in room 2.

Figure 4.2: VNA measurements campaign in room 1 and room 2 using 2 GHz swept frequency up-converted from 15 GHz to 60 GHz.

4.2.2 Results

Figure 4.3 shows, for the measurements in room 1, TDOA values estimated by determining the periodicity of S_{21} parameter using the NLS algorithm presented in chapter 3. Results are presented by considering two different τ_p and changing the position of MD from RD with range R differences of 1 m and 1.5 m and with θ varying from $-90°$ to $90°$ for each case.

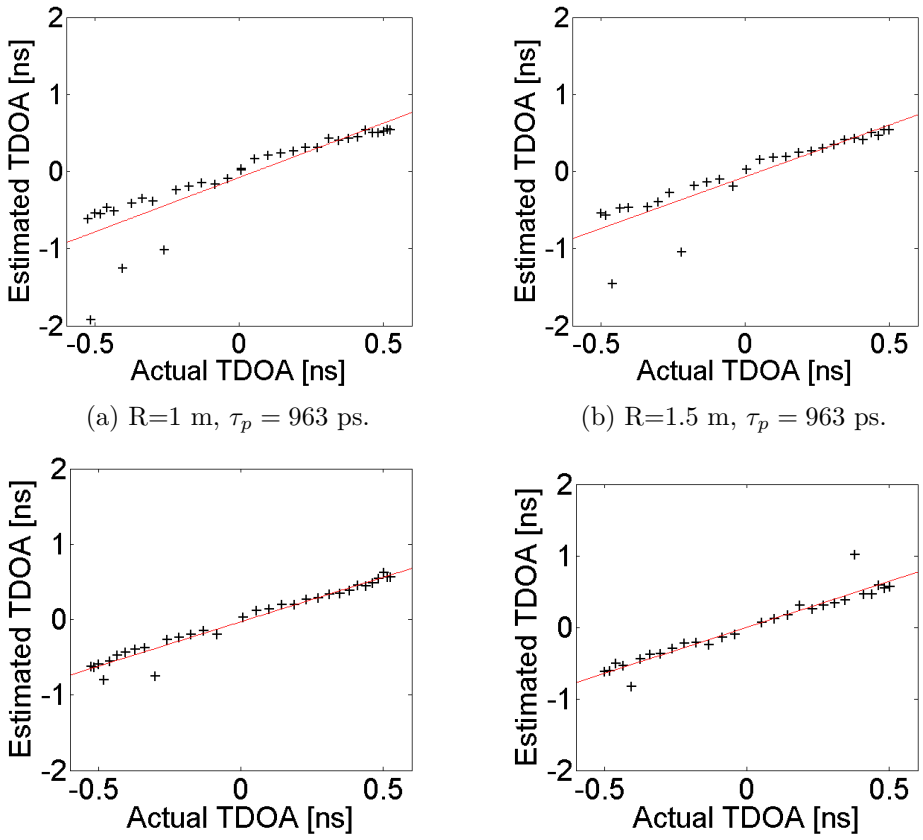

(a) R=1 m, $\tau_p = 963$ ps.

(b) R=1.5 m, $\tau_p = 963$ ps.

(c) R=1 m, $\tau_p = 1300$ ps.

(d) R=1.5 m, $\tau_p = 1300$ ps.

Figure 4.3: TDOA extracted from S_{21} parameter measurements results using ZVA24 in room 1 considering 2 different τ_p, baseline=16 cm, bandwidth: 2 GHz swept frequency.

The obtained results follow a similar behavior than simulation ones, errors being larger when R (the distance between RD and MD) is larger. Compared to simulation, additional errors are due to the system errors such as phase noise, errors regarding mixers and amplifiers frequency responses and also reference positions errors. Due to the material limitations, it is not possible to obtain the exact theoretical values of τ_p. In consequence two different delays, $\tau_p = 1300$ ps and $\tau_p = 963$ ps are obtained by using waveguides with different lengths.

	R=1 m	**R=1.5 m**
$\tau_p = 1300$ ps	0.21 m	0.37 m
$\tau_p = 963$ ps	0.31 m	0.6 m

Table 4.1: Average error in spatial domain considering different τ, room 1.

	R=1 m	**R=1.5 m**	**R=2 m**	**R=2.5 m**
Average error	0.18 m	0.31 m	0.44 m	0.61 m
RMSE	0.25 m	0.44 m	0.6 m	1.14 m

Table 4.2: Average error in spatial domain and RMSE for room 2.

As expected, the results obtained for $\tau_p = 1300$ ps which is closer to the optimum theoretical value of $\tau_p = 1283$ ps according to section 3.3.2, show a better precision. The average error in spatial domain, as shown in Table 4.1, for R=1 m and R=1.5 m for $\tau_p = 1300$ ps, are respectively 0.21 m and 0.37 m whereas for $\tau_p = 963$ ps are respectively 0.36 m and 0.61 m. Also the RMSE for R=1 m and R=1.5 m for $\tau_p = 1300$ ps, are respectively 0.31 m and 0.6 m whereas for $\tau_p = 963$ ps they are respectively 0.77 m and 1.5 m.

Fig. 4.4 shows estimated TDOA error results for the measurements implemented in room 2, considering $\tau_p = 1300$ ps and changing the position of MD from RD with range differences of 1 m and 2.5 m and with a θ varying from -90° to 90° for each case.

As presented in this figure, the results are better compared to room 1, because of less multipath effects of this room. Average error in spatial domain for R=1 m, R=1.5 m, R=2 m and R=2.5 m in room 2, as shown in Table 4.2, are respectively 0.18 m, 0.31 m, 0.44 m and 0.61 m. Also the RMSE for R=1 m, R=1.5 m, R=2 m, and R=2.5 m in room 2, are respectively 0.25 m, 0.44 m, 0.6 m, and 1.14 m.

4.2.3 Conclusion

The measurement campaign led in this section uses the vectorial network analyzer in order to validate the main analytical and simulated results concerning TDOA estimation. The good agreement observed confirms predicted results and allows us to consider these measurements as a reference. However this approach does not take into account any modulation formats usually used in HDR systems and appeals other measurement campaigns more suited for communication issues.

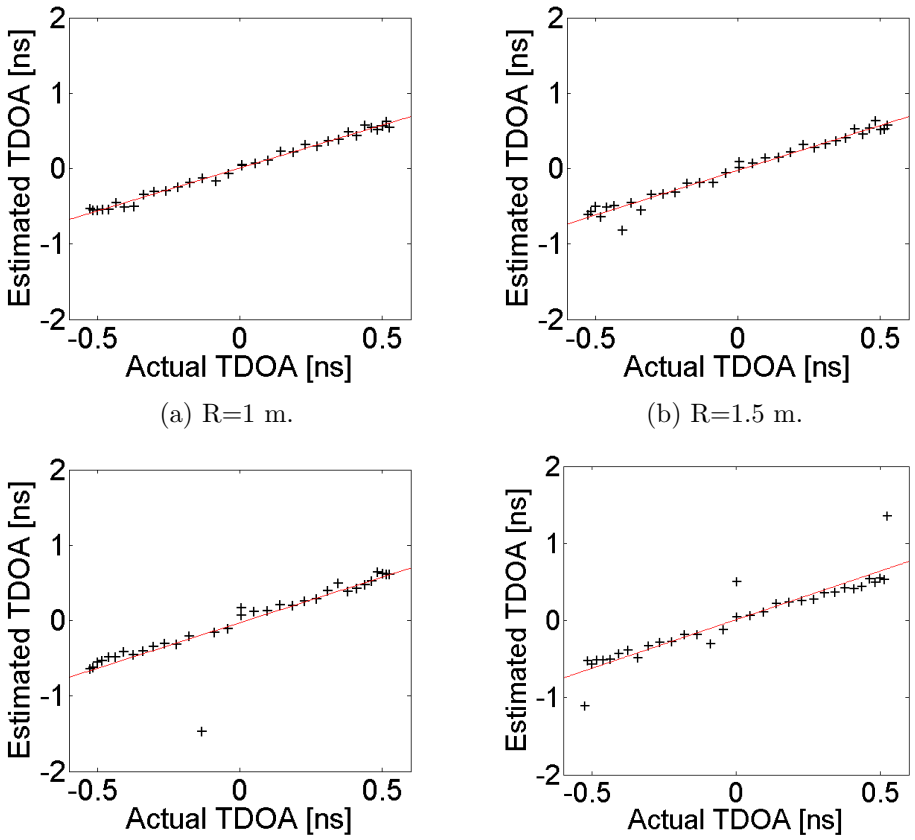

(a) R=1 m.

(b) R=1.5 m.

(c) R=2 m.

(d) R=2.5 m.

Figure 4.4: TDOA measurements results using ZVA24 in room 2, τ_p = 1300 ps, baseline=16 cm, bandwidth: 2 GHz swept frequency.

4.3 Measurements using Vubiq and VSA

4.3.1 Experimental setups

This campaign of measurement is led using a commercially available 60 GHz band communication system called Vubiq. To meet WiGig standard requirements, communication signals using OFDM format are built in SystemVue and Matlab. An AWG (Arbitrary Waveform Generator) is used to physically generate these different signals which in turn drive the 60 GHz communication system. The role of receiver is played by a digital storage oscilloscope including the vectorial signal analysis interface (VSA). The measurements setup and the global view are illustrated in Figure 4.5 and Figure 4.6.

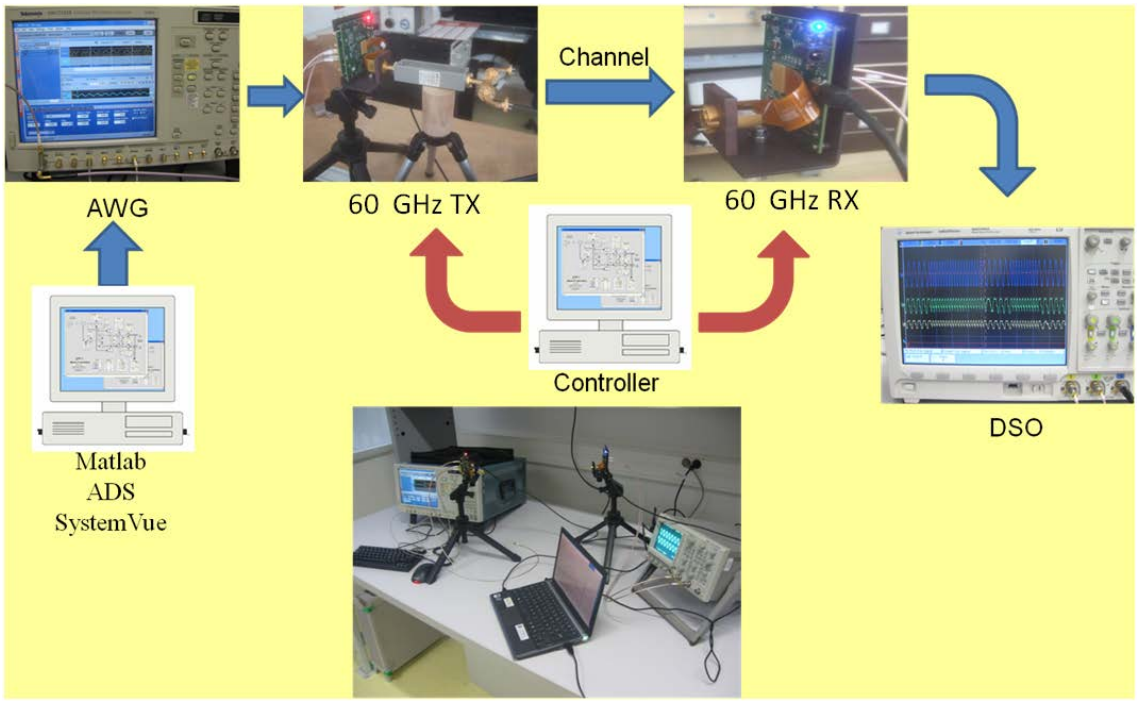

Figure 4.5: Measurement setup using commercialy campaign.

Base-band signals, prepared with Matlab and SystemVue and generated by the AWG, are connected via the high speed baseband connector on the rear side of each Vubiq board. The signals are sent through the 60 GHz Tx and captured by 60 GHz Rx. The received signal is then treated by a DSO and the main communication features are displayed. In next sections, the main parts of this measurement campaign are described further.

4.3.1.1 Arbitrary waveform generator (AWG)

Main characteristic of the Tektronix AWG7000 Series, used as AWG are:

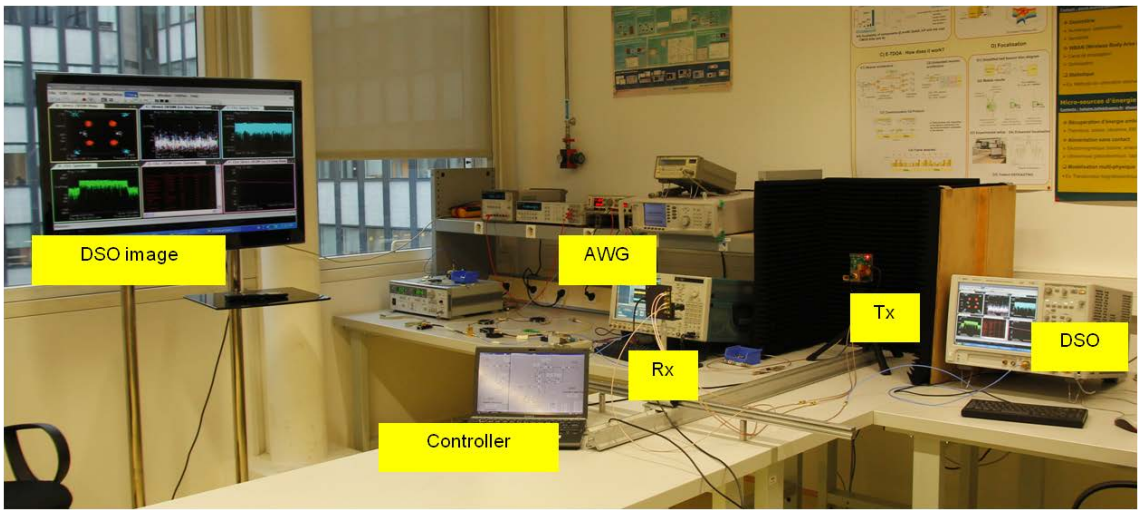

Figure 4.6: Measurement setup global view

.

- Sample rate (24 Gsample/sec)
- Wide analog bandwidth (up to 7.5 GHz)
- Deep memory(up to 129,600,000 points)

With sample rates up to 24 Gsample/sec (with up to 10-Bit resolution), together with one or two channel, complex UWB OFDM signals or other complex signals can be generated.

4.3.1.2 60 GHz waveguide module development system (V60WGD02)

The V60WGD02 development system of the VubIQ company is used in order to study the communication system at 60 GHz. This product is composed of a millimeter transmitter board and receiver board which operate in the 57 to 64 GHz band. Both Tx and Rx can be controlled by a PC via a simple USB interface on each board. Each board can drive its power from the USB connection (standard operation) or from a separate AC powered 5 volt supply. The high sensibility and the high gain of Rx (56-70 dB) can be helpful to detect the signals in a proper way. The basic parts of this product are presented in appendix.

Transmitter operates in the 57 to 64 GHz unlicensed band and its output power can reach up to 10 mW. More than 500 MHz baseband channels can be transmitted about each central frequency while at 60 GHz, up to 1.5 GHz (modulated) bandwidth can be obtained. However, due to system impairments, frequency bandwidth of less than 300 MHz can actually be properly transmitted, which limits the performance of this system. Receiver operates also in the 57 to 64 GHz unlicensed band with the same characteristics and has a 6 dB noise figure.

It should be mentioned that the 1 dB compression point (P1dB) for the transmitter output power is typically +10 dBm. The maximum recommended input signal level to the transmitter (I and Q inputs) is 100 mVPP differential. Saturation of the receiver input stage is approximately at -30 dBm (P1dB). Distance between the Tx and Rx will depend on system bandwidth, information rate (symbol rate if using digital modulation), antenna gains, and the path characteristics (such as completely free space or multipath). As an example, using only the waveguide apertures as antennas (about 7 dBi gain for each waveguide, Tx and Rx), at a distance of 1 meter (68 dB path loss), the received signal power level is driven by:

$$\text{TxPower + WaveguideGain (x2) - path loss} = 10\ dBm + 14\ dB - 68\ dB = -44\ dBm.$$

The waveguide radiation patterns are very wide (in the range of 70° to 80°), so multi-path in high bit rate systems will be an issue. With horn antennas, the signal level to the receiver is increased by the horn gain(s) and the multi-path situation is largely improved due to the narrow beam widths. Far field is determined by the aperture of the antenna(s). Generally, the far field is equal to $2D^2/\lambda$, where D is the largest dimension of the antenna aperture. So while using open waveguides as radiating structure, the far field occurs as soon as 7.2 cm.

4.3.1.3 SystemVue interface

Used mainly as a simulator tool in chapter 3, SystemVue can also play the role of OFDM coding signal able to drive hardware communication systems. So, different OFDM signals were generated in this research work until now, but just some are selected and presented to be observed more precisely in this chapter. All these signals are generated by using the FlexOFDM source block in SystemVue. As shown in Figure 4.7, this block gives the users the ability of changing and modifying all important parameters considered in an OFDM signal such as carrier Frequency, OFDM Sample frequency, DFT size, number of guard sub-carriers, data mapping type, preamble and pilot characteristics, etc. So one is capable to create his customized OFDM signal.

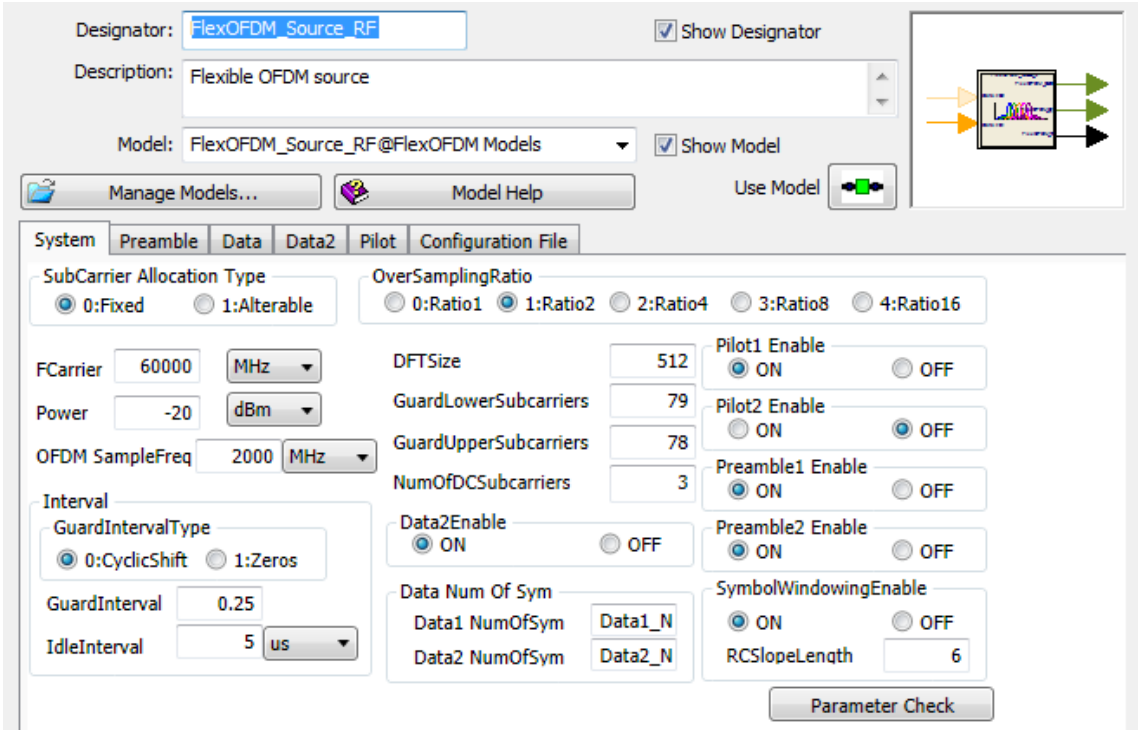

Figure 4.7: OFDM source block GUI in SystemVue.

As shown in Figure 4.8, an OFDM signal that corresponds to the WiGig standard characteristics is generated with the OFDM source block and then the transmitted signal is captured and demodulated by the VSA89600 (Vectorial Signal Analyzer). In this case a 256 QAM mapping type is chosen. In Figure 4.9 the constellation, OFDM spectrum, EVM, OFDM summary characteristics, OFDM time signal, and equivalent channel frequency response in the VSA are shown.

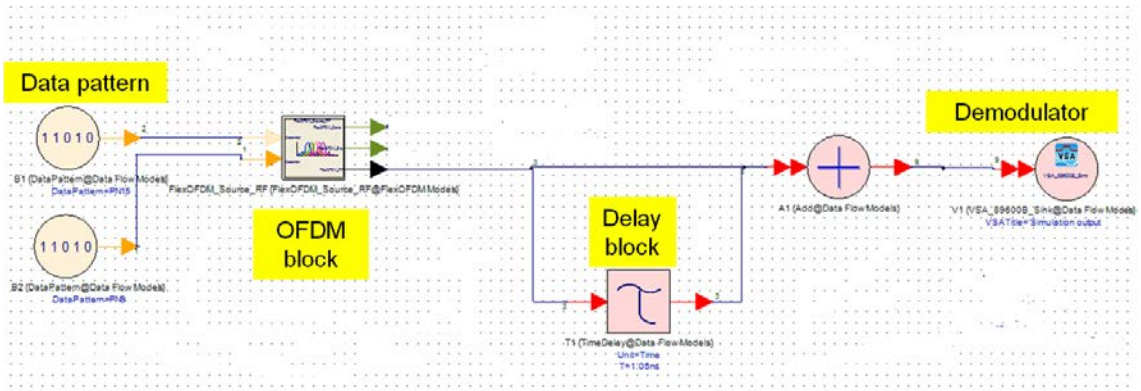

Figure 4.8: OFDM source block and VSA in SystemVue schematic.

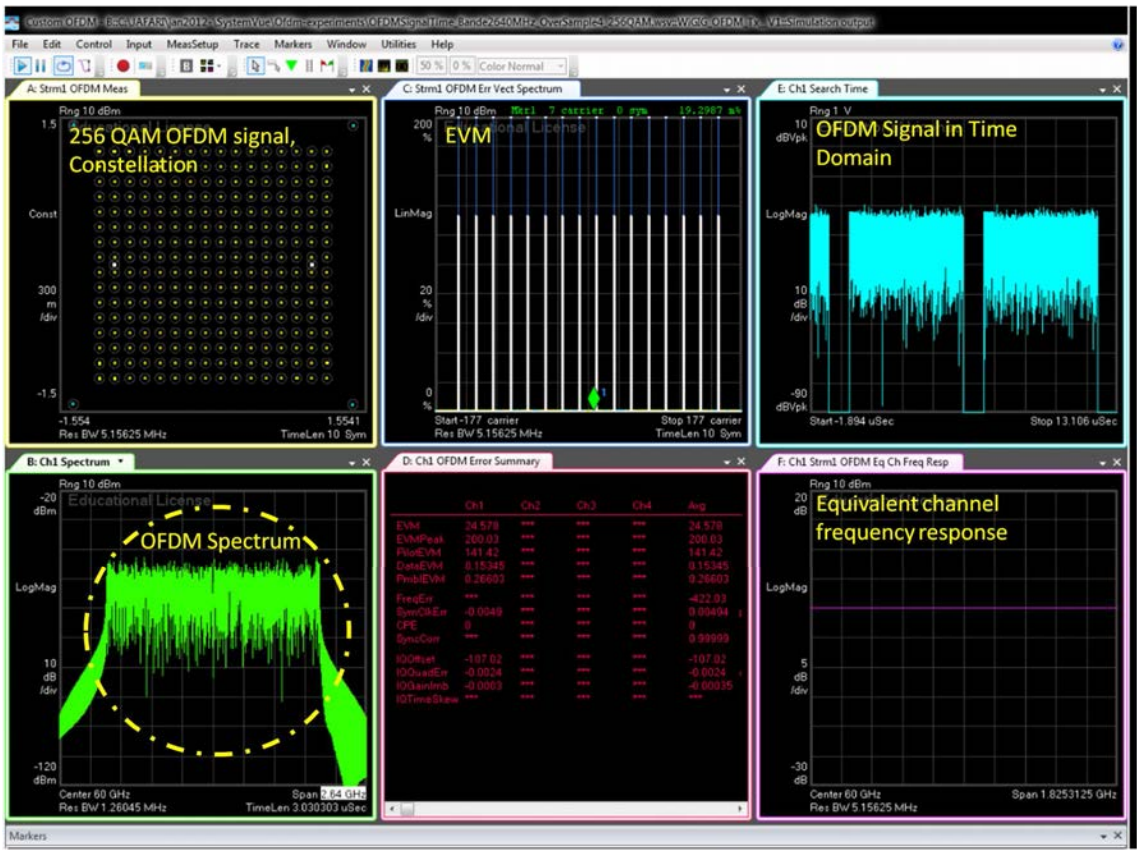

Figure 4.9: General display of the received OFDM signal using digital storage oscilloscope (DSO) with vectorial signal analyzer interface (VSA).

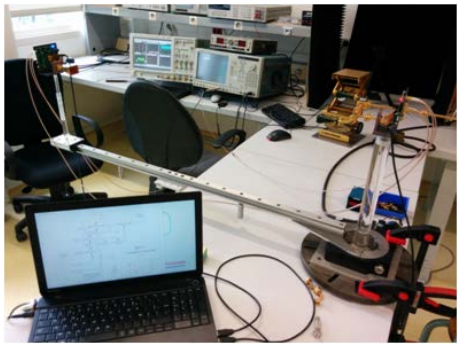

(a) The whole experimental setup

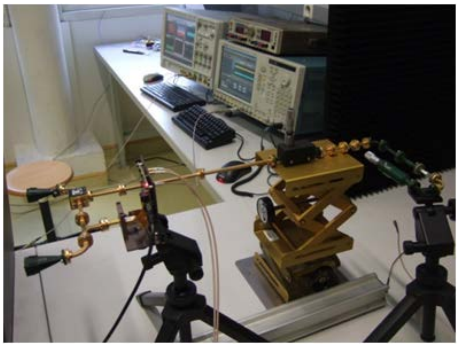

(b) Dual antenna system with delay line

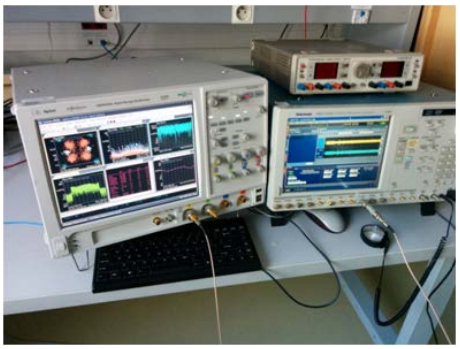

(c) DSO and AWG

Figure 4.10: Measurements using Vubiq and DSO with open waveguides

4.3.2 Measurements results

4.3.2.1 Free space measurements

Experiments were carried out in lab for wireless communication measurements using UWB OFDM signals (following the WiGig standard) for different values of TDOA over a range of frequencies. As shown in Figure 4.10, different experiments are performed and some results are presented in Figure 4.11. We can see that the communication, by means of constellation diagram, is performed even if the spectrum exhibits nulls while the average EVM is high enough, as expected. However, some communications trouble often occurred due to the difficulty to synchronize properly RD and MD. Indeed during tests, a 400 KHz sine-wave signal was observed at the Rx outputs even without inserting any signals at Tx. The fact is that the receiver sees the transmitter's clock (which is about 400 KHz difference between its own clock), when the two are tuned to the same channel. This essentially produces a CW (continuous wave) signal but it is normal and due to the fact that the Tx and Rx have their own 285.714 MHz reference oscillators that are close in frequency but are never going to be exact. So the third mode of synchronization is chosen in which the Tx and Rx oscillator are connected to each other to overcome this

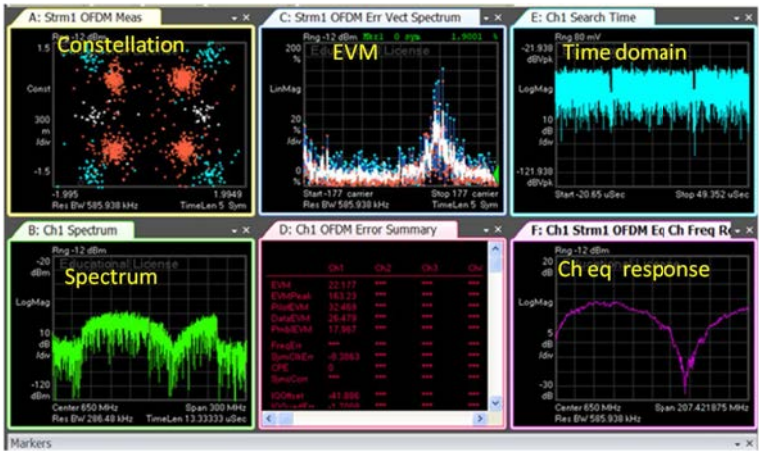

Figure 4.11: An example of measurement results using Vubiq and DSO with open waveguides, QAM OFDM, EVM= 24%, baseline= 18 cm.

problem.

But yet, the obtained TDOA measurements are not close to the expected values. In the next step of experimental work, to recognize whether the sources of error are due to the channel or the vubiq system a guided measurement campaign is explored.

4.3.2.2 Guided mono-band measurements

Experiments were carried out in lab using UWB OFDM signals (following the WiGig standard) for different values of TDOA over a range of frequencies.

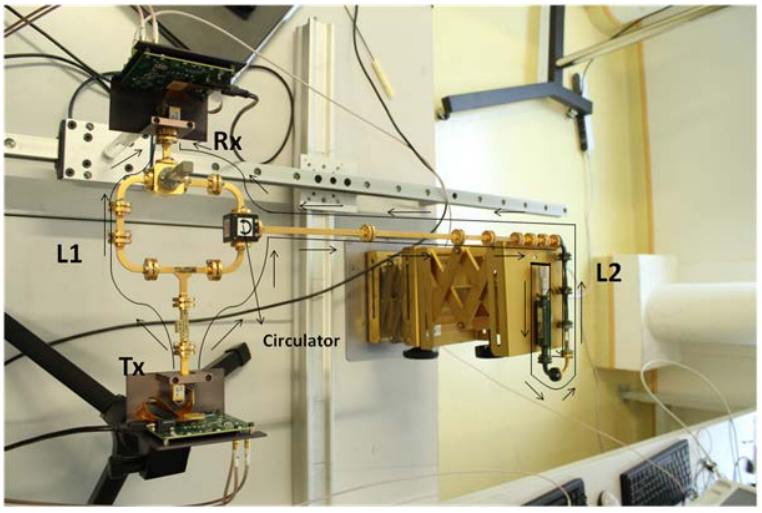

Figure 4.12: Experimental setup with Vubiq using ideal channel emulated by WR rectangular waveguides

.

As shown in Figure 4.12, the setup used for these experiments is a guided measurement, which consists in an attenuator, a power splitter to emulate the dual Tx antenna, a power combiner, and a circulator. A delay line is added in one path to introduce τ_t and the path followed by the signals indicated with arrows in Figure 4.12. Data obtained from these measurements were processed in Vector Signal Analysis (VSA) software to extract, by means of post processing, τ_t.

First a mono-band approach is considered at $F_0 = 60$ GHz. In Figure 4.13, an example of received signal is presented. As illustrated in this figure, the expected interferometry pattern is obtained on the spectrum which has naturally an influence on EVM and ECR. But the constellation indicates that the overall average EVM is still reasonable to perform the communication. Unfortunately, due to the unsuitability of the system, the estimated TDOA are not close to the expected values and high errors are observed. Now, this is clear that the errors are due to the Vubiq system impairments. Actually, the frequency response over the whole bandwidth of different functions (filters, amplifiers,...) may be very perturbed. So one can try to reduce the impact of the frequency response by working with multiple narrow bands. In the next step of experimental work, a multi-band system will be implemented to explore the possibility of improving the obtained results.

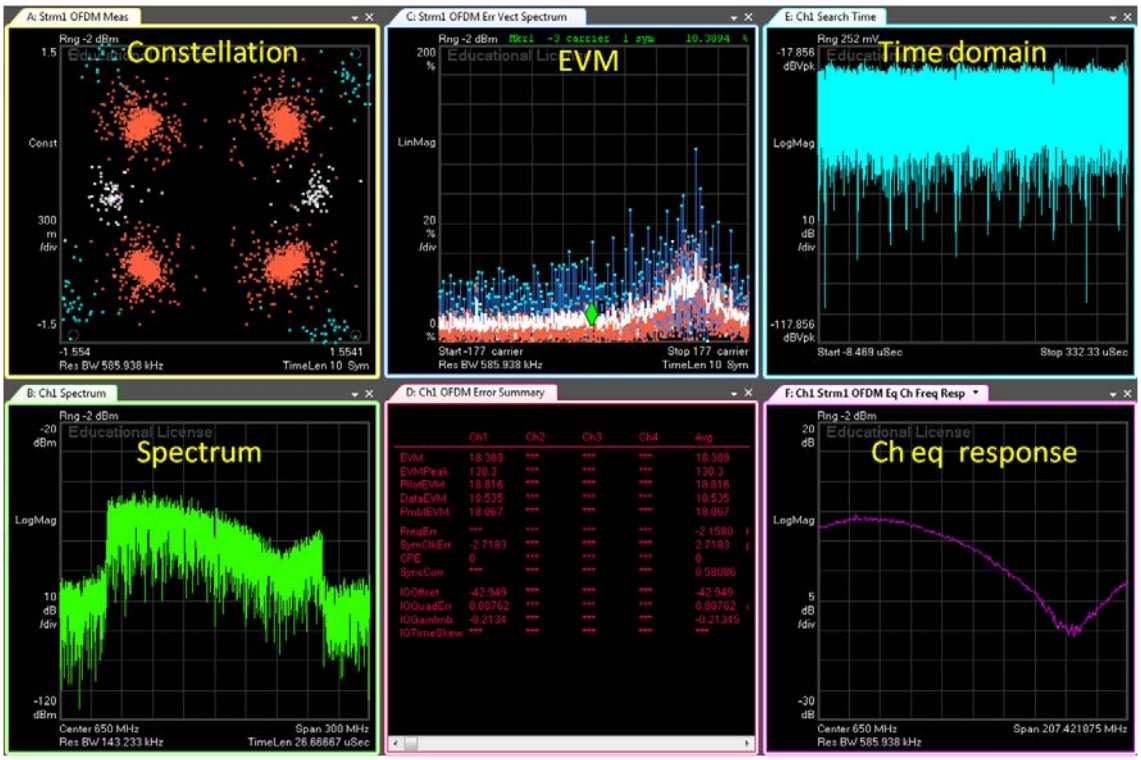

Figure 4.13: Mono band Measurements results with Vubiq system using “ideal ”channel emulated by WR rectangular waveguide.

4.3.2.3 Guided multi-band measurements

A multi-band approach is hence considered by using 8 different bands centered about 8 carriers from 57 to 61 GHz (each with about 200 MHz bandwidth). In Figure 4.14, the multi-band received signals are presented.

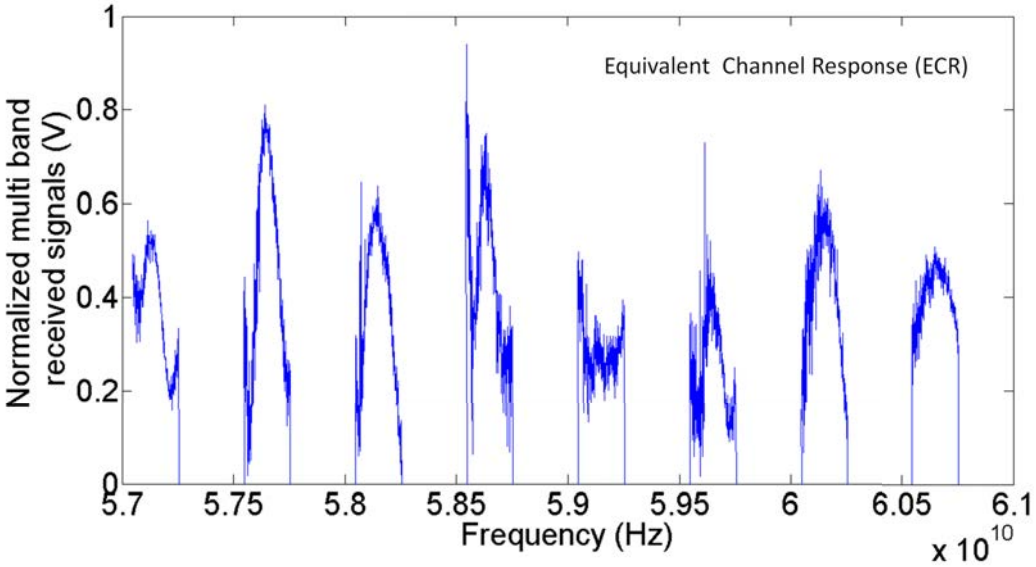

Figure 4.14: Multi band Measurements results with Vubiq system using ideal channel emulated by WR rectangular waveguide.

To estimate the TDOA from these measurements, the NLS estimation method, already presented in chapter 3, is applied for each band. Here again, in spite of obtaining good fit-curving for almost all cases (Figure 4.15), the estimated TDOA values exhibit large errors. However, it should be noticed that the feasibility of our proposed approach has already been proven by VNA and it can be inferred that an important portion of errors are due to the Vubiq circuits impairments. To be able to have coherent results using a 60 GHz system, in the next stage, another system which is called "Highrate Transceiver"is considered for the measurements.

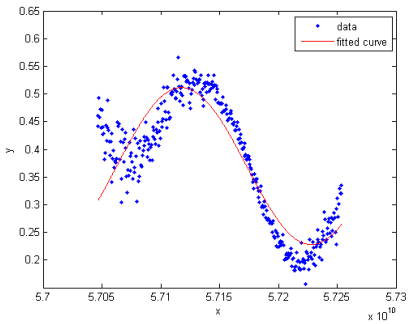

(a) First band

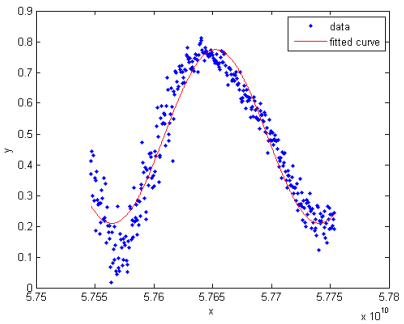

(b) Second band

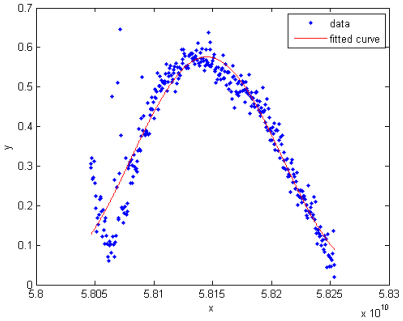

(c) Third band

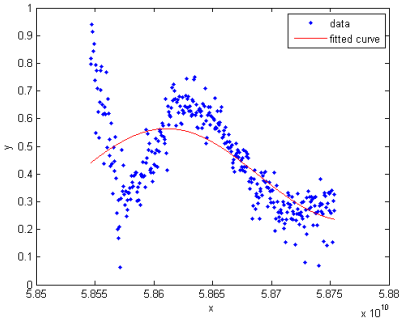

(d) Forth band

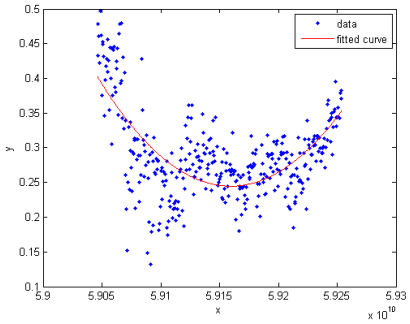

(e) Fifth band

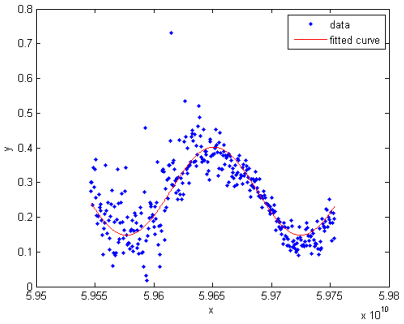

(f) Sixth band

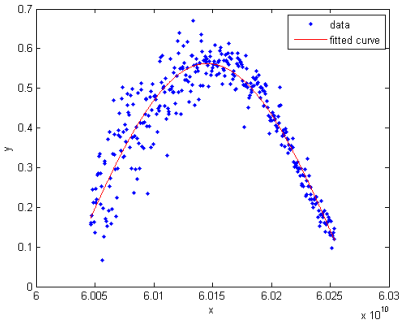

(g) Seventh band

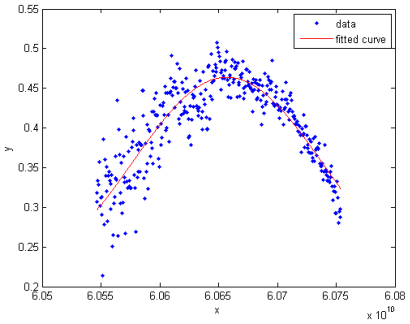

(h) Eighth band

Figure 4.15: Multi band Measurements: TDOA NLS regression for all bands.

4.4 Measurements using Highrate transceiver

4.4.1 Experimental setup and test condition

Almost the same configuration is considered for the measurements but instead of Vubiq system, a transceiver, which is called "Highrate Transceiver", is used. This transceiver, shown in Figure 4.16, has a 2*2 MIMO capabilities and is composed, at the transmitting part, by amplifier and IQ modulator and, at the receiving part, by LNA and IQ mixer. Receiver local oscillator and transmitter local oscillator are given by the same reference oscillator which also drives the sample clock. Digital signal control and processing are led by FPGA. The software interfaces considered in this system enable real-time implementations [112].

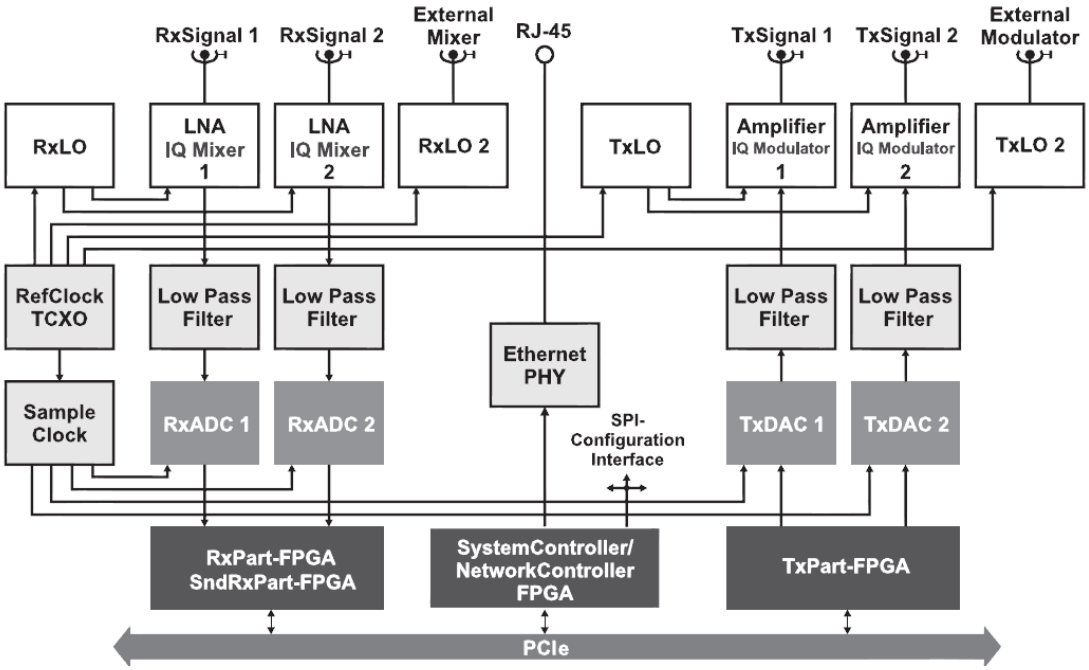

Figure 4.16: Highrate transceiver structure.

The maximum possible bandwidth which can be generated by this transceiver is only 250 MHz. Table 4.25 and Table 4.4 gives the main features and specifications of this system [112].

Parameter	Specification
Bandwidth	250 MHz
Number of subcarriers	64
Loaded subcarriers	48
Pilot subcarriers	12
Guard interval / cyclic prefix	8 clock cycles
Subcarrier modulation	QPSK, QAM16, QAM64
Coding	Code spreading on subcarriers

Table 4.3: Highrate transceiver characteristics.

Using the scenario presented in Figure 4.17, a 250 MHz flat OFDM spectrum is generated and then transmitted at a central frequency $F_0 = 60$ GHz by using quadruplers, and mixers. The baseline is here longer and is set to 34 cm.

Component	Specifications[a]
FPGAs	4×Altera Stratix III with 260K logic elements
TX DACs	2×IQ DACs, 250 MSps (internal: 500 MSps), 16 bit res. SNR: 45 dB, SFDR: 82 dBc, DNL: 2.1 LSB, INL: 3.7 LSB
RX DACs	2×IQ DACs, 500 MSps, 8 bit resolution SNR: 45 dB, SFDR: 54 dBc, ENOB: 7.2
On-board memory	8 MS per channel at Tx, 16 MS/channel at RX

[a]SFDR: spurious-free dynamic range, DNL: differential nonlinearity, LSB: least significant bit, INL: integral nonlinearity, ENOB: effective number of bits

Table 4.4: Highrate transceiver specifications.

Due to the fact that a long delay line is required to visualize the periodicity in a 250 MHz bandwidth, the power transmitted from the dual antenna system at RD is not the same at A_1 and A_2. In order to compensate this, an amplifier and a variable attenuator are added after the delay line to be able to equalize this power difference, which imposes a longer baseline. The setup is shown in Figure 4.17 .

4.4.2 Results

The TDOA is now estimated from the channel equalization performed within the OFDM communication. Different positions for mobile are considered: 1 to 2 m range differences from the reference device and with a θ varying from 0° to 90°, leading to an excursion of about 1.1 ns in the time domain.

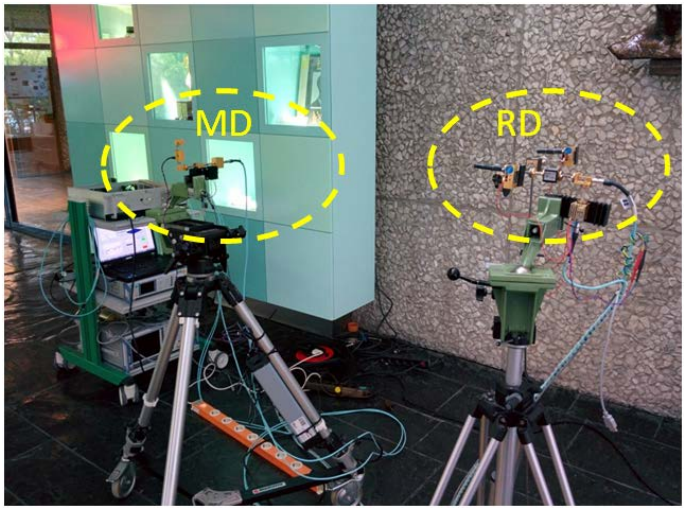

Figure 4.17: Scenario of the measurements campaign using Highrate transceiver with 250 MHz OFDM signal (room 2, lobby), B=34 cm.

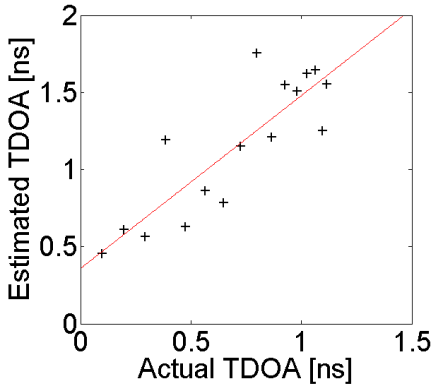

(a) measurement error results in spatial domain

Figure 4.18: TDOA Measurements results using Highrate transceiver with 250 MHz OFDM signal (room 2, lobby), B=34 cm.

An example of error results is shown in Figure 4.18. It can be observed that obtained results exhibit coherence with expected values but using this smaller bandwidth causes, as expected, much higher estimation errors. Therefore, the obtained values are drastically different from the simulation results and the first measurement campaign using VNA, but seem coherent.

4.5 Multi-band measurements with base-band signals

The theory and simulations regarding multi-band approach is already explored in chapter 3. Due to the instrumental limitations (highlighted in previous sections), the simulation, presented in chapter 3, with the same bandwidth and in the wireless environment cannot be implemented experimentally. But to prove our idea experimentally a wire-line communication and signals at lower frequency are chosen. As shown in Figure 4.19, to introduce the delay, two wires with different lengths were connected to the two channels of AWG where the same OFDM signals were generated. To introduce the additioner, a power combiner which works at 1-4 GHz is used. The two wire-lines are connected at the power combiner outputs, and the VSA to its input for detecting the received signal. For the multi-band approach, 6 OFDM signals with 500 MHz bandwidth but with different center frequencies are generated in a manner that the whole 3 GHz bandwidth which is available between 1 to 4 GHz can be utilized. In this range, no up-conversion is required as the AWG can directly transmit such frequencies. In each experiment, one of these 6 OFDM signals is transmitted. The received signals are shown in Figure 4.20 (in this figure, all these received signals are for a delay corresponding to 45 cm difference in lengths of the two wirelines). At the end, the saved results are concatenated to achieve the whole spectrum. Depending on the different delays, the position of zeros are changed in the spectrum as expected. Three different delays are studied by changing the relative length of the two input wire-lines of the additioner.

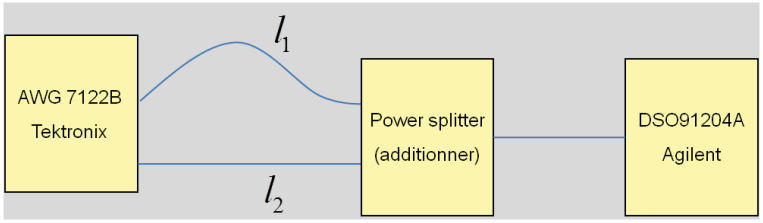

Figure 4.19: Multi band experimental schematic.

As shown in Figure 4.21 to extract higher TDOA values, just one window of 500 MHz may be sufficient, but to extract lower values, more windows (thus more equivalent bandwidth) is required, hence the usefulness of the proposed multi-band approach is demonstrated. As presented in Figure 4.21, by implementing the multi-band approach and concatenating the results of each transmission, a higher bandwidth can be used to extract the TDOA. The comparison between estimated values and expected one are presented in Figure 4.22. They exhibit a very good agreement validating the proposed approach.

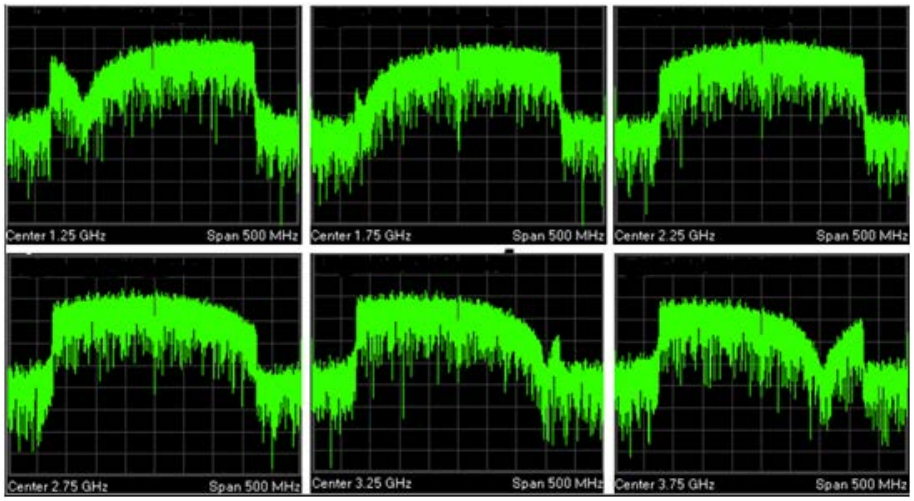

Figure 4.20: 6 received signals for 6 different RF signals.

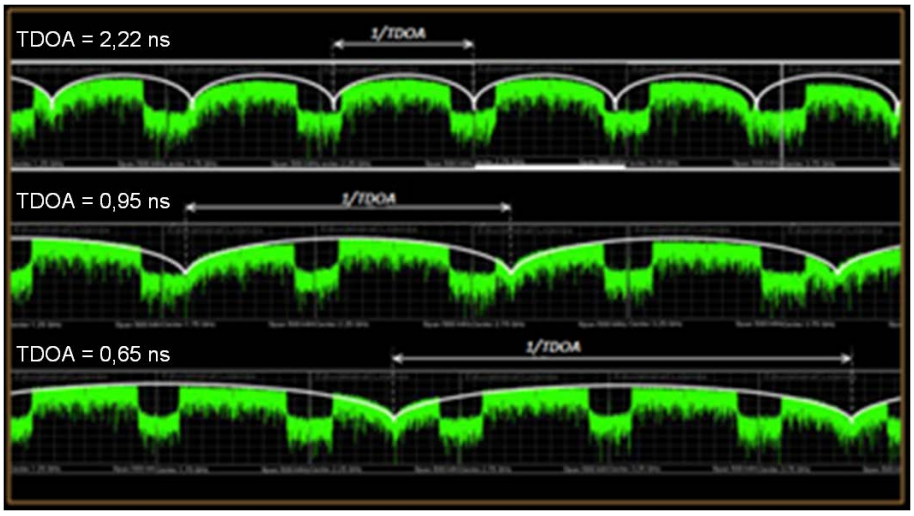

Figure 4.21: Concatenated multi-band received signals in three different cases.

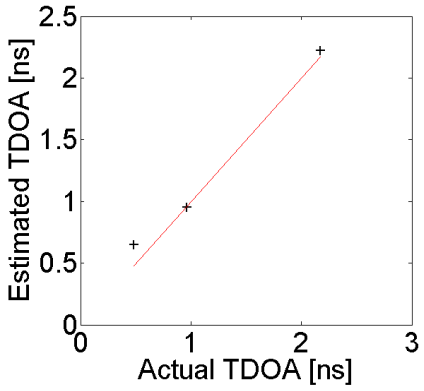

Figure 4.22: TDOA Measurements results using multi-band approach with base-band signals.

4.6 Conclusion

In this chapter, experimental works validating the new proposed method for estimating the TDOA, particularly well suited for communication systems in indoor applications operating at 60 GHz and using UWB OFDM signals, are presented.

In section 1, measurements using VNA are presented. Due to the 2 GHz bandwidth and to well defined calibration procedure, the results are in good agreements with analytical and modeling approaches.

In section 2, measurements using Vubiq and VSA are presented using free space measurements, guided mono-band and guided multi-band approaches. The mono-band solution shows that the proposed solution is qualitatively interesting but important enhancement are required to develop an operational system. The multi-band, due to the concatenation of several narrow band seems to be an interesting compromise in this approach. But due to the system impairments, the TDOA estimated values are not close to expected values.

In section 3, measurements using Highrate transceiver, are explored using a narrow bandwidth, and exhibit coherent results but with errors that are not yet compatible with current applications.

In section 4, base-band multi-band measurements are explored and coherent results in good agreement with expected values are obtained. These campaigns of measurements point-out the ability of already existing communication systems to perform localization. However to reach accurate solutions some effort are needed in both hardware and software aspects.

Conclusion and perspectives

The emerging concepts of Internet of Things (IoT), Internet of Everything (IoE) and more extensively Internet of Space (IoS), associated with green radio communication and energy saving solutions, require further exploitation of spatial resources. This research work contributes to this purpose, which appears as a very promising trend. Furthermore, millimeter wave band communication and especially the 60 GHz band has gained increased interest thanks to the availability of a huge unlicensed spectrum about 60 GHz and to the development of the IEEE 802.11.ad standard for indoor systems.

By developing a new method for the Time Difference Of Arrival estimation, that has been proven particularly well suited for modern millimeter wave high data rate communication systems in indoor applications, we demonstrate the possibility to perform in real time localization functionality in a standard communication system.

After a brief description of the context, rich of numerous applications, we presented a global overview including the state of art of 60 GHz communication systems and positioning techniques. Different topics, dealing with channel issues, technological aspects, standard and metrics, are presented and discussed. Such review demonstrates the potentiality of the 60 GHz OFDM system to perform High Data rate (HDR), low Bit Error Rate (BER) communication, and accurate real time localization as well.

A focus on the ability of the TDOA metric to provide accurate localization function in the context of mobile connected objects, led to the definition of a compact and energy aware solution allowing the extraction of TDOA information from communication signals and data. This wide-band interferometry-based method permits TDOA estimation by using available features in an OFDM receiver such as Error Vector Magnitude (EVM) or Equivalent Channel Response (ECR). The useful bandwidth is sometimes considered as a mono-band centered on 60 GHz, or as a concatenation of adjacent multiple bands, each of them centered about different frequency carriers in the range of 57 GHz to 66 GHz. In case of non adjacent multiple bands, interpolation could be proposed.

Theory of this approach is firstly studied in the case of an ideal channel. The ana-

lytical solution is validated by a set of simulations performed by a commercial simulator "SystemView". Experimental measurement, carried out by means of a vectorial network analyzer, validates the predicted results and confirms the relevance of the proposed solution.

In order to cope with realistic millimeter wave communication environment, channel issues are taken into account. We first define a simple LOS-NLOS channel and then implement a dedicated IEEE 802.11ad channel model. Simulation results of both channel models are in good agreement with analytical results. For the experimental part, many campaigns of measurement were carried out using commercial HDR communication system. The first system, called Vubiq is a 60 GHz TX and RX module offering about 500 MHz bandwidth at fourteen different center frequencies in a range of 57-63 GHz. The second system called Highrate Transceiver is a flexible digital radio testbed providing a bandwidth of 250 MHz and 2x2 MIMO capabilities that lead to reach rapid real-time implementations .

For the whole measurement carried out by these communication systems, the experimental results are qualitatively in good agreement with the theory. However due to many imperfections including frequency response of filters and the non linearity of active devices, the results, obtained at 60 GHz band, are not very accurate. More precise results are obtained when measurement are carried out with the base-band signals between 1 GHz and 4 GHz. In this case, TDOA measured with an error less than 12 % has been presented.

This preliminary work demonstrates the feasibility of the solution consisting in the extraction, from communication patterns, of relevant parameters able to determine the TDOA and hence the localization of a connected object. But there is room for enhancing this approach, stating the perspectives of this work, by developing high quality hardware and advanced software.

For the hardware part, efforts are first expected in the calibration of the receiving system. The fine knowledge of the transfer function for each component can help to define a more realistic direct model, which in turn, makes easier the solution of the inverse problem. Therefore, efforts should also be oriented toward the design of millimeter wave devices involving preferentially CMOS technology. Actually CMOS technology is becoming a must technology for implementing energy efficient and low cost connected objects. Strong efforts are also expected in the signal processing part. The use of advanced estimating method dealing for example with Extended Kalman Filtering or Particle Filtering can overcome some hardware imperfections.

Finally for localization purpose, it would be very interesting to define, as for communication issue, a specific channel of localization. The performance criteria would not be the

bit error rate (BER) but the accuracy of location. One should also be able to discriminate line of sight contribution from non-line of sight contribution. New channel characterization and modeling would be of high interest for this research area. Furthermore, to reach a better accuracy and more precise system, a combination of AOA and proposed TDOA approach can be taken in consideration for further investigations. In addition, the same approach may be explored in outdoor environment regarding the recent researches using millimeter wave communication in 5G mobile networks.

Appendix A : 60 GHz Vubiq Modules

Transmitter and receiver

As presented in Figure. 4.23 and Figure. 4.24 the Tx and Rx circuits are heterodyne systems utilizing the low phase noise crystal oscillators that provide the clock reference frequency for the Tx/Rx synthesizers.

The frequency of the oscillator is 285.714 MHz and has a stability rating over temperature of 25 ppm. There may be certain system level applications that require the transmitter and/or receiver to be phase locked to an external source. The Tx/Rx RF boards are set up to provide the following options for oscillator reference source:

- Internal: separate crystal oscillators (default)
- External: 285.714 MHz signal source such as a laboratory signal generator
- Transmitter sourcing the receiver (Tx master/RX slave) from the Tx internal oscillator:
  The optional reference oscillator settings are implemented via zero-ohm resistor (or wire jumper).

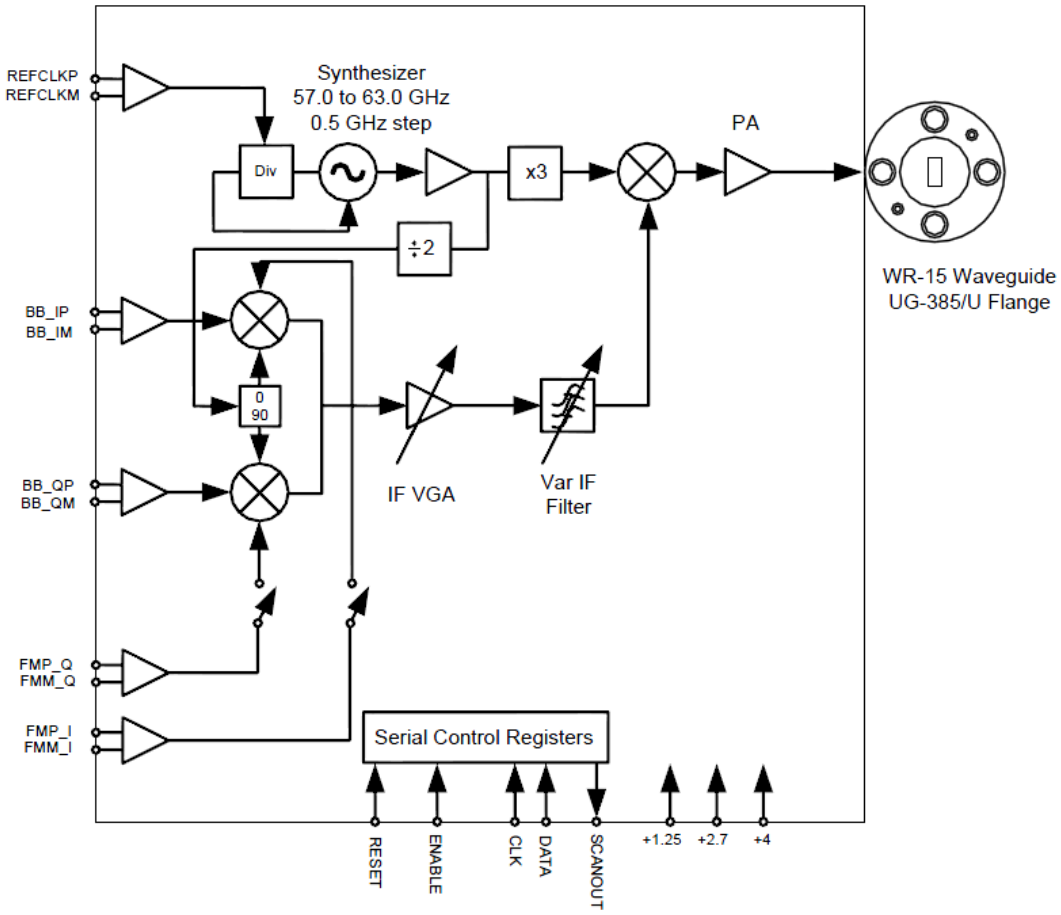

Figure 4.23: 60 GHz transmitter circuit

.

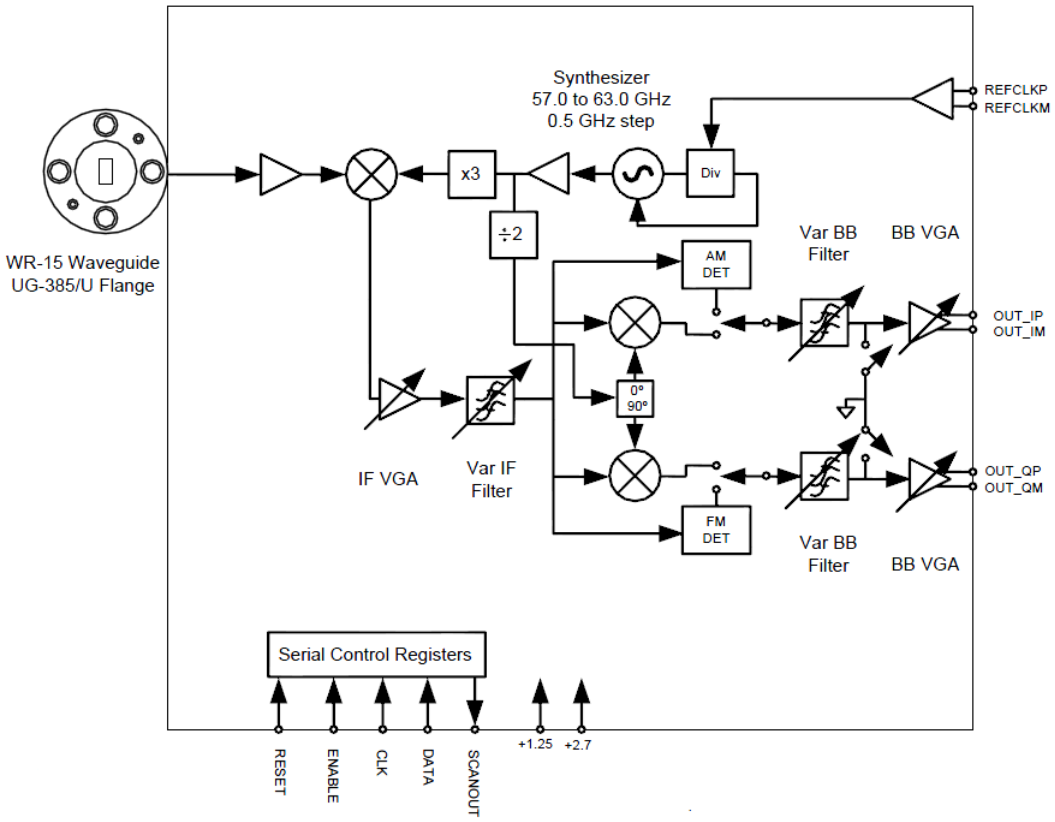

Figure 4.24: 60 GHz receiver circuit

.

Appendix B : Highrate Transceiver

Receiver

The receiver side of Higrate Transceiver is shown in Figure 4.25.

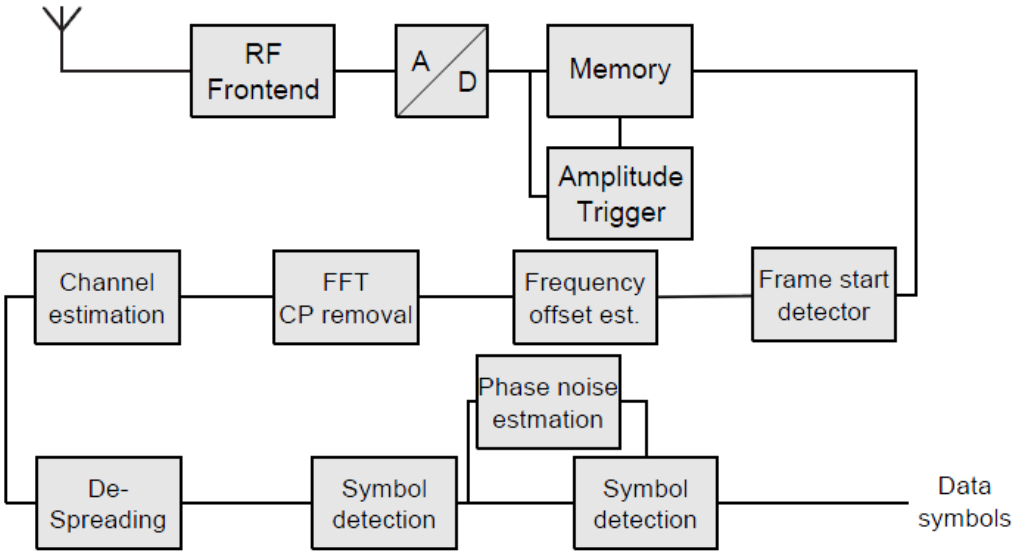

Figure 4.25: Highrate Transceiver Rx block diagram.

Appendix C : List of publications

Journal paper

1.TDOA estimation method using 60 GHz OFDM spectrum
Ahmadreza Jafari, Luca Petrillo, Julien Sarrazin, David Lautru, Philippe De Doncker, Aziz Benlarbi-Delai International Journal of Microwave and Wireless Technologies, vol. 7, pp. 31-35, 2 2015.

International and national conferences

1.NLOS Influence on 60 GHz Indoor Localization Based on a New TDOA Extraction Approach
A. Jafari, J. Sarrazin, L. Petrillo, D. Lautru, P. De Doncker, A. Benlarbi-Delai, in 2013 European Microwave Conference (EuMC), Oct 2013, pp. 330-333.

2.Simultaneous Communication and Localization for 60 GHz UWB OFDM systems
A. Jafari, J. Sarrazin, L. Petrillo, D. Lautru, P. De Doncker, A. Benlarbi-Delai in 2013 IEEE Antennas and Propagation Society International Symposium (AP-SURSI), July 2013, pp. 1948-1949.

3.Localisation Indoor: Nouvelle Méthode d'Estimation de la TDOA à Partir des Signaux de Communication Millimétrique OFDM
A. Jafari, J. Sarrazin, L. Petrillo, T. Mavridis, P. De Doncker, A. Benlarbi-Delaï URSI 2014, Paris, France, Mars 2014.

4.Solutions de Communication et de Localisation Simultanées en Bande Millimétrique

A. Jafari, J. Sarrazin, L. Petrillo, D. Lautru, P. De Doncker, A. Benlarbi-Delai Journees Nationales Micro-ondes JNM 2013, Paris, France, Mai 2013.

5.Communication et Radio Localisation Simultanées en Bande Millimétrique

A. Jafari, L. petrilllo, J. Sarrazin, D. lautru, P. De Doncker, A. Benlarbi-delai URSI 2013, Paris, France, mars 2013.

Bibliography

[1] T. Baykas, C.-S. Sum, Z. Lan, J. Wang, M. Rahman, H. Harada, and S. Kato, "IEEE 802.15.3c: the first IEEE wireless standard for data rates over 1 Gb/s," *IEEE Communications Magazine*, vol. 49, no. 7, pp. 114–121, July 2011.

[2] S. Yong and C.-C. Chong, "An overview of multigigabit wireless through millimeter wave technology: Potentials and technical challenges," *EURASIP Journal on Wireless Communications and Networking*, vol. 2007, no. 1, p. 078907, 2007. [Online]. Available: http://jwcn.eurasipjournals.com/content/2007/1/078907

[3] T. Rappaport, S. Sun, R. Mayzus, H. Zhao, Y. Azar, K. Wang, G. Wong, J. Schulz, M. Samimi, and F. Gutierrez, "Millimeter wave mobile communications for 5G cellular: It will work!" *IEEE Access*, vol. 1, pp. 335–349, 2013.

[4] W. Roh, J.-Y. Seol, J. Park, B. Lee, J. Lee, Y. Kim, J. Cho, K. Cheun, and F. Aryanfar, "Millimeter-wave beamforming as an enabling technology for 5G cellular communications: theoretical feasibility and prototype results," *IEEE Communications Magazine*, vol. 52, no. 2, pp. 106–113, February 2014.

[5] T. Rappaport, J. Murdock, and F. Gutierrez, "State of the art in 60-GHz integrated circuits and systems for wireless communications," *Proceedings of the IEEE*, vol. 99, no. 8, pp. 1390–1436, Aug 2011.

[6] A. Technologies, *Wireless LAN at 60 GHz - IEEE 802.11ad Explained.* Agilent Technologies, Inc. 2012, 2013 Published in USA, May 30, 2013 5990-9697EN, 2010.

[7] M.-T. Z. Shao-Qiu Xiao and Y. Zhang, *Millimeter Wave Technology in Wireless PAN, LAN, and MAN.* Auerbach Publications , Taylor and Francis Group, 2008.

[8] I. C. Gusenbauer, D. and J. Krösche, "Self-contained indoor positioning on off-the-shelf mobile devices," 2010.

[9] "Miweba, Millimetre-Wave Evolution for Backhaul and Access," 2014, http://www.miweba.eu/.

[10] "Metis, Mobile and wireless communications Enablers for the Twenty-twenty Information Society," 2014, https://www.metis2020.com/.

[11] C. Dehos, J. Gonzalez, A. De Domenico, D. Ktenas, and L. Dussopt, "Millimeter-wave access and backhauling: the solution to the exponential data traffic increase in 5G mobile communications systems?" *IEEE Communications Magazine*, vol. 52, no. 9, pp. 88–95, September 2014.

[12] R. Weiler, M. Peter, W. Keusgen, E. Calvanese-Strinati, A. De Domenico, I. Filippini, A. Capone, I. Siaud, A.-M. Ulmer-Moll, A. Maltsev, T. Haustein, and K. Sakaguchi, "Enabling 5G backhaul and access with millimeter-waves," in *European Conference on Networks and Communications (EuCNC)*, June 2014, pp. 1–5.

[13] G. Li, T. Irnich, and C. Shi, "Coordination context-based spectrum sharing for 5G millimeter-wave networks," in *9th International Conference on Cognitive Radio Oriented Wireless Networks and Communications (CROWNCOM)*, June 2014, pp. 32–38.

[14] C. Hansen, "Wigig: Multi-gigabit wireless communications in the 60 GHz band," *IEEE Wireless Communications*, vol. 18, no. 6, pp. 6–7, 2011.

[15] F. Khan, Z. Pi, and S. Rajagopal, "Millimeter-wave mobile broadband with large scale spatial processing for 5g mobile communication," in *50th Annual Allerton Conference on Communication, Control, and Computing (Allerton)*, Oct 2012, pp. 1517–1523.

[16] K. P. F. Gutierrez, S. Agarwal and T. S. Rappaport., "On-chip integrated antenna structures in CMOS for 60 GHz WPAN systems,", *Proceedings of IEEE Global Communications Conference (Globecom)*, Honolulu, HI, November 30December 4, 2009.

[17] G. Minassian, J. Borowski and J. Tom, "Portable wireless data storage," Google Patents, US Patent 7,742,741, 2010.

[18] C. Park and T. Rappaport, "Short-range wireless communications for next-generation networks: UWB, 60 GHz millimeter-wave WPAN, and zigbee," *IEEE Wireless Communications*, vol. 14, no. 4, pp. 70–78, 2007.

[19] N. Patwari, J. Ash, S. Kyperountas, A. Hero, R. Moses, and N. Correal, "Locating the nodes: cooperative localization in wireless sensor networks," *IEEE Signal Processing Magazine*, vol. 22, no. 4, pp. 54–69, 2005.

[20] J. Al-Karaki and A. Kamal, "Routing techniques in wireless sensor networks: a survey," *IEEE Wireless Communications*, vol. 11, no. 6, pp. 6–28, 2004.

[21] S. Zhang, Y. Chen, and S. Xu, "Improving energy efficiency through bandwidth, power, and adaptive modulation," in *IEEE 72nd Vehicular Technology Conference Fall (VTC 2010-Fall)*, Sept 2010, pp. 1–5.

[22] B. Van Veen and K. Buckley, "Beamforming: a versatile approach to spatial filtering," *IEEE ASSP Magazine*, vol. 5, no. 2, pp. 4–24, April 1988.

[23] E. Perahia, C. Cordeiro, M. Park, and L. Yang, "IEEE 802.11ad: Defining the next generation multi-Gbps wi-fi," in *7th IEEE Consumer Communications and Networking Conference (CCNC)*, Jan 2010, pp. 1–5.

[24] L. Li, J. Y. Halpern, P. Bahl, Y.-M. Wang, and R. Wattenhofer, "A cone-based distributed topology-control algorithm for wireless multi-hop networks," *IEEE/ACM Transactions on Networking*, vol. 13, no. 1, pp. 147–159, Feb 2005.

[25] D. R. Mautzt., "Indoor positioning technologies," Habilitation Thesis submitted to ETH Zurich, 2012.

[26] "Loctronix company," 2014, http://www.loctronix.com/en/default.htm.

[27] B. Ye and Z. Zhang, "Improved pilot design and channel estimation for 60 GHz OFDM based on IEEE 802.11.ad," in *IEEE Wireless Communications and Networking Conference (WCNC)*, April 2013, pp. 4129–4133.

[28] H. Zhu and J. Wang, "Chunk-based resource allocation in OFDMA systems - part i: chunk allocation," *IEEE Transactions on Communications*, vol. 57, no. 9, pp. 2734–2744, September 2009.

[29] H. Yang, P. Smulders, and M. Herben, "Frequency selectivity of 60-GHz los and nlos indoor radio channels," in *IEEE 63rd Vehicular Technology Conference, VTC*, vol. 6, May 2006, pp. 2727–2731.

[30] T. Manabe, K. Sato, H. Masuzawa, K. Taira, T. Ihara, Y. Kasashima, and K. Yamaki, "Polarization dependence of multipath propagation and high-speed transmission characteristics of indoor millimeter-wave channel at 60 GHz," *IEEE Transactions on Vehicular Technology*, vol. 44, no. 2, pp. 268–274, May 1995.

[31] E. Violette, R. Espeland, R. DeBolt, and F. Schwering, "Millimeter-wave propagation at street level in an urban environment," *IEEE Transactions on Geoscience and Remote Sensing*, vol. 26, no. 3, pp. 368–380, May 1988.

[32] C. Anderson and T. Rappaport, "In-building wideband partition loss measurements at 2.5 and 60 GHz," *IEEE Transactions on Wireless Communications*, vol. 3, no. 3, pp. 922–928, May 2004.

[33] B. Langen, G. Lober, and W. Herzig, "Reflection and transmission behaviour of building materials at 60 GHz," in *5th IEEE International Symposium on Personal, Indoor and Mobile Radio Communications, 1994. Wireless Networks - Catching the Mobile Future*, Sep 1994, pp. 505–509 vol.2.

[34] C. Balanis, *Advanced Engineering Electromagnetics*, ser. CourseSmart Series. Wiley, 2012. [Online]. Available: http://books.google.fr/books?id=_q35KChOfVwC

[35] N. Chahat, M. Zhadobov, and R. Sauleau, "Broadband tissue-equivalent phantom for ban applications at millimeter waves," *IEEE Transactions on Microwave Theory and Techniques*, vol. 60, no. 7, pp. 2259–2266, July 2012.

[36] B. Leite, E. Kerherve, A. Ghiotto, A. Larie, B. Martineau, and D. Belot, "60 GHz 28 nm cmos transformer-coupled power amplifier for wigig applications," *Electronics Letters*, vol. 50, no. 20, pp. 1451–1453, September 2014.

[37] C. Doan, S. Emami, A. Niknejad, and R. Brodersen, "Millimeter-wave CMOS design," *IEEE Journal of Solid-State Circuits*, vol. 40, no. 1, pp. 144–155, Jan 2005.

[38] J.-S. Rieh and D.-H. Kim, "An overview of semiconductor technologies and circuits for Terahertz communication applications," in *IEEE GLOBECOM Workshops*, Nov 2009, pp. 1–6.

[39] D. Sobel and R. Brodersen, "A 1 Gb/s mixed-signal baseband analog front-end for a 60 GHz wireless receiver," *IEEE Journal of Solid-State Circuits*, vol. 44, no. 4, pp. 1281–1289, April 2009.

[40] A. Niknejad, "Siliconization of 60 ghz," *IEEE Microwave Magazine*, vol. 11, no. 1, pp. 78–85, Feb 2010.

[41] J. Lee and Y. Lin, "3.88 db nf 60 GHz CMOS UWB LNA with small group-delay-variation," *Electronics Letters*, vol. 49, no. 7, pp. 472–474, March 2013.

[42] G. Liu, P. Haldi, T.-J. K. Liu, and A. Niknejad, "Fully integrated CMOS power amplifier with efficiency enhancement at power back-off," *IEEE Journal of Solid-State Circuits*, vol. 43, no. 3, pp. 600–609, March 2008.

[43] M. Apostolidou, M. van der Heijden, D. Leenaerts, J. Sonsky, A. Heringa, and I. Volokhine, "A 65 nm CMOS 30 dBm class-e RF power amplifier with 60 % PAE and 40 % PAE at 16 dB back-off," *IEEE Journal of Solid-State Circuits*, vol. 44, no. 5, pp. 1372–1379, May 2009.

[44] J. Choi, D. Kang, D. Kim, and B. Kim, "Optimized envelope tracking operation of Doherty power amplifier for high efficiency over an extended dynamic range," *IEEE Transactions on Microwave Theory and Techniques*, vol. 57, no. 6, pp. 1508–1515, June 2009.

[45] P. Asbeck, L. Larson, D. Kimball, S. Pornpromlikit, J.-H. Jeong, C. Presti, T. Hung, F. Wang, and Y. Zhao, "Design options for high efficiency linear handset power amplifiers," in *IEEE Topical Meeting on Silicon Monolithic Integrated Circuits in RF Systems*, Jan 2009, pp. 1–4.

[46] A. M. Niknejad and H. Hashemi, "Mm-wave silicon technology," *New York: Springer-Verlag*, 2008.

[47] M. Varonen, M. Karkkainen, J. Riska, P. Kangaslahti, and K. Halonen, "Resistive HEMT mixers for 60-GHz broad-band telecommunication," *IEEE Transactions on Microwave Theory and Techniques*, vol. 53, no. 4, pp. 1322–1330, April 2005.

[48] B. Motlagh, S. Gunnarsson, M. Ferndahl, and H. Zirath, "Fully integrated 60-GHz single-ended resistive mixer in 90-nm CMOS technology," *IEEE Microwave and Wireless Components Letters*, vol. 16, no. 1, pp. 25–27, Jan 2006.

[49] L. H. Chen, L. Li, and T. J. Cui, "Four-channel 60 GHz up-conversion mixer with 14 dB gain and 2.5 dBm p1dB using transformer matching network," *Electronics Letters*, vol. 50, no. 11, pp. 814–815, May 2014.

[50] J. Borremans, M. Dehan, K. Scheir, M. Kuijk, and P. Wambacq, "VCO design for 60 GHz applications using differential shielded inductors in 0.13 um CMOS," in *IEEE Radio Frequency Integrated Circuits Symposium, 2008. RFIC*, June 2008, pp. 135–138.

[51] L. Wu and H. Luong, "A 49-to-62 GHz quadrature VCO with bimodal enhanced-magnetic-tuning technique," *IEEE Transactions on Circuits and Systems I: Regular Papers*, vol. 61, no. 10, pp. 3025–3033, Oct 2014.

[52] L. Kuang, X. Yu, H. Jia, L. Chen, W. Zhu, M. Wei, Z. Song, Z. Wang, and B. Chi, "A fully integrated 60-GHz 5-Gb/s QPSK transceiver with t/r switch in 65-nm CMOS," *IEEE Transactions on Microwave Theory and Techniques*, vol. 62, no. 12, pp. 3131–3145, Dec 2014.

[53] J. Murdock, E. Ben-Dor, F. Gutierrez, and T. Rappaport, "Challenges and approaches to on-chip millimeter wave antenna pattern measurements," in *IEEE MTT-S International Microwave Symposium Digest (MTT)*, June 2011, pp. 1–4.

[54] L. Ragan, A. Hassibi, T. Rappaport, and C. Christianson, "Novel on-chip antenna structures and frequency selective surface (FSS) approaches for millimeter wave devices," in *IEEE 66th Vehicular Technology Conference, 2007. VTC-2007 Fall*, Sept 2007, pp. 2051–2055.

[55] J. Buckwalter, A. Babakhani, A. Komijani, and A. Hajimiri, "An integrated subharmonic coupled-oscillator scheme for a 60-GHz phased-array transmitter," *IEEE Transactions on Microwave Theory and Techniques*, vol. 54, no. 12, pp. 4271–4280, Dec 2006.

[56] S. Gunnarsson, C. Karnfelt, H. Zirath, R. Kozhuharov, D. Kuylenstierna, A. Alping, and C. Fager, "Highly integrated 60 GHz transmitter and receiver MMIC in a GaAs PHEMT technology," *IEEE Journal of Solid-State Circuits*, vol. 40, no. 11, pp. 2174–2186, Nov 2005.

[57] B. Floyd, S. Reynolds, U. Pfeiffer, T. Zwick, T. Beukema, and B. Gaucher, "SiGe bipolar transceiver circuits operating at 60 GHz," *IEEE Journal of Solid-State Circuits*, vol. 40, no. 1, pp. 156–167, Jan 2005.

[58] S. Reynolds, A. Natarajan, M.-D. Tsai, S. Nicolson, J.-H. Zhan, D. Liu, D. Kam, O. Huang, A. Valdes-Garcia, and B. Floyd, "A 16-element phased-array receiver IC

for 60-GHz communications in sige BICMOS," in *IEEE Radio Frequency Integrated Circuits Symposium (RFIC)*, May 2010, pp. 461–464.

[59] E. Torkildson, H. Zhang, and U. Madhow, "Channel modeling for millimeter wave MIMO," in *Information Theory and Applications Workshop (ITA)*, Jan 2010, pp. 1–8.

[60] B. Razavi, "A 60-GHz CMOS receiver front-end," *IEEE Journal of Solid-State Circuits*, vol. 41, no. 1, pp. 17–22, Jan 2006.

[61] D. Alldred, B. Cousins, and S. Voinigescu, "A 1.2v, 60-GHz radio receiver with on-chip transformers and inductors in 90-nm CMOS," in *IEEE Compound Semiconductor Integrated Circuit Symposium, CSIC*, Nov 2006, pp. 51–54.

[62] M. Lei, I. Lakkis, C.-S. Sum, T. Baykas, J.-Y. Wang, M. Rahman, R. Kimura, R. Funada, Y. Shoji, H. Harada, and S. Kato, "Hardware impairments on LPDC coded SC-FDE and ofdm in multi-Gbps WPAN (IEEE 802.15.3c)," in *IEEE Wireless Communications and Networking Conference, WCNC*, March 2008, pp. 442–446.

[63] J. Tan and G. Stuber, "Frequency-domain equalization for continuous phase modulation," *IEEE Transactions on Wireless Communications*, vol. 4, no. 5, pp. 2479–2490, Sept 2005.

[64] H. Singh, S.-K. Yong, J. Oh, and C. Ngo, "Principles of IEEE 802.15.3c: Multi-gigabit millimeter-wave wireless PAN," in *Proceedings of 18th Internatonal Conference on Computer Communications and Networks, ICCCN*, Aug 2009, pp. 1–6.

[65] R. C. Johnson, "IBM, mediatek to debut 60-GHz chipset," *EE Times, accessed on May 31, 2010 [Online]. Available: http://www.eetimes.com/news/ latest/showArticle.jhtml?articleID= 225000143.*

[66] *High Rate 60 GHz PHY, MAC, and HDMI PAL, Standard ECMA-387,*, vol. 1st ed, p. 344, Dec. 2008.

[67] E. Perahia, C. Cordeiro, M. Park, and L. Yang, "Ieee 802.11ad: Defining the next generation multi-Gbps Wi-Fi," in *7th IEEE Consumer Communications and Networking Conference (CCNC)*, Jan 2010, pp. 1–5.

[68] H. Liu, H. Darabi, P. Banerjee, and J. Liu, "Survey of wireless indoor positioning techniques and systems," *IEEE Transactions on Systems, Man, and Cybernetics, Part C: Applications and Reviews*, vol. 37, no. 6, pp. 1067–1080, 2007.

[69] M. Kanaan and K. Pahlavan, "A comparison of wireless geolocation algorithms in the indoor environment," in *IEEE Wireless Communications and Networking Conference, WCNC*, vol. 1, 2004, pp. 177–182 Vol.1.

[70] X. Li, K. Pahlavan, M. Latva-aho, and M. Ylianttila, "Comparison of indoor geolocation methods in DSSS and OFDM wireless LAN systems," in *52nd IEEE-VTS Fall VTC Vehicular Technology Conference*, vol. 6, 2000, pp. 3015–3020 vol.6.

[71] G. Mao, B. Fidan, and B. D. O. Anderson, "Wireless sensor network localization techniques," *Comput. Netw.*, vol. 51, no. 10, pp. 2529–2553, Jul. 2007. [Online]. Available: http://dx.doi.org/10.1016/j.comnet.2006.11.018

[72] D. Koks, "Numerical calculations for passive geolocation scenarios," *Tech. Rep. DSTO-RR-0000*, 2005, http://catalogue.nla.gov.au/Record/4367609.

[73] T. Rappaport, J. Reed, and B. Woerner, "Position location using wireless communications on highways of the future," *IEEE Communications Magazine*, vol. 34, no. 10, pp. 33–41, Oct 1996.

[74] R. Schmidt, "Multiple emitter location and signal parameter estimation," *IEEE Transactions on Antennas and Propagation*, vol. 34, no. 3, pp. 276–280, Mar 1986.

[75] R. Roy and T. Kailath, "Esprit-estimation of signal parameters via rotational invariance techniques," *IEEE Transactions on Acoustics, Speech and Signal Processing*, vol. 37, no. 7, pp. 984–995, Jul 1989.

[76] A. Paulraj, R. Roy, and T. Kailath, "A subspace rotation approach to signal parameter estimation," *Proceedings of the IEEE*, vol. 74, no. 7, pp. 1044–1046, July 1986.

[77] N. Tayem and H. Kwon, "Conjugate esprit (c-sprit)," *IEEE Transactions on Antennas and Propagation*, vol. 52, no. 10, pp. 2618–2624, Oct 2004.

[78] P. Bergamo and G. Mazzini, "Localization in sensor networks with fading and mobility," in *13th IEEE International Symposium on Personal, Indoor and Mobile Radio Communications*, vol. 2, Sept 2002, pp. 750–754 vol.2.

[79] E. Elnahrawy, X. Li, and R. Martin, "The limits of localization using signal strength: a comparative study," in *First Annual IEEE Communications Society Conference on Sensor and Ad Hoc Communications and Networks*, Oct 2004, pp. 406–414.

[80] T. S. Rappaport, "Wireless communications: Principles and practice," *2nd ed. Prentice Hall PTR*, 2001.

[81] R. Bernhardt, "Macroscopic diversity in frequency reuse radio systems," *IEEE Journal on Selected Areas in Communications*, vol. 5, no. 5, pp. 862–870, Jun 1987.

[82] D. McCrady, L. Doyle, H. Forstrom, T. Dempsey, and M. Martorana, "Mobile ranging using low-accuracy clocks," *IEEE Transactions on Microwave Theory and Techniques*, vol. 48, no. 6, pp. 951–958, Jun 2000.

[83] G. Carter, "Coherence and time delay estimation," *Proceedings of the IEEE*, vol. 75, no. 2, pp. 236–255, Feb 1987.

[84] C. Knapp and G. Carter, "The generalized correlation method for estimation of time delay," *IEEE Transactions on Acoustics, Speech and Signal Processing*, vol. 24, no. 4, pp. 320–327, Aug 1976.

[85] S. Hara, D. Anzai, T. Yabu, K. Lee, T. Derham, and R. Zemek, "A perturbation analysis on the performance of TOA and TDOA localization in mixed LOS/NLOS environments," *IEEE Transactions on Communications*, vol. 61, no. 2, pp. 679–689, February 2013.

[86] C. Schaible, "Mobile radiotelephone station two-way ranging system," *US Patent, US4229620 A*, 12 Jan 1982.

[87] N. B. Priyantha, A. Chakraborty, and H. Balakrishnan, "The cricket location-support system," in *Proceedings of the 6th Annual International Conference on Mobile Computing and Networking*, ser. MobiCom '00. New York, NY, USA: ACM, 2000, pp. 32–43. [Online]. Available: http://doi.acm.org/10.1145/345910.345917

[88] J.-Y. Lee and R. Scholtz, "Ranging in a dense multipath environment using an UWB radio link," *IEEE Journal on Selected Areas in Communications*, vol. 20, no. 9, pp. 1677–1683, Dec 2002.

[89] S. Gezici, Z. Tian, G. Giannakis, H. Kobayashi, A. Molisch, H. Poor, and Z. Sahinoglu, "Localization via ultra-wideband radios: a look at positioning aspects for future sensor networks," *IEEE Signal Processing Magazine*, vol. 22, no. 4, pp. 70–84, July 2005.

[90] C.-K. Chen and W. Gardner, "Signal-selective time-difference of arrival estimation for passive location of man-made signal sources in highly corruptive environments. ii. algorithms and performance," *IEEE Transactions on Signal Processing*, vol. 40, no. 5, pp. 1185–1197, May 1992.

[91] W. Gardner and C.-K. Chen, "Signal-selective time-difference-of-arrival estimation for passive location of man-made signal sources in highly corruptive environments. i. theory and method," *IEEE Transactions on Signal Processing,* , vol. 40, no. 5, pp. 1168–1184, May 1992.

[92] L. Zwirello, T. Schipper, M. Harter, and T. Zwick, "UWB localization system for indoor applications: Concept, realization and analysis," *JECE*, vol. 2012, pp. 4:1–4:11, Jan. 2012. [Online]. Available: http://dx.doi.org/10.1155/2012/849638

[93] A. Ward, A. Jones, and A. Hopper, "A new location technique for the active office," *IEEE Personal Communications*, vol. 4, no. 5, pp. 42–47, Oct 1997.

[94] "Active Bat ultrasonic location system," *http://www.cl.cam.ac.uk/research/dtg/attarchive/bat/*.

[95] D. N. Hatfield, "A report on technical and operational issues impacting the provision of wireless enhanced 911 services," *Federal Communications Commission*, 2002.

[96] F. Gustafsson and F. Gunnarsson, "Mobile positioning using wireless networks: possibilities and fundamental limitations based on available wireless network measurements," *IEEE Signal Processing Magazine*, vol. 22, no. 4, pp. 41–53, July 2005.

[97] G. Goth, "Wi-Fi making big new waves: "in-room" high-speed uses to get big boost from wireless mainstay," *IEEE Internet Computing*, vol. 15, no. 5, pp. 7–10, 2011.

[98] A. Pekou, V. Nastos, N. Moraitis, and P. Constantitiou, "Time delay and coherence bandwidth measurements at 60 GHz in an indoor environment for WLANs," in *IEEE 59th Vehicular Technology Conference, VTC 2004-Spring*, vol. 1, 2004, pp. 93–97 Vol.1.

[99] I. Oppermann, M. Hamalainen, and J. Iinatti, "UWB theory and applications," in *John Wiley and Sons Ltd 2004*, vol. 1, 2004, pp. 3–10, 42–43.

[100] A. Jafari, J. Sarrazin, D. Lautru, A. Benlarbi-Delai, L. Petrillo, and P. De Doncker, "NLOS influence on 60 GHz indoor localization based on a new TDOA extraction approach," in *2013 European Microwave Conference (EuMC)*, Oct 2013, pp. 330–333.

[101] A. Jafari, J. Sarrazin, D. Lautru, A. Benlarbi-Delai, L. Petrillo, and P. De Doncker, "Simultaneous communication and localization for 60 GHz UWB OFDM systems," in *2013 IEEE Antennas and Propagation Society International Symposium (APSURSI)*, July 2013, pp. 1948–1949.

[102] A. Jafari, L. Petrillo, J. Sarrazin, D. Lautru, P. De Doncker, and A. Benlarbi-Delai, "TDOA estimation method using 60 GHz OFDM spectrum," *International Journal of Microwave and Wireless Technologies*, vol. 7, pp. 31–35, 2 2015. [Online]. Available: http://journals.cambridge.org/article-S1759078714000324

[103] F. P. Fontan and P. M. Espieira, *Modelling the Wireless Propagation Channel: A Simulation Approach with Matlab*. Wiley Publishing, 2008.

[104] K. Panta and J. Armstrong, "Indoor localisation using white LEDs," *Electronics Letters*, vol. 48, no. 4, pp. 228–230, 2012.

[105] M. Ghosh, "Improved equalization for coded, zero-padded OFDM (ZP-OFDM) systems," in *IEEE International Conference on Communications, ICC*, June 2007, pp. 4263–4268.

[106] C. De Marziani, J. Urena, A. Hernandez, J. Garcia, A. Jimenez, M. Perez, F. Alvarez, and J. Villadangos, "Relative localization and mapping combining multidimensional scaling and Levenberg-Marquardt optimization," in *IEEE International Symposium on Intelligent Signal Processing*, Aug 2009, pp. 43–47.

[107] D. Lowe, "Fitting parameterized three-dimensional models to images," *IEEE Transactions on Pattern Analysis and Machine Intelligence*, vol. 13, no. 5, pp. 441–450, May 1991.

[108] W. Y. Y. C. G. K. Yong Soo Cho, Jaekwon Kim, *MIMO-OFDM WIRELESS COMMUNICATIONS WITH MATLAB*. John Wiley and Sons (Asia) Pte Ltd, 2010.

[109] B. Sklar, *Digital Communications: Fundamentals and Applications 2/E.* Prentice Hall, 2002.

[110] T. Mavridis, L. Petrillo, P. De Doncker, J. Sarrazin, D. Lautru, and A. Benlarbi-Delai, "A 60 GHz off-body channel implementation," in *2013 IEEE Antennas and Propagation Society International Symposium (APSURSI)*, July 2013, pp. 1786–1787.

[111] R. Felbecker, W. Keusgen, and M. Peter, "Estimation of permitivitty and loss tangent of high frequency materials in the millimeter wave band using a hemispherical open resonator," in *2011 IEEE International Conference on Microwaves, Communications, Antennas and Electronics Systems (COMCAS)*, Nov 2011, pp. 1–8.

[112] W. Keusgen, A. Kortke, M. Peter, and R. Weiler, "A highly flexible digital radio testbed and 60 GHz application examples," in *2013 European Microwave Conference (EuMC)*, Oct 2013, pp. 740–743.